FIN OPTIMIZATION IN A FLOW FIELD INDUCED BY PIEZOELECTRIC FAN

PİEZOELEKTRİK FAN KULLANILARAK OLUŞTURULAN BİR AKIŞ ALANINDA FİN OPTİMİZASYONU

EROL UÇ

ASSIST. PROF. DR. ÖZGÜR EKİCİ
Supervisor

Submitted to Graduate School of Science and Engineering of Hacettepe University
as a Partial Fulfillment to the Requirements
for the Award of the Degree of Master of Science
in Mechanical Engineering

2018

This work named "**Fin Optimization in a Flow Field Induced by Piezoelectric Fan**" by **EROL UÇ** has been approved as a thesis for the Degree of **MASTER OF SCIENCE IN MECHANICAL ENGINEERING** by the below mentioned Examining Committee Members.

Prof. Dr. Murat KÖKSAL
Head .....

Assist. Prof. Dr. Özgür EKİCİ
Supervisor ..... 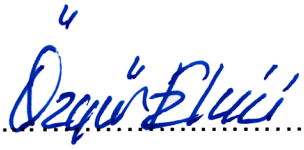

Assoc. Prof. Dr. Metin YAVUZ
Member .....

Assist. Prof. Dr. Okan GÖRTAN
Member .....

Assist. Prof. Dr. Bilsay SÜMER
Member ..... 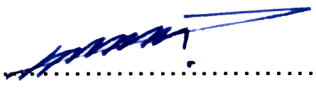

This thesis has been approved as a thesis for the Degree of **MASTER OF SCIENCE IN MECHANICAL ENGINEERING** by Board of Directors of the Institute for Graduate School of Science and Engineering.

Prof. Dr. Menemşe GÜMÜŞDERELİOĞLU
Director of the Institute of
Graduate School of Science and Engineering

YAYINLAMA VE FİKRİ MÜLKİYET HAKLARI BEYANI

Enstitü tarafından onaylanan lisansüstü tezimin/raporumun tamamını veya herhangi bir kısmını, basılı (kağıt) ve elektronik formatta arşivleme ve aşağıda verilen koşullarla kullanıma açma iznini Hacettepe üniversitesine verdiğimi bildiririm. Bu izinle Üniversiteye verilen kullanım hakları dışındaki tüm fikri mülkiyet haklarım bende kalacak, tezimin tamamının ya da bir bölümünün gelecekteki çalışmalarda (makale, kitap, lisans ve patent vb.) kullanım hakları bana ait olacaktır.

Tezin kendi orijinal çalışmam olduğunu, başkalarının haklarını ihlal etmediğimi ve tezimin tek yetkili sahibi olduğumu beyan ve taahhüt ederim. Tezimde yer alan telif hakkı bulunan ve sahiplerinden yazılı izin alınarak kullanması zorunlu metinlerin yazılı izin alarak kullandığımı ve istenildiğinde suretlerini Üniversiteye teslim etmeyi taahhüt ederim.

☒ **Tezimin/Raporumun tamamı dünya çapında erişime açılabilir ve bir kısmı veya tamamının fotokopisi alınabilir.**
(Bu seçenekle teziniz arama motorlarında indekslenebilecek, daha sonra tezinizin erişim statüsünün değiştirilmesini talep etseniz ve kütüphane bu talebinizi yerine getirse bile, tezinin arama motorlarının önbelleklerinde kalmaya devam edebilecektir.)

☐ **Tezimin/Raporumun ..... tarihine kadar erişime açılmasını ve fotokopi alınmasını (İç Kapak, Özet, İçindekiler ve Kaynakça hariç) istemiyorum.**
(Bu sürenin sonunda uzatma için başvuruda bulunmadığım taktirde, tezimin/raporumun tamamı her yerden erişime açılabilir, kaynak gösterilmek şartıyla bir kısmı ve ya tamamının fotokopisi alınabilir)

☐ **Tezimin/Raporumun ..... tarihine kadar erişime açılmasını istemiyorum, ancak kaynak gösterilmek şartıyla bir kısmı veya tamamının fotokopisinin alınmasını onaylıyorum.**

☐ **Serbest Seçenek/Yazarın Seçimi**

17 / 04 / 2018

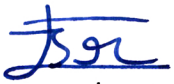

(İmza)

Erol UÇ

Öğrencinin Adı Soyadı

Dedicated to my family

ETHICS

In this thesis study, prepared in accordance with spelling rules of Institute of Graduate Studies in Science of Hacettepe University.

I declared that

- all the information and documents have been obtained in the base of the academic rules
- all audio-visual and written information and results have been presented according to the rules of scientific ethics
- in case of using other Works, related studies have been cited in accordance with the scientific standards
- all cited studies have been fully referenced
- I did not do any distortion in the data set
- And any part of this thesis has not been presented as another thesis study at this or any other university.

17/04/2018

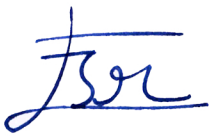

EROL UÇ

ABSTRACT

FIN OPTIMIZATION IN A FLOW FIELD INDUCED BY PIEZOELECTRIC FAN

EROL UÇ

Master of Science, Department of Mechanical Engineering

Supervisor: Assist. Prof. Dr. Özgür Ekici

April 2018, 100 pages

In recent years, piezoelectric fans have been investigated for forced convection heat transfer applications as an alternative to conventional fans. Basically, it consists of a piezoelectric and a non-piezoelectric patch. When AC current is applied, piezoelectric part vibrates with a certain amplitude at that specific AC frequency. In this study, forced convection heat transfer driven by a piezoelectric fan is investigated for fin optimization problem. A 3-dimensional numerical model is implemented with CFD approach employing a commercial CFD solver: Ansys Fluent 17.2. In this model, a piezoelectric fan with a known movement function is simulated in time domain to generate air flow first with a horizontal fan arrangement. The generated air flow is directed to a fin block which is placed at a certain distance from the piezoelectric fan. As a design parameter, the number of fins in fin block is increased. The fin block is formed by attaching conjugated cylindrical fins side by side. The number of conjugated fins is increased from 1 to 10, resulting in 10 different fin block configurations. In this study, there are two boundary conditions applied. Firstly, the total amount of applied heat remains the same. In each configuration 0.8064 W heat is applied to the base of fin block as a

boundary condition. Secondly, the applied heat flux remains the same. In each configuration 50400 W/m^2 heat flux is applied to the base of fin block as a boundary condition. The average surface temperature of fin blocks, the average surface temperature difference between natural and forced convection, heat transfer augmentation ratio and average base temperature of fin blocks are compared. This comparison results in the optimum number of fins for each criterion. When the heat transfer augmentation ratio is evaluated, the 2-fin-block configuration for the constant total heat boundary condition and the 1-fin-block configuration for the constant heat flux boundary condition gives the best results, respectively. Additionally, a vertical fan arrangement is employed and the results are compared to a horizontal fan arrangement for a specified fin configuration. For the studied fin geometry the horizontal fan arrangement is found to provide better cooling performance in all fin configurations compared to the vertical fan arrangement.

Keywords: piezoelectric material, piezoelectric fan, fin optimization,

ÖZET

PİEZOELEKTRİK FAN KULLANILARAK OLUŞTURULAN BİR AKIŞ ALANINDA FİN OPTİMİZASYONU

EROL UÇ

Yüksek Lisans, Makina Mühendisliği Bölümü

Tez Danışmanı: Yrd. Doç. Dr. Özgür Ekici

Nisan 2018, 100 sayfa

Son yıllarda, geleneksel fanlara alternatif olarak piezoelektrik fanlar zorlanmış iletimsel ısı transferi uygulamaları için araştırılmıştır. Bu fanlar, temel olarak, bir piezoelektrik ve bir piezoelektrik olmayan parça içerir. Alternatif akım uygulandığında, piezoelektrik parça belirli bir alternatif akım frekansında belirli bir genlikte titreşir. Bu çalışmada, fin eniyileme problemi için bir piezoelektrik fan yardımıyla zorlanmış iletimsel ısı transferi araştırılmıştır. Ticari bir CFD çözümleyicisi olan Ansys Fluent 17.2 kullanılarak CFD yaklaşımı ile 3 boyutlu bir sayısal model uygulanmaktadır. Bu modelde, bilinen bir hareket fonksiyonuna sahip bir piezoelektrik fan, ilk olarak yatay fan düzenlemesi ile hava akışı oluşturmak üzere zaman etki alanında benzeşim yapılmıştır. Oluşan hava akışı piezoelektrik fanın belirli bir mesafesine yerleştirilen bir fin bloğuna yönlendirilmiştir. Bir tasarım parametresi olarak, fin bloğundaki finlerin sayısı arttırılmıştır. Fin kanalı, eşlenik silindirik finlerin yan yana eklenmesiyle oluşturulmuştur. Eşlenik finlerin sayısı 1'den 10'a çıkarılarak 10 farklı fin bloğu konfigürasyonu elde edilmiştir. Bu çalışmada, uygulanan iki sınır şartı

bulunmaktadır. İlk sınır şartı olarak uygulanan toplam ısı miktarı sabit tutulmuştur. Her konfigürasyonda, sınır koşulu olarak fin blokun tabanına 0.8064 W ısı uygulanır. İkinci sınır şartında uygulanan ısı akısı sabit tutulmuştur. Her konfigürasyonda 50400 W/m^2 ısı akışı sınır koşulu olarak fin bloğun tabanına uygulanır. Fin bloklarının ortalama yüzey sıcaklığı, doğal ve zorlanmış konveksiyon arasındaki ortalama yüzey sıcaklıkları farkı, ısı transfer artış oranı ve fin blokların ortalama taban sıcaklığı karşılaştırılmıştır. Bu karşılaştırmanın nihai sonucu, her kriter için optimum fin sayısıdır. Isı transferi artış oranı değerlendirildiğinde toplam sabit ısı sınır koşulu için 2 finli konfigürasyon en iyi sonucu verirken; sabit ısı akısı sınır koşulunda 1 finli konfigürasyon en iyi sonucu vermektedir. Ayrıca dikey fan düzenlemesi kullanılmış ve dikey fan düzenlemesine ait sonuçlar belirtilen fin konfigürasyonu için yatay fan düzenlemesi ile karşılaştırılmıştır. Çalışılan fin geometrisi için, yatay fan yerleşiminin dikey fan yerleşimine göre tüm fin konfigürasyonları için daha iyi bir soğutma performansı sağladığı görülmüştür.

Anahtar Kelimeler: piezoelektrik malzeme, piezoelektrik fan, fin optimizasyonu,

ACKNOWLEDGEMENTS

I would like to express my deepest thanks to the supportive advisor Dr. Özgür Ekici, who helped in the initiation, orientation and completion of this thesis. The belief in me, in the toughest moments he gave greatest support to finish this study.

I would also like to thank Dr. Murat Köksal, Dr. Metin Yavuz, Dr. Bilsay Sümer and Dr. Okan Görtan, who are members of the jury committee that gives me directions and suggestions.

I would also like to thank Mr. Selçuk Öksüz, who I have exchanged ideas about the thesis topic, and who started this thesis idea.

I thank my mother, my father and my sister for their trust in me in my graduate studies for many years. I express my deepest gratitude to my wife and son for their dedication, patience and support.

TABLE OF CONTENTS

Page

ABSTRACT i
ÖZET iii
ACKNOWLEDGEMENTS v
TABLE OF CONTENTS vi
LIST OF FIGURES viii
LIST OF TABLES xiii
LIST OF ABBREVIATIONS xiv
NOMENCLATURE xv
CHAPTER 1 1
INTRODUCTION AND LITERATURE REVIEW 1
1.1 Introduction 1
1.2 Principles of a Piezoelectric Fan 1
1.3 Literature Review 4
1.4 Aim and Scope of the Thesis 7
CHAPTER 2 9
THEORY AND MODELING 9
2.1 Motion of the Piezoelectric Fan 9
2.2 Model and Domain of the Study 11
CHAPTER 3 19
VALIDATION OF THE MODEL AND MODEL PARAMETERS 19
3.1 Model of the Validation Study 19
3.2 Study of Validation 23
3.3 Results of Validation 25
CHAPTER 4 27
RESULTS AND DISCUSSION 27
4.1 Flow Field Analysis 29
4.2 Results for Constant Total Heat Boundary Condition with Horizontal Fan Arrangement 40
4.3 Results for Constant Heat Flux Boundary Condition with Horizontal Fan Arrangement 46

4.4 Results for Constant Total Heat Boundary Condition with Vertical Fan Arrangement 52
4.5 Results for Constant Heat Flux Boundary Condition with Vertical Fan Arrangement 58
CHAPTER 5 64
CONCLUSIONS AND FUTURE WORK 64
REFERENCES 67
APPENDIX A 70
Constant Total Heat - Temperature Distribution in Transient Solution - Horizontal Fan Arrangement 70
APPENDIX B 80
Constant Heat Flux - Temperature Distribution in Transient Solution – Horizontal Fan Arrangement 80
APPENDIX C 90
Constant Total Heat - Temperature Distribution in Transient Solution – Vertical Fan Arrangement 90
APPENDIX D 93
Constant Heat Flux - Temperature Distribution in Transient Solution – Vertical Fan Arrangement 93
APPENDIX E 96
UDF of Thesis Study 96
APPENDIX F 98
UDF of Validation Study 98

LIST OF FIGURES

Page

Figure 1.1 General view of a typical piezoelectric fan [6] 2
Figure 1.2 First three mode shapes of a piezoelectric fan [7] 3
Figure 2.1 General view of piezoelectric fan geometry [12] 9
Figure 2.2 Dimensionless positions of piezoelectric fan 11
Figure 2.3 CFD domain in side view (in mm) 13
Figure 2.4 CFD domain in top view (in mm) 14
Figure 2.5 Dimensions of the piezoelectric fan and 1-fin-block in side view (in mm) 14
Figure 2.6 Dimensions of the piezoelectric fan and 1-fin-block in top view (in mm) 15
Figure 2.7 10-fin-block geometry in front view (in mm) 15
Figure 2.8 10-fin-block geometry in top view (in mm) 16
Figure 2.9 Solution Steps of the Study 18
Figure 3.1 Geometry of the cylinder (in mm) [20] 20
Figure 3.2 Dimensionless positions of piezoelectric fan 21
Figure 3.3 Dimensions of CDF domain (in mm) [20] 21
Figure 3.4 General view of experimental setup [20] 22
Figure 3.5 General view of the CFD domain with δ=1.5 23
Figure 3.6 Variations of heat transfer augmentation ratio as function of dimensionless distance between piezoelectric fan tip and heated surface [20] 24
Figure 4.1 Horizontal fan arrangement with 10-fin-block configuration 27
Figure 4.2 Vertical fan arrangement with 10-fin-block configuration 28
Figure 4.3 Velocity distribution of the airflow for horizontal fan arrangement front view 30
Figure 4.4 Velocity distribution of the airflow for vertical fan arrangement front view 30
Figure 4.5 Velocity distribution of the airflow for horizontal fan arrangement top view 31
Figure 4.6 Velocity distribution of the airflow for vertical fan arrangement top view 31

Figure 4.7 Velocity vectors of the airflow for horizontal fan arrangement front view 32
Figure 4.8 Velocity vectors of the airflow for vertical fan arrangement front view . 33
Figure 4.9 Velocity vectors of the airflow for horizontal fan arrangement top view-1 34
Figure 4.10 Velocity vectors of the airflow for vertical fan arrangement top view-1 35
Figure 4.11 Velocity vectors of the airflow for horizontal fan arrangement top view-2 36
Figure 4.12 Velocity vectors of the airflow for vertical fan arrangement top view-2 37
Figure 4.13 Temperature distribution of the airflow for horizontal fan arrangement top view 38
Figure 4.14 Temperature distribution of the airflow for vertical fan arrangement top view 39
Figure 4.15 Temperature distribution of the airflow for horizontal fan arrangement front view 39
Figure 4.16 Temperature distribution of the airflow for vertical fan arrangement front view 40
Figure 4.17 Average surface temperature of 1-fin-block for constant total heat ... 42
Figure 4.18 Temperature distribution (in K) of 1-fin-block after natural convection (a) and piezoelectric fan cooling (b) 43
Figure 4.19 Average surface temperatures of fin blocks for constant total heat boundary condition for natural and forced convection cooling 44
Figure 4.20 Heat transfer augmentation ratio for constant total heat 44
Figure 4.21 Temperature difference between natural and forced convection for constant total heat 45
Figure 4.22 Base temperature of the fin blocks 46
Figure 4.23 Average surface temperature of 2-fin-block for constant heat flux 47
Figure 4.24 Temperature distribution (in K) of 2-fin-block after natural convection (a) and piezoelectric fan cooling (b) 48
Figure 4.25 Average surface temperatures of fin blocks for constant heat flux for natural and forced convection cooling 49
Figure 4.26 Heat transfer augmentation ratio for constant heat flux 50

Figure 4.27 Temperature difference between natural and forced convection for constant heat flux 51
Figure 4.28 Base temperature of the fin blocks 52
Figure 4.29 Average surface temperature of 2-fin-block for constant total heat ... 53
Figure 4.30 Temperature distribution (in K) of 2-fin-block after natural convection (a) and piezoelectric fan cooling (b) 54
Figure 4.31 Average surface temperatures of fin blocks for constant total heat ... 55
Figure 4.32 Heat transfer augmentation ratio for constant total heat..... 55
Figure 4.33 Temperature distribution (in K) of 10-fin-block for constant total heat boundary condition with (a) horizontal and (b) vertical fan arrangement 57
Figure 4.34 Average surface temperature of 2-fin-block for constant heat flux for horizontal and vertical fan arrangement 59
Figure 4.35 Temperature distribution (in K) of 2-fin-block after natural convection (a) and piezoelectric fan cooling (b) 60
Figure 4.36 Average surface temperatures of fin blocks for constant heat flux 61
Figure 4.37 Heat transfer augmentation ratio for constant heat flux..... 61
Figure 4.38 Temperature distribution (in K) of 10-fin-block for constant heat flux boundary condition with (a) horizontal and (b) vertical fan arrangement 62
Figure 5.1 Nested fin and piezoelectric fan arrangement example [4]..... 66
Figure 7.1 Average surface temperature of 1-fin-block 70
Figure 7.2 Temperature distribution (in K) of 1-fin-block 70
Figure 7.3 Average surface temperature of 2-fin-block 71
Figure 7.4 Temperature distribution (in K) of 2-fin-block 71
Figure 7.5 Average surface temperature of 3-fin-block 72
Figure 7.6 Temperature distribution (in K) of 3-fin-block 72
Figure 7.7 Average surface temperature of 4-fin-block 73
Figure 7.8 Temperature distribution (in K) of 4-fin-block 73
Figure 7.9 Average surface temperature of 5-fin-block 74
Figure 7.10 Temperature distribution (in K) of 5-fin-block 74
Figure 7.11 Average surface temperature of 6-fin-block 75
Figure 7.12 Temperature distribution (in K) of 6-fin-block 75
Figure 7.13 Average surface temperature of 7-fin-block 76
Figure 7.14 Temperature distribution (in K) of 7-fin-block 76
Figure 7.15 Average surface temperature of 8-fin-block 77

Figure 7.16 Temperature distribution (in K) of 8-fin-block 77
Figure 7.17 Average surface temperature of 9-fin-block 78
Figure 7.18 Temperature distribution (in K) of 9-fin-block 78
Figure 7.19 Average surface temperature of 10-fin-block 79
Figure 7.20 Temperature distribution (in K) of 10-fin-block 79
Figure 8.1 Average surface temperature of 1-fin-block 80
Figure 8.2 Temperature distribution (in K) of 1-fin-block 80
Figure 8.3 Average surface temperature of 2-fin-block 81
Figure 8.4 Temperature distribution (in K) of 2-fin-block 81
Figure 8.5 Average surface temperature of 3-fin-block 82
Figure 8.6 Temperature distribution (in K) of 3-fin-block 82
Figure 8.7 Average surface temperature of 4-fin-block 83
Figure 8.8 Temperature distribution (in K) of 4-fin-block 83
Figure 8.9 Average surface temperature of 5-fin-block 84
Figure 8.10 Temperature distribution (in K) of 5-fin-block 84
Figure 8.11 Average surface temperature of 6-fin-block 85
Figure 8.12 Temperature distribution (in K) of 6-fin-block 85
Figure 8.13 Average surface temperature of 7-fin-block 86
Figure 8.14 Temperature distribution (in K) of 7-fin-block 86
Figure 8.15 Average surface temperature of 8-fin-block 87
Figure 8.16 Temperature distribution (in K) of 8-fin-block 87
Figure 8.17 Average surface temperature of 9-fin-block 88
Figure 8.18 Temperature distribution (in K) of 9-fin-block 88
Figure 8.19 Average surface temperature of 10-fin-block 89
Figure 8.20 Temperature distribution (in K) of 10-fin-block 89
Figure 9.1 Average surface temperature of 2-fin-block 90
Figure 9.2 Temperature distribution (in K) of 2-fin-block 90
Figure 9.3 Average surface temperature of 5-fin-block 91
Figure 9.4 Temperature distribution (in K) of 5-fin-block 91
Figure 9.5 Average surface temperature of 10-fin-block 92
Figure 9.6 Temperature distribution (in K) of 5-fin-block 92
Figure 10.1 Average surface temperature of 2-fin-block 93
Figure 10.2 Temperature distribution (in K) of 2-fin-block 93
Figure 10.3 Average surface temperature of 5-fin-block 94

Figure 10.4 Temperature distribution (in K) of 5-fin-block 94
Figure 10.5 Average surface temperature of 10-fin-block 95
Figure 10.6 Temperature distribution (in K) of 10-fin-block 95

LIST OF TABLES

Page

Table 1-1 Tabulated literature summary 5
Table 2-1 Mesh dependency study results 17
Table 3-1 Average surface temperature for natural and forced convection 24
Table 3-2 Heat transfer augmentation ratio results 25
Table 3-3 Heat transfer augmentation ratio comparison 26
Table 4-1 Heat transfer augmentation ratio and the average surface temperatures of fin blocks for the constant total heat of 0.8064 W 43
Table 4-2 Heat transfer augmentation ratio and the average surface temperatures of fin blocks for constant heat flux of 50400 W/m2 49
Table 4-3 Average surface temperatures of fin blocks for constant total heat 54
Table 4-4 Heat transfer augmentation ratio comparison between horizontal and vertical fan arrangement 58
Table 4-5 Average surface temperatures of fin blocks for constant heat flux 60
Table 4-6 Heat transfer augmentation ratio comparison between horizontal and vertical fan arrangement 63

LIST OF ABBREVIATIONS

PDA	Personal Data Assistant
AC	Alternating Current
CFD	Computational Fluid Dynamics
3D	Three Dimensional
SIMPLE	Semi Implicit Method for Pressure Linked Equations
UDF	User Defined Function

NOMENCLATURE

c_p Specific heat capacity ($Jkg^{-1}K^{-1}$)

g Gravitational acceleration (m^2s^{-1})

k Thermal conductivity ($Wm^{-1}K^{-1}$)

p Pressure (Pa)

q_s Heat flux applied (W/m^2)

q_a Heat flux applied for model (W/m2)

T Temperature (K)

t Time (s)

f_r Frequency of AC Voltage (Hz)

$u_{i,j}$ Air velocity (ms^{-1})

ρ Density (kgm^{-3})

β Thermal expansion coefficient (K^{-1})

μ Dynamic viscosity (Nsm^{-2})

ξ Heat Transfer Augmentation Ratio

h_{pf} Heat Transfer Coefficient under Forced Convection ($Wm^{-1}K^{-1}$)

h_n Heat Transfer Coefficient under Natural Convection ($Wm^{-1}K^{-1}$)

κ Turbulent Kinetic Energy

ε Turbulent Dissipation

E_{ij} Component of Rate of Deformation

μ_t Eddy Viscosity

δ Dimensionless Distance between Fan Tip and Heated Surface (δ=d/w)

α Dimensionless Amplitude of Piezoelectric Fan (α=a/w)

w Width of Piezoelectric Fan (mm)

a Amplitude of Piezoelectric Fan (mm)

d Distance between Fan Tip and Heated Surface (mm)

Subscripts

a Ambient

n Natural Convection

pf Forced Convection

s Location on Fin Block

CHAPTER 1
INTRODUCTION AND LITERATURE REVIEW

1.1 Introduction

In recent years, with the extensive development of technology and the shrinking dimensions of electronic systems, the importance of heat transfer and cooling has increased in parallel to power consumption and thermal management requirements of these systems. So that, the limits of progress in electronics are to be determined by how much the thermal problem issues are solved. In this case, the current research in the area of electronics cooling seeks new ways to increase the heat transfer by various approaches such as incorporating multi-phase cooling, much stronger fans, magnetic cooling and utilizing the material technologies [1], [2].

Besides the advantages of existing conventional heat transfer methods, there are also disadvantages, some of which are high power consumption, larger volume, narrow operating temperature range, high noise and high failure rate. Therefore in mobile systems, computers and PDAs, piezoelectric fans have emerged as an alternative in recent years with advantages such as low volume requirement, low power consumption, silent operation and a long life expectancy [3]–[5].

1.2 Principles of a Piezoelectric Fan

Piezoelectric materials convert electrical energy into mechanical energy when AC voltage is applied and vice versa. The piezoelectric fan is generally formed by inserting a metal or non-metal patch to a piezoelectric patch. The parts forming a typical piezoelectric fan are given in Figure 1.1.

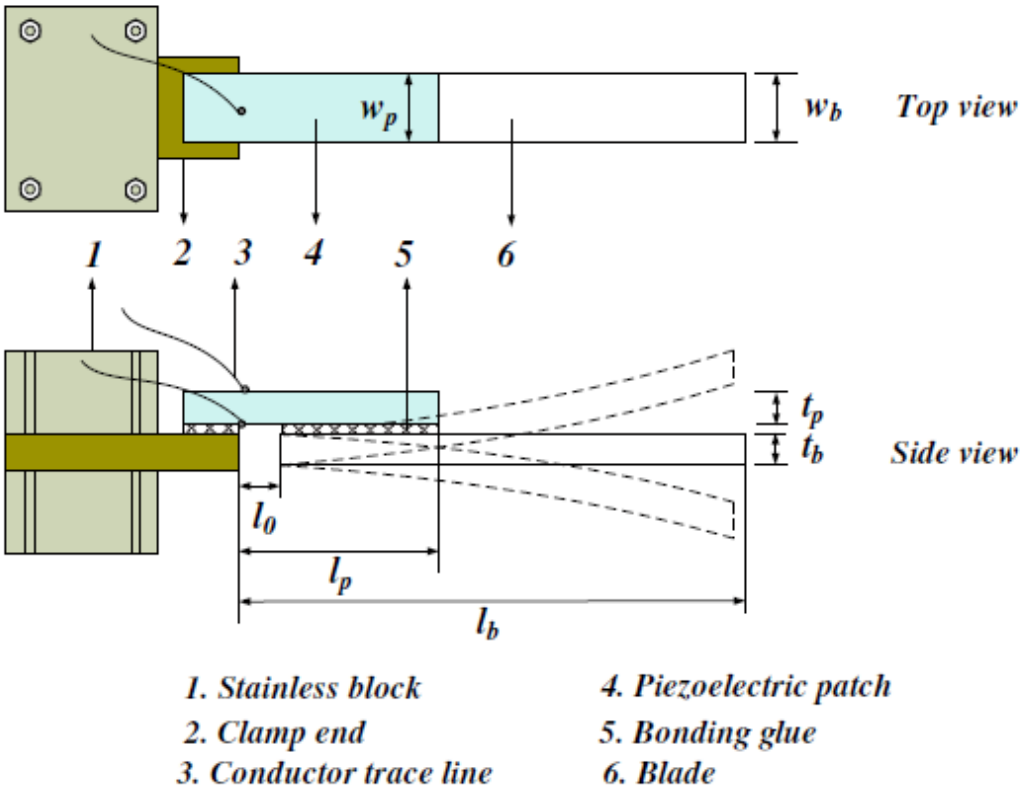

Figure 1.1 General view of a typical piezoelectric fan [6]

The first three mode shapes of a piezoelectric fan are shown in Figure 1.2. The largest amplitude is seen in the first mode, also known as the fundamental mode or frequency. In the case where the piezoelectric fan is supplied with AC voltage whose frequency is equal to the fundamental natural frequency, it oscillates in the mode shape corresponding to this natural frequency. The amplitude of the piezoelectric fan depends on the voltage of the AC power; the higher the applied voltage is, the larger the generated amplitude is.

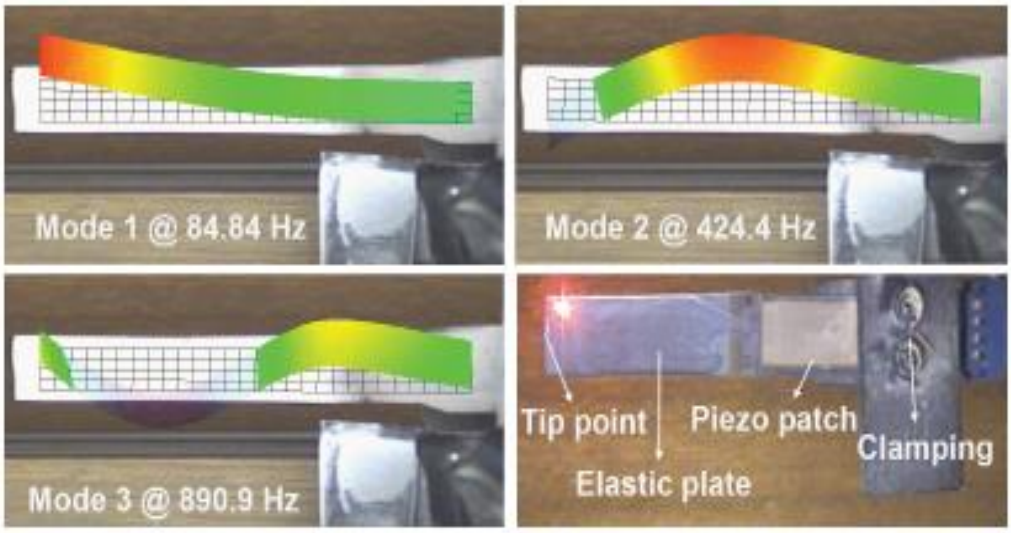

Figure 1.2 First three mode shapes of a piezoelectric fan [7]

There are three basic features about the piezoelectric fans.

Firstly, the important point here is to ensure that the frequency of the AC voltage to be supplied is equal to or very close to the fundamental natural frequency of the two-piece piezoelectric fan. In this case, the piezoelectric fan will resonate and the oscillation amplitude will increase. This is one of the basic features that distinguish a piezoelectric fan from conventional rotary fans. In his work, Kimber et al [8] has found that it is possible to generate more flow with much less power compared to rotary fans.

Secondly, since the relevant properties of the material used are not affected by the environmental conditions, piezoelectric fans can work under very wide environmental conditions. It can operate from -55°C to +125°C without loss of performance under relative humidity values up to 95%. Thus, cooling under extreme conditions is one of the most convenient features of piezoelectric fans which makes them suitable for demanding applications such as those existing in aerospace & military fields.

Thirdly, piezoelectric fans have a very long service life without any maintenance requirement. This is because materials requiring maintenance and limited-life such as rotors and bearings are not used. The resulting flow is created by using the property inherent in the natural structure of the material. The Piezoflo firm has

already stated that it will have a lifetime of more than 15 years, while still carrying out the tests [9].

1.3 Literature Review

The piezoelectric fan was first discovered and introduced in 1979 by Toda [10]. Then there was no new work in this area until the early 2000s. As a result of scientists' research into new methods to meet the increased cooling needs of electronic units, efforts have been made to work more seriously on piezoelectric fans.

A piezoelectric fan, as mentioned above offers various advantages compared to conventional fans. This first appeared in 1979 when Toda [10] and his team vibrated a piezo ceramic material easily when AC power was applied at its fundamental natural frequency. Also as the AC voltage was increased, piezoelectric fan amplitudes increased as well. By inducing a flow induced by vibrating on a piece of television receiver with a sample piezoelectric fan, they experienced an additional temperature drop of 17°C with an increase in heat transfer compared to natural convection only.

Açıkalın et al. [11] performed an experimental study in 2004 with horizontal and vertical orientations with full, half and no coverage locations for a given fin block. This experimental work is important because it is the first study to prove that a piezoelectric fan can be used as a commercial product. In this study, valuable information such as heat transfer augmentation ratio, fan curve and fan efficiency are generated. As a result, it is concluded that piezoelectric fans are more suitable to be used with conventional rotary fans for larger devices such as laptop and computers, and suitable for stand-alone use for smaller devices.

In another work of Açıkalın et al. [3] five parameters related to piezoelectric fan and heat source interaction were investigated experimentally. These parameters are; voltage and frequency of AC power, length of piezoelectric fan, horizontal and vertical distances to the heat source from the piezoelectric fan tip. The temperature of the heat source is plotted according to the specified parameters. In the same study, a CFD solution model was also implemented. A 2-D CFD solution were created because the preferred 3-D solution requires computational time on the order of years to complete. However, this model did not reflect reality well, 2-D

CFD simulation could not predict results accurate enough for the complete domain.

In earlier literature, piezoelectric fan studies started with establishing experimental setup to find out fan characteristics, then cooling performance studies were conducted. With the development of computing power, 2D and 3D CFD solutions have been introduced. In this thesis, 3D CFD solution will be implemented.

The studies were conducted recently can be summarized under 5 different categories. These 5 different categories are described according to:

- different methods: experimental or CFD simulation,
- different number of piezoelectric fans: 1, 2 or multiple with magnetic effect,
- different piezoelectric fan arrangements: vertical or horizontal,
- different fin configurations: plate, channel, cylinder fin or square fin,
- different purposes: optimization, piezoelectric fan performance measurement or comparison.

The tabulated literature survey for 5 different categories is given in Table 1-1.

Table 1-1 Tabulated literature summary

Author of the Study	Year	Method	Number of Piezoelectric fan	Piezoelectric Fan Arrangement	Fin	Purpose
C.H. Huang et al [12]	2012	Experimental + CFD Simulation	1	Horizontal	Plate	Optimization
C.N. Lin [13]	2012	Experimental + CFD Simulation	1	Vertical	Plate	Optimization
T. Açıkalın et al [3]	2007	Experimental + CFD Simulation	1	Vertical	Plate	Optimization
P. Bürmann et al [14]	2003	CFD Simulation	1	Horizontal	Not Applicable	Piezofan Performance Measurement
S.F. Sufian et al [15]	2013	Experimental + CFD Simulation	1	Vertical	Channel	Optimization
S.F Sufian et al [16]	2013	CFD Simulation	2	Vertical	Plate	Comparison
M. Choi et al [17]	2014	CFD Simulation	2	Vertical	Not Applicable	Piezofan Performance Measurement
T. Açıkalın et al [11]	2004	Experimental	1	Horizontal+Vertical	Plate	Comparison
M. Kimber et al [18]	2009	Experimental	2	Horizontal+Vertical	Not Applicable	Piezofan Performance Measurement

S.F. Liu et al [6]	2009	Experimental	1	Horizontal+Vertical	Plate	Piezofan Performance Measurement
H.Y. Li et al [19]	2016	Experimental	2	Vertical	Fin (Square)	Piezofan Performance Measurement
C.N. Lin et al [20]	2013	CFD Simulation	1	Vertical	Fin (Cylinder)	Comparison
H.K. Ma et al [21]	2014	Experimental	Magnetic Fan Arrays	Vertical	Channel	Piezofan Performance Measurement
H.C. Su et al [22]	2013	Experimental + CFD Simulation	Magnetic Fan Arrays	Vertical	Channel	Piezofan Performance Measurement
H.K. Ma et al [5]	2012	Experimental + CFD Simulation	1	Vertical	Channel	Optimization
M. Kimber et al [23]	2009	Experimental	1	Horizontal	Plate	Optimization
M.K. Abdullah et al [24]	2009	Experimental + CFD Simulation	1	Horizontal	Plate	Optimization
M. Choi et al [25]	2012	CFD Simulation	2	Vertical	Not Applicable	Piezofan Performance Measurement
J. Petroski et al [4]	2010	Experimental + CFD Simulation	2	Vertical	Channel	Optimization
H.K. Ma et al [26]	2014	Experimental	Magnetic Fan Arrays	Vertical	Plate	Optimization
M.K. Abdullah [27]	2012	Experimental + CFD Simulation	Multiple	Horizontal+Vertical	Channel	Optimization
M. Kimber et al [8]	2009	Experimental	1	Horizontal	Not Applicable	Piezofan Performance Measurement
M. Kimber et al [28]	2008	Experimental	1	Horizontal	Not Applicable	Piezofan Performance Measurement
C.N. Lin et al [29]	2014	CFD Simulation	2	Horizontal+Vertical	Fin (Cylinder)	Comparison
S.F Sufian [30]	2014	Experimental + CFD Simulation	2	Vertical	Plate	Comparison
H.Y. Li et al [31]	2013	Experimental	1	Horizontal+Vertical	Fin (Square)	Optimization
M. Toda et al [10]	1979	Experimental	1	Horizontal	Plate	Piezofan Performance Measurement

As a result of the literature survey, the following deductions have been made:

• A flow is generated when the piezoelectric material structure vibrates at its resonance frequency.

• Convective heat transfer is increased when this flow is directed to a heated material.

• Orientation, coverage and distance of fan tip and fin block relative to each other are important factors that affect the fan performance.

• CFD simulations show results close to experimental results.

• Piezoelectric fans are more energy efficient than conventional rotor fans.

• By placing magnets at the tip of the fans, one active fan and two passive fans can be used to increase energy efficiency.

Referring to the previous studies and the categories presented in Table 1-1, this study will employ;

- 3-D CFD simulation as a method,
- 1 piezoelectric fan as a flow source,
- Horizontal piezoelectric fan arrangement with vertical piezoelectric fan arrangement comparison,
- Cylinder fin blocks as a fin configuration,
- Fin optimization as a purpose.

1.4 Aim and Scope of the Thesis

Recent years, since piezoelectric fans have been recognized as a remarkable technology that can be utilized in heat transfer problems, a significant number of studies have been performed on piezoelectric fan applications. After these studies were introduced, different parameters were used to study the usage areas of the piezoelectric fan. Nevertheless, these conducted studies mainly focused on the cooling of a single cylinder or square cross section or a duct cooling. To the best of author's knowledge, there is no literature investigating the domain of influence of the piezoelectric fan by changing the target width. In the conducted studies, the fin arrangement within a constant cross-sectional envelope or the height of fin block are the only geometric parameters changed. In this study, the number of fins is increased to examine the effects of increasing target width on the cooling performance. In this way, the largest fin block is formed up to 3 times wider than the width of the piezoelectric fan.

The aims of this thesis are;

- To establish a validated model by referring to a similar piezoelectric fan study from the literature

- To investigate the optimum number of fins in a row so that the piezoelectric fan provides an efficient cooling
- To investigate the maximum average surface temperature difference between natural and forced convection cooling configurations
- To investigate the minimum average base temperature of the fin block
- To compare and reveal the cooling performance of vertically and horizontally oriented piezoelectric fan arrangement for a specified fin block geometry

CHAPTER 2
THEORY AND MODELING

In this thesis, a 3D CFD model of the flow generated and directed onto a fin block using a commercial piezoelectric fan is developed. The design parameter is specified as the number of fins in the fin block. The structure consists of identical fins lined up side by side. The number of these fins is increased and an attempt to find an optimum number of fins by focusing on different interpretations of obtained results will be made. The validation of the model is done by comparing the results of the current study against the results obtained using a similar model of Lin's [20] work.

2.1 Motion of the Piezoelectric Fan

A commercial piezoelectric fan is used in this study [9]. The general view of the piezoelectric fan used in this study is given in Figure 2.1.

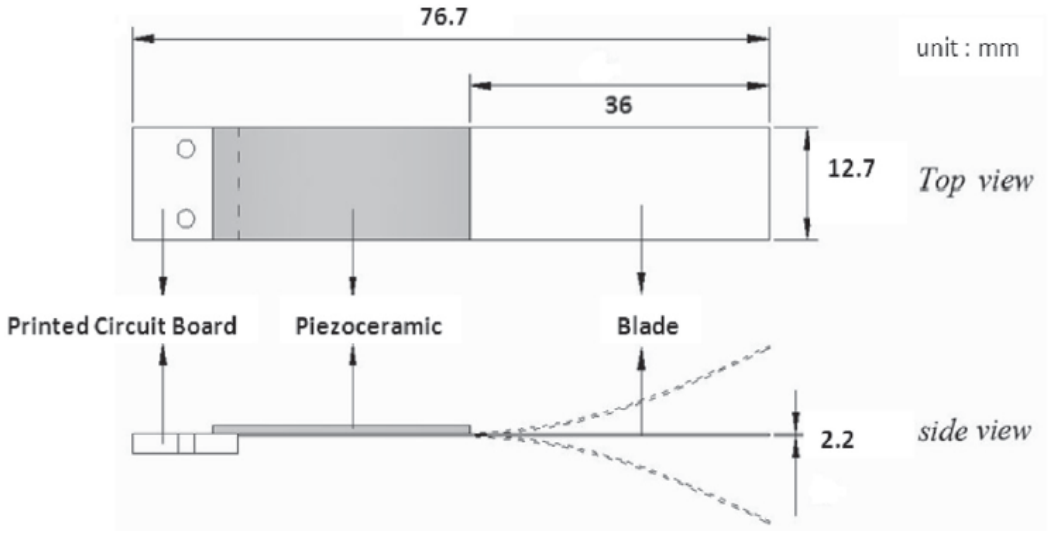

Figure 2.1 General view of piezoelectric fan geometry [12]

The total length of the piezoelectric fan given in Figure 2.1 is 76.7 mm. The moving part of the piezoelectric fan is 64 mm which includes both ceramic and piezoelectric materials. The 28 mm from the left of the 64 mm length of the oscillating part is a piezoelectric material. The last 36 mm of the 64 mm length of the oscillating part is Mylar material. In the CFD model, the 12.7 mm section used

for fixing the piezoelectric fan is not included and only the oscillating part (piezoelectric and non-piezoelectric part) is modeled.

The oscillation of piezoelectric fans is in the form of a sinus curve due to the shape of the AC voltage. In addition, the fan motion curve changes depending on the choice of material, dimensions, AC frequency and the applied voltage. For a given piezoelectric fan in which the piezoelectric material is PZT, the motion of the piezoelectric fan curve at a given frequency and voltage can be tracked and generated by the measurements with a laser displacement sensor. In this thesis, the motion of a specific Mylar piezoelectric fan is modeled as the transverse displacement of slender beam [3], [32], [33].

The seventh-degree polynomial, which simulates the motion of a piezoelectric fan, is given Eq. (1):

$$z(y)=-42.34\times y^2+33587\times y^3-2.732\times 10^6\times y^3+9.053\times 10^7\times y^4 \\ -1.265\times 10^9\times y^6+6.34496\times 10^9\times y^7, 0<y<64\text{mm} \quad (1)$$

where z(y) is the dimensionless amplitude of the piezoelectric fan and y is the length of the piezoelectric fan. Dimensionless fan amplitude is calculated as the piezoelectric fan tip amplitude divided by the length of the piezoelectric fan.

The sinus function of the AC voltage is given below:

$$\sin(2\pi \times f_r \times t) \quad (2)$$

where f_r is the frequency of the AC power and t is the time. Multiplication of Eq. (1) and Eq. (2) gives the motion of the piezoelectric fan with respect to time.

In the works carried out within the scope of the thesis, the commercial piezoelectric fan was operated at 100 Hz which is very close to its fundamental natural frequency. The amplitude of the piezoelectric fan is 25.4 mm and the length of the piezoelectric fan is 64 mm. According to the frequency and amplitude of the AC voltage supplied, the main modes of the fan movement are shown in Figure 2.2. This figure represents the piezoelectric fan movement normalized with the amplitude of fan displacement by the variable phase angle (Theta, θ) values. This normalized height is defined as dimensionless height and calculated as the

height of the piezoelectric fan divided by the length of piezoelectric fan. Phase angles simulate alternating phase angles of applied AC voltage.

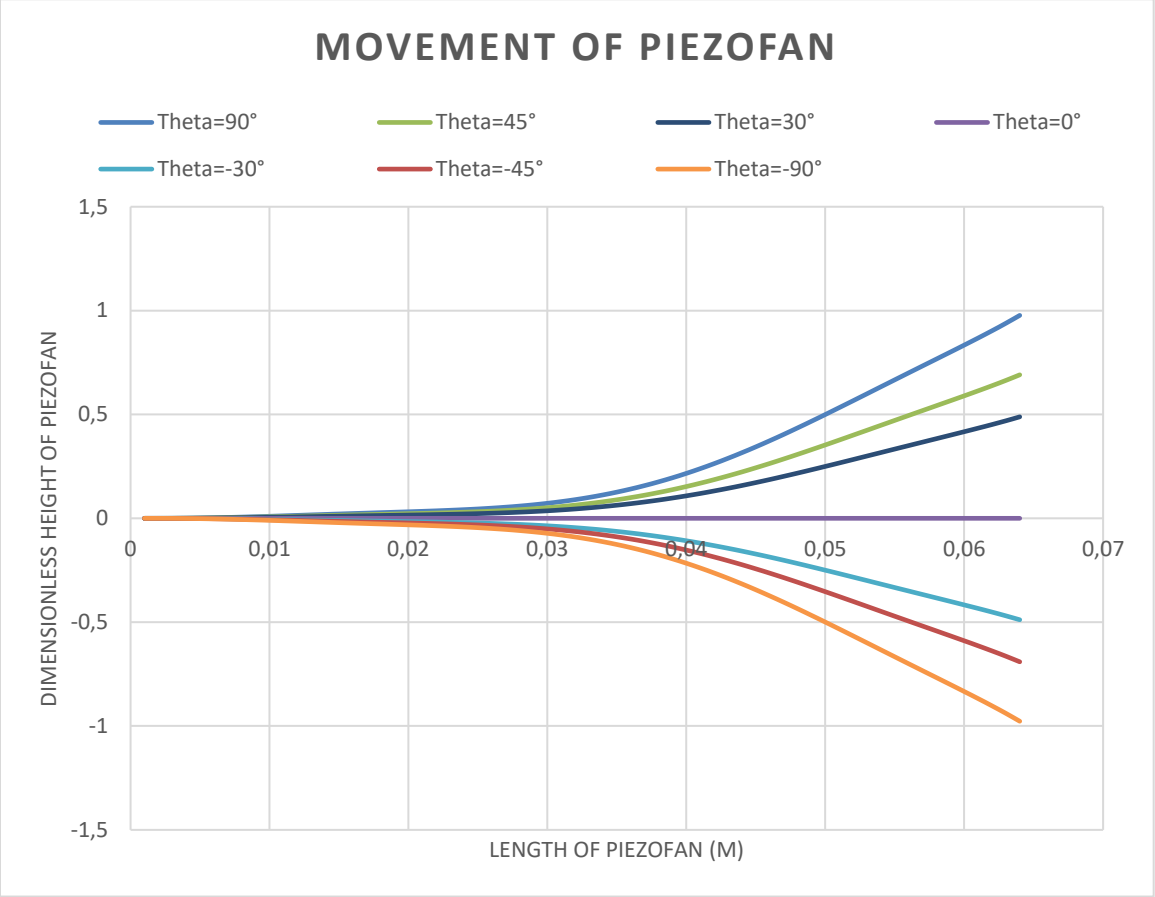

Figure 2.2 Dimensionless positions of piezoelectric fan

2.2 Model and Domain of the Study

The Reynold number is calculated as about 200 with the following parameters: hydraulic diameter is 2 mm, mean velocity is 2 m/s, kinematic viscosity is 2.056×10^{-5} m^2/s. Regardless of the calculated value, as has been discussed in in the explained in Bejan [34], the Re numbers at which the transition from the laminar to turbulent could occur at small number on the order 10^2. In addition, the piezoelectric fan creates vortices while vibrating. Thus a turbulence modeling is preferred and the standard κ-ε turbulence model is used in this study to solve the governing equations.

Continuity, momentum and energy equations used in the mathematical model for thermal and flow fields modeling in transient form are given in Eq. (3). This set of equations in Eq. (3) is used to obtain the transient solution when the piezoelectric

fan is on. For natural convection comparisons steady state solutions are obtained taking the time dependent terms zero.

$$\frac{\partial \rho}{\partial \tau} + \frac{\partial}{\partial x_i}(\rho u_i) = 0$$
$$\frac{\partial}{\partial \tau}(\rho u_i) + \frac{\partial}{\partial x_j}(\rho u_i u_j) = -\frac{\partial p}{\partial x_i} + \mu \frac{\partial^2 u_i}{\partial x_j^2} + \rho g \qquad (3)$$
$$\frac{\partial}{\partial \tau}(\rho c_p T) + \frac{\partial}{\partial x_j}(\rho u_i c_p T) = k \frac{\partial^2 T}{\partial x_j^2}$$

Transport equations for standard κ-ε model are given in Eq. (4). For turbulent kinetic energy, κ is;

$$\frac{\partial}{\partial t}(\rho\kappa) + \frac{\partial}{\partial x_i}(\rho\kappa u_i) = \frac{\partial}{\partial x_j}\left[\frac{\mu_t}{\sigma_\kappa}\frac{\partial \kappa}{\partial x_j}\right] + 2\mu_t E_{ij} E_{ij} - \rho\varepsilon \qquad (4)$$

Where, σ_κ=1.00.

For dissipation ε is;

$$\frac{\partial}{\partial t}(\rho\varepsilon) + \frac{\partial}{\partial x_i}(\rho\varepsilon u_i) = \frac{\partial}{\partial x_j}\left[\frac{\mu_t}{\sigma_\varepsilon}\frac{\partial \varepsilon}{\partial x_j}\right] + C_{1\varepsilon}\frac{\varepsilon}{\kappa} 2\mu_t E_{ij} E_{ij} - C_{2\varepsilon}\rho\frac{\varepsilon^2}{\kappa} \qquad (5)$$

Where, σ_ε=1.30; $C_{1\varepsilon}$=1.44; $C_{2\varepsilon}$=1.92.

$$\mu_t = \rho C_\mu \frac{\kappa^2}{\varepsilon} \qquad (6)$$

Where, C_μ=0.09.

The buoyancy forces in the air due to temperature differences in the domain is modeled by employing Boussinesq approximation with an ideal gas assumption $\beta = 1/T_0$. The equation is given in Eq. (7):

$$\rho = \rho_0 - \rho_0 \beta (T - T_0) \qquad (7)$$

Figure 2.3 and Figure 2.4 show the dimensions of the piezoelectric fan, fin block and the CFD domain. Accordingly, the domain of the flow is 200 X 200 X 130 (Height x Width x Length) mm. This domain consists of two parts. The first part is 200 x 200 x 70 mm and consists of the dynamic mesh in which the piezoelectric

fan is located and the model moves with respect to time. The second part is 200 x 200 x 60 mm. This part is the fixed part where the fin block is located and the mesh does not change over time. These two domains are interconnected by the interface. The gap between piezoelectric fan tip and fin is also 12.7 mm as the piezoelectric fan width, shown in Figure 2.5 and Figure 2.6. As a boundary conditions, the inlet is defined as pressure inlet; outlet is defined as pressure outlet and the ambient temperature is 300 K. Side walls are treated as pressure boundaries, permitting the airflow inward or outward with ambient temperature of 300 K.

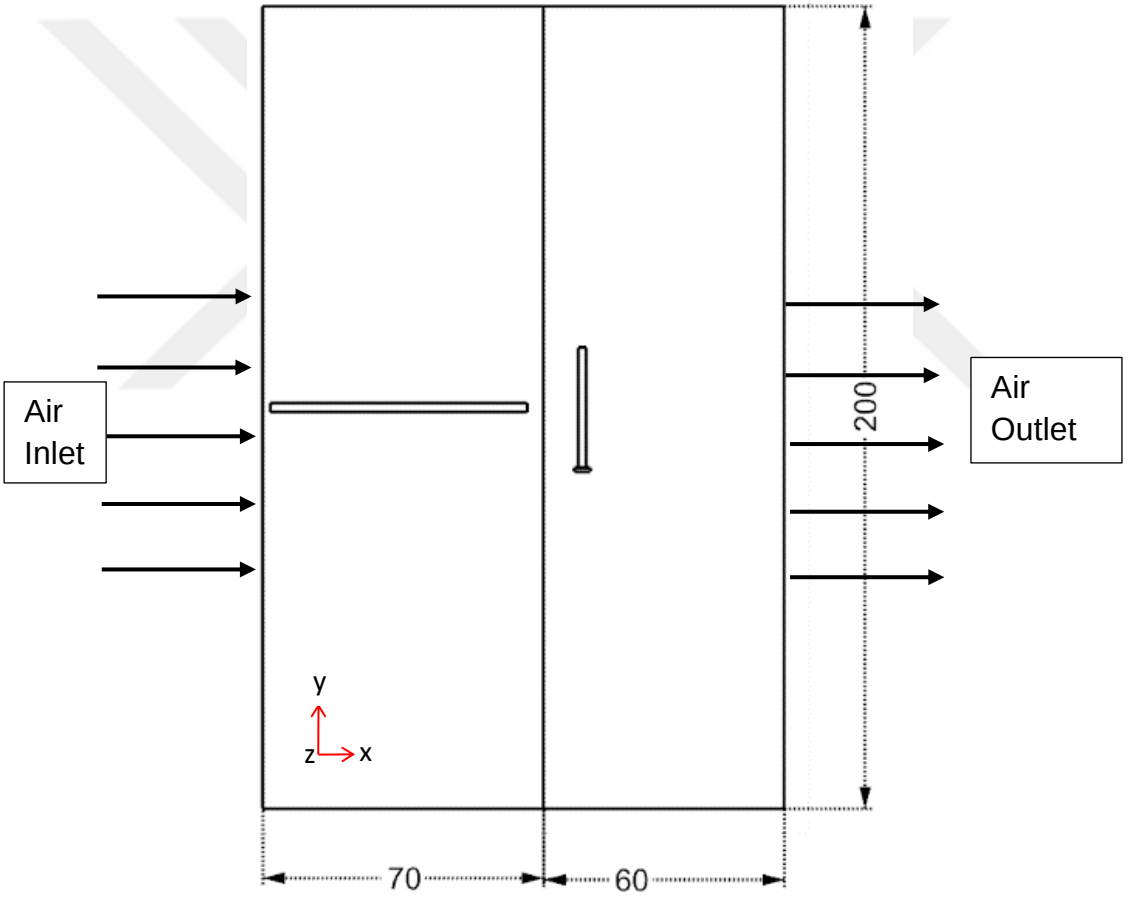

Figure 2.3 CFD domain in side view (in mm)

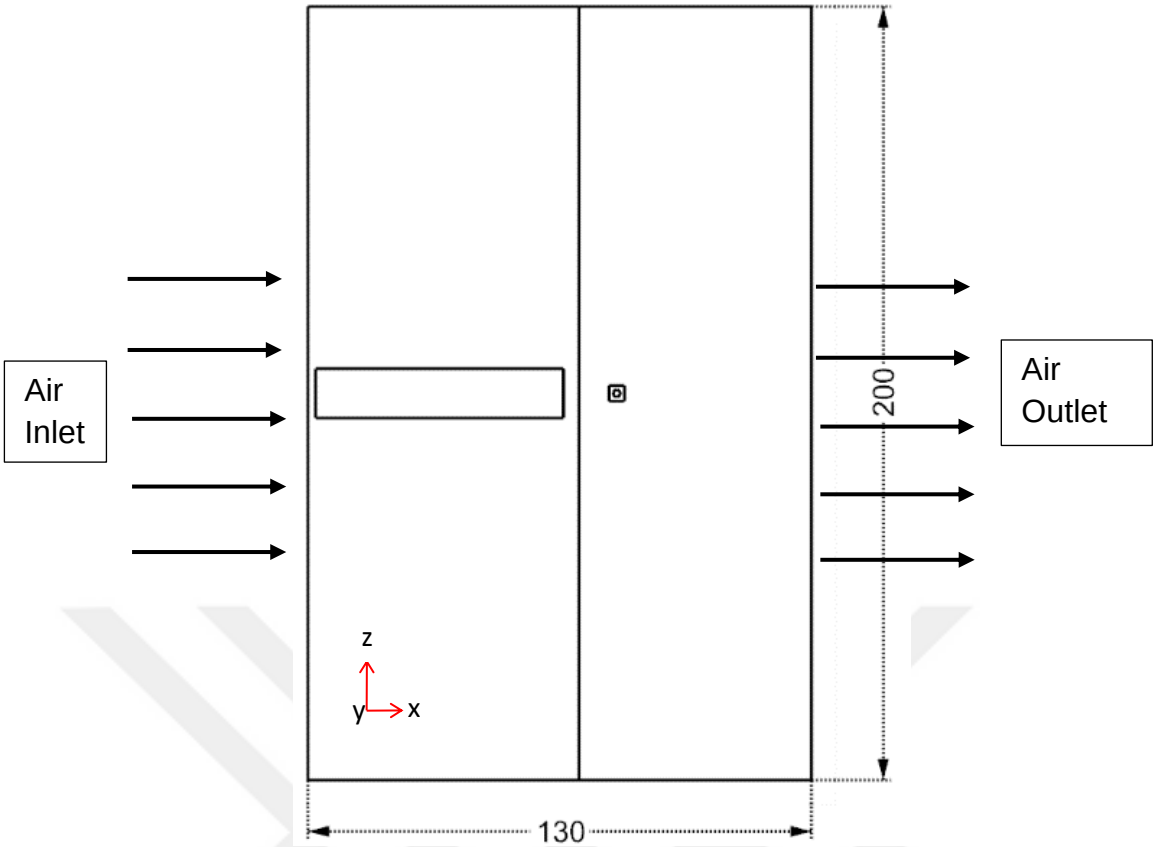

Figure 2.4 CFD domain in top view (in mm)

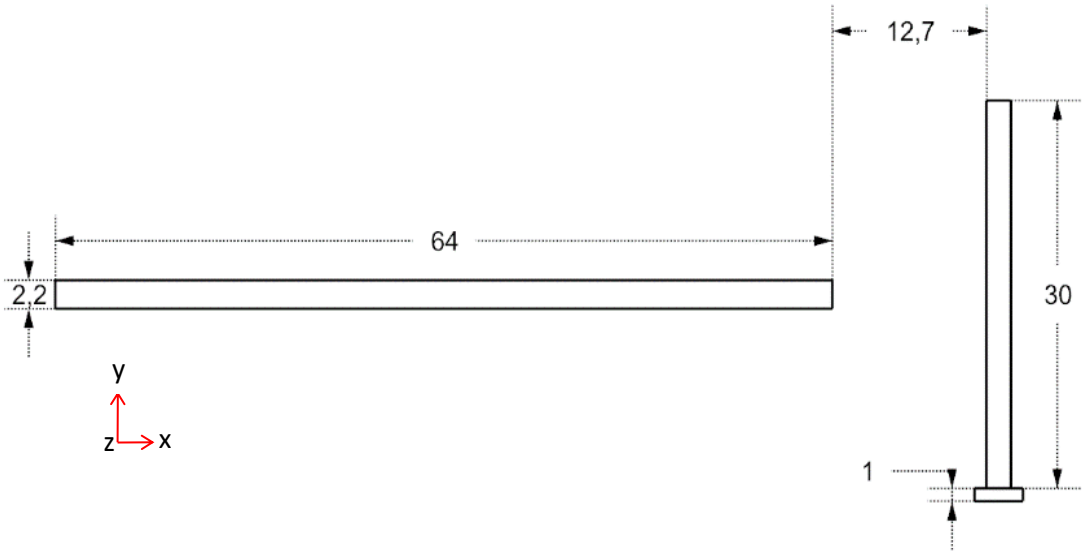

Figure 2.5 Dimensions of the piezoelectric fan and 1-fin-block in side view (in mm)

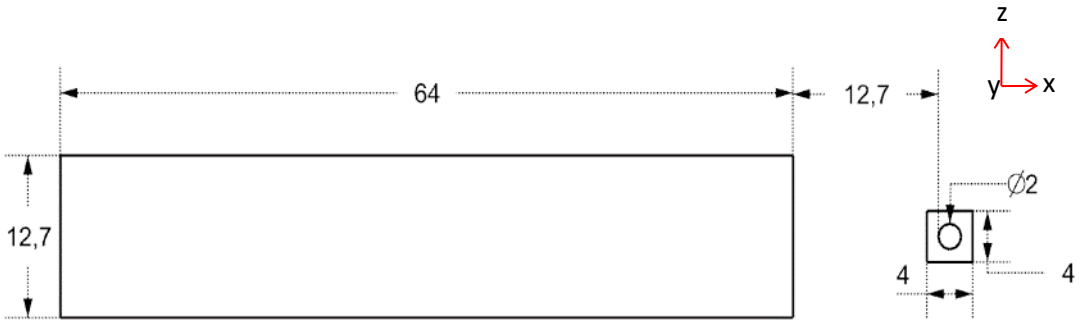

Figure 2.6 Dimensions of the piezoelectric fan and 1-fin-block in top view (in mm)

For the aluminum fin block used, a fin with a height of 30 mm and a diameter of 2 mm was used on a 4 × 4 mm^2 base with a height of 1 mm as shown in Figure 2.5 and Figure 2.6. The same fin is used when it is desired to increase the number of conjugate fins mounted side by side in the fin block. The dimensions for the 10-fin configuration is given in Figure 2.7 and Figure 2.8. The units are mm.

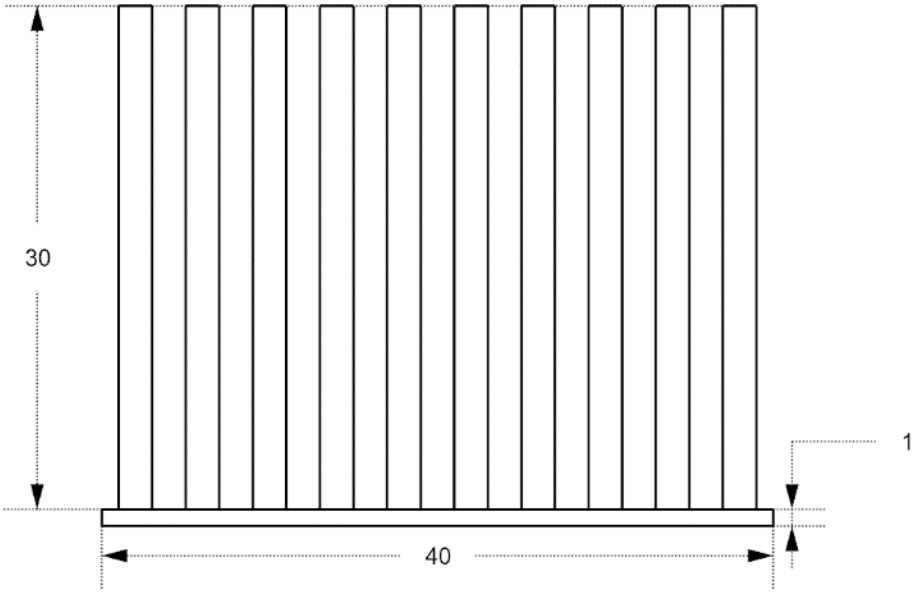

Figure 2.7 10-fin-block geometry in front view (in mm)

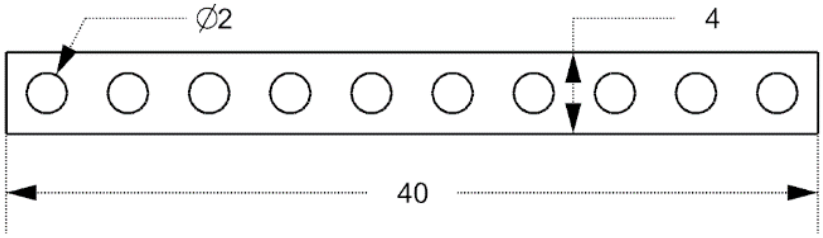

Figure 2.8 10-fin-block geometry in top view (in mm)

The CFD model is implemented using a commercial package, Ansys Fluent 17.2 solver, after the 3D CAD model was created. The movement of the fan is coded with a user defined function (UDF) which is given in Appendix E. In this CFD method, the pressure and velocity coupling equations are solved using the SIMPLE scheme, in which the convective terms are discretized with an upwind scheme. The k-ε model is used for turbulence transport. The motion is oscillating at a frequency of 100 Hz, almost coinciding with the fundamental natural frequency of the fan. Each period of piezoelectric fan is divided into 200 parts and $5x10^{-5}$ s time step is used. With this time step, the dynamic mesh is defined as the skewness is not allowed to be above 0.85. So the CFD package remeshes the volume mesh for each time step using this criterion. If the time step is used above $5x10^{-5}$ s, the solution fails before the pseudo steady-state solution is reached since the skewness of some elements exceeds the skewness criterion. The air is modeled using Boussinesq approximation in which the nominal density value was taken as 1.2 kg/m^3 and the β was set to 0.0033 1/K.

In this study, the simulation results were evaluated based on three different parameters, which are the heat transfer coefficient augmentation ratio (ξ), the base temperature of fin block and the average temperature difference between natural and forced convection. The formulation of the heat transfer augmentation ratio is given in Eq. (8):

$$\xi = \frac{h_{pf}}{h_n} = \frac{\dfrac{q_s}{T_{s,pf} - T_a}}{\dfrac{q_s}{T_{s,n} - T_a}} = \frac{T_{s,n} - T_a}{T_{s,pf} - T_a} \qquad (8)$$

In order to examine whether the solution in the study is mesh independent, mesh independency test is done as in the studies [20], [29]. Simulations were performed with different computational domains having 226823, 782642 and 2797777 cells in 1-fin-block configuration. The results are given in Table 2-1.

Table 2-1 Mesh dependency study results

	Case 1	Case 2	Case 3
Number of Cells in Domain	226823	782642	2797777
Average Surface Temperature after Natural Convection (K)	454.40	451.98	453.12
Variation from Case 1 (%)	NA	0.53%	0.28%
Variation from Case 2 (%)	0.53%	NA	0.25%
Average Surface Temperature after Forced Convection (K)	344.46	339.56	339.67
Variation from Case 1 (%)	NA	1.42%	1.39%
Variation from Case 2 (%)	1.42%	NA	0.03%

The steady state solution under natural convection resulted in average fin surface temperature of 454.40 K, 451.98 K and 453.12 K, for three different mesh configurations tested. After the piezoelectric fan vibrates, those temperature values dropped to 344.46 K, 339.56 K and 339.67 K, at the time when the pseudo-steady state is reached. The maximum variation in average surface temperatures is about 1.42% for Case 1 and Case 2. The maximum variation in average surface temperatures is below 0.25% for Case 2 and Case 3. For this reason, a mesh of 782642 cells was used. The same mesh properties are employed for the other fin configurations.

As a solution procedure the following steps are performed: Under natural convection, first, the steady state solution is achieved with the given boundary conditions. Then, the transient solution is activated using the steady state solution results as initial conditions. Under the transient forced convection conditions provided by a piezoelectric fan, pseudo-steady state is reached. This means heat transfer augmentation ratio and average surface temperature differences between

forced and natural convection could be calculated as well as average base temperature values. Solution steps performed in this study is summarized in Figure 2.9.

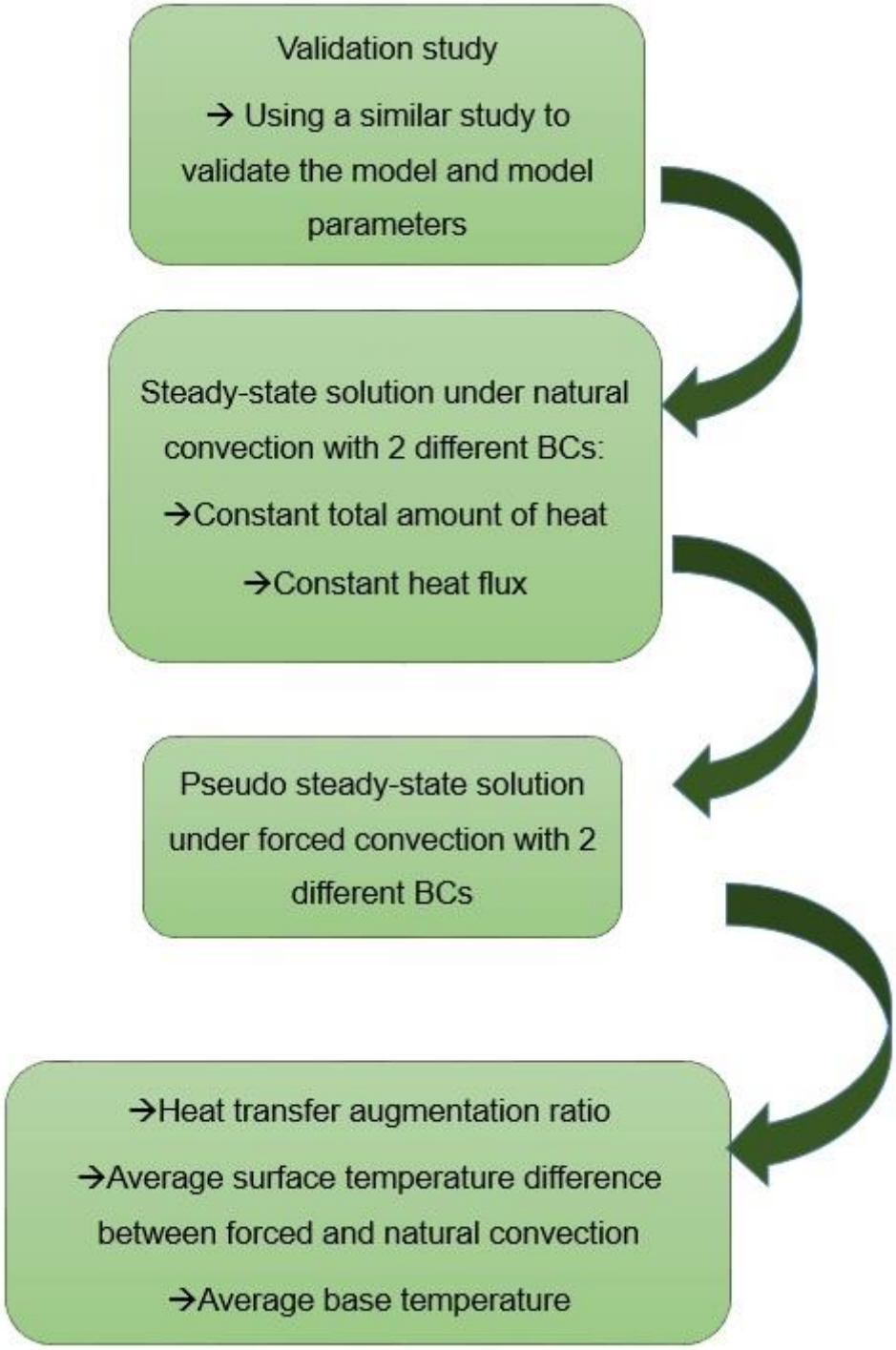

Figure 2.9 Solution Steps of the Study

CHAPTER 3
VALIDATION OF THE MODEL AND MODEL PARAMETERS

In order to validate the computational model before proceeding to fin optimization cases the work of Lin [20] presented in 2013 will be used.

The reasons for using this study are listed below:

1. Experimental and 3D CFD solutions worked together and the results were compared.
2. Piezoelectric fan width and piezoelectric fan amplitude used in the study are the same as the piezoelectric fan model used in the thesis.
3. The heat flux applied on a cylinder which is similar to fins used in the current study was tried to be cooled.
4. The surface to be cooled is at a similar distance with the current study.

For these reasons, the model in Lin's [20] work is created to check whether comparable results are achieved as has been detailed in the following sections. Thus, a model validated by the test results will be used in the validation study to model the motion of another piezoelectric fan.

3.1 Model of the Validation Study

In Lin's study [20] , a cylinder having a height of 50.8 mm, a diameter of 22.2 mm and a thickness of 0.5 mm is used, the dimensions of which are given in Figure 3.1. In the experimental study, heaters were placed on the inner surface of the cylinder and an average heat flux of 1000 W/m^2 was applied. This heat flux corresponds to a total heat load of 3.52 W.

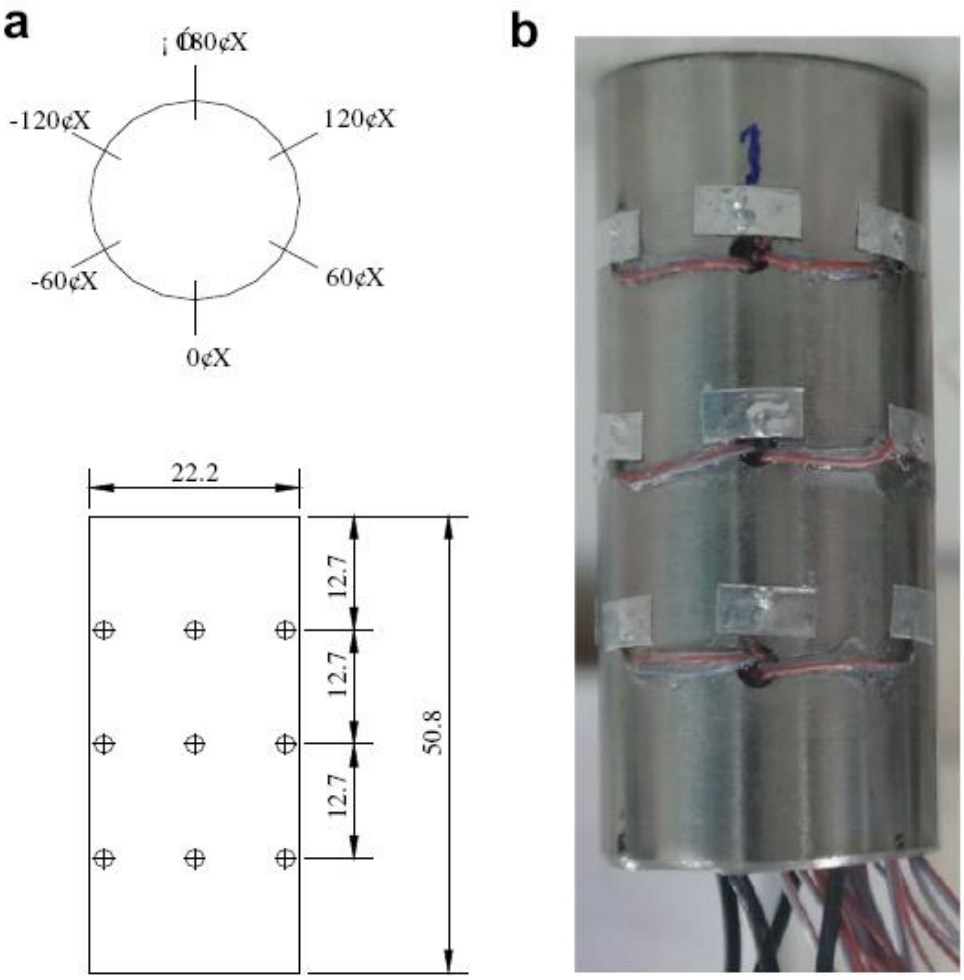

Figure 3.1 Geometry of the cylinder (in mm) [20]

The geometry of the piezoelectric fan used is defined by the dimensions of 75 x 12.7 x 0.5 mm. The measured natural frequency of this particular fan is 35.714 Hz. The function of the movement of the piezoelectric fan is given in Eq. (9):

$$y_1(x) = a(c_0 + c_1x + c_2x^2 + c_3x^3); 0 \le x \le L_1$$
$$y_2(x) = a(c_4 + c_5x + c_6x^2 + c_7x^3 + c_8x^4); L_1 \le x \le L_2 \quad (9)$$

where,

$L_1 = 29$ mm, $L_2 = 75$ mm,
$c_0 = -8.772 \times 10^{-5}$, $c_1 = 1.819 \times 10^{-4}\,mm^{-1}$,
$c_2 = 7.000 \times 10^{-4}\,mm^{-2}$, $c_3 = -4.763 \times 10^{-6}\,mm^{-3}$,
$c_4 = 1.159$, $c_5 = -9.419 \times 10^{-2}\,mm^{-1}$,
$c_6 = 3.567 \times 10^{-3}\,mm^{-2}$, $c_7 = -2.488 \times 10^{-5}\,mm^{-3}$,
$c_8 = 9.372 \times 10^{-8}\,mm^{-4}$, $a = 25.4$

Figure 3.2 simulates the piezoelectric fan positions normalized to the fan's amplitude value according to the phase angle values of the AC power source:

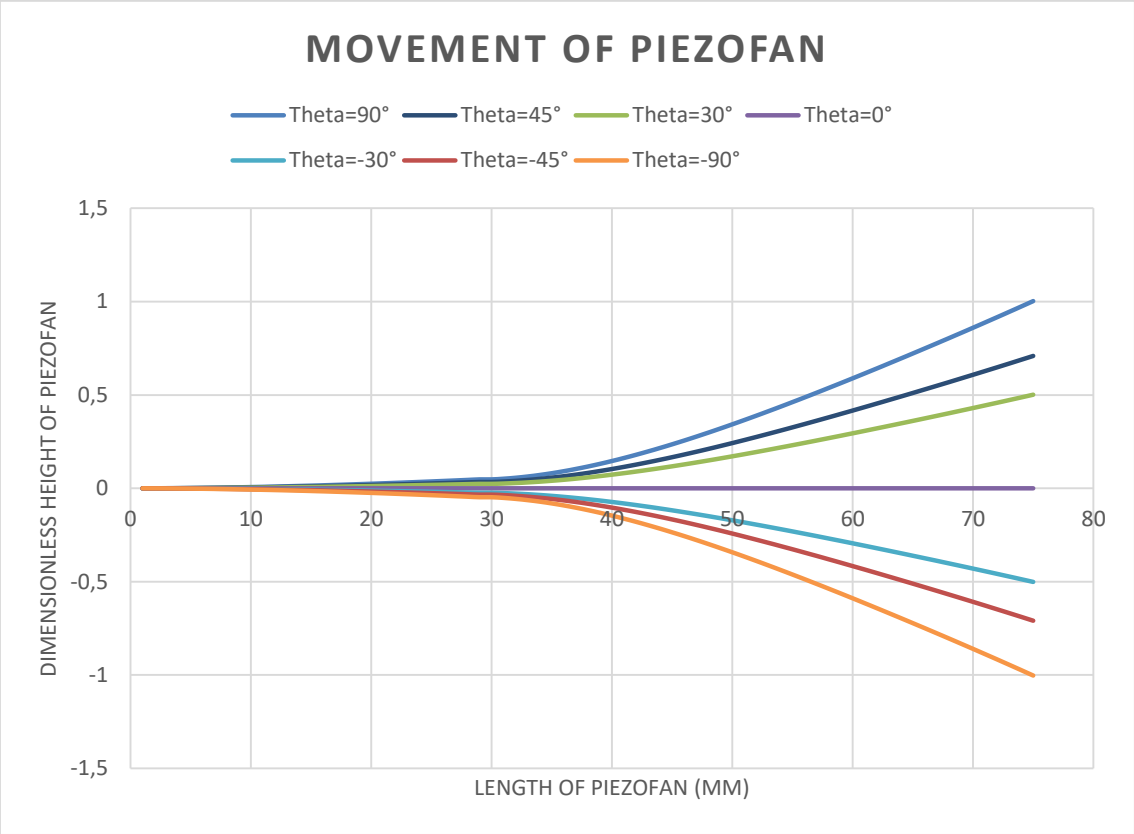

Figure 3.2 Dimensionless positions of piezoelectric fan

As shown in Figure 3.3, the heated cylinder is positioned at a certain distance to the piezoelectric fan and then cooled by piezoelectric fan vibration.

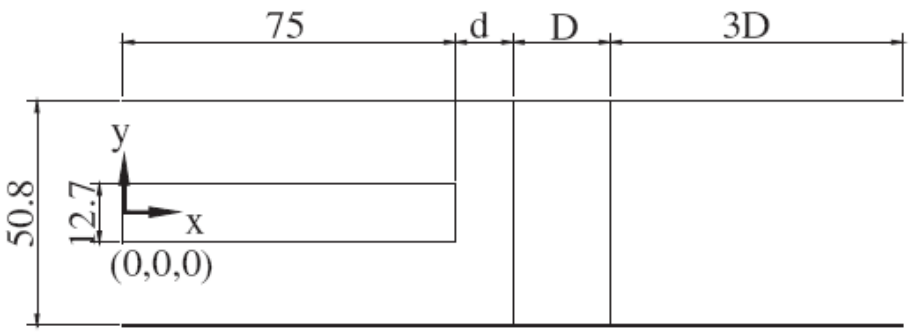

Figure 3.3 Dimensions of CDF domain (in mm) [20]

The flow domain is selected as 600 x 400 x 170 (Height x Width x Length) mm which is compatible with the reference work [20]. The left 600 x 400 x 90 mm part of this domain consists of the dynamic mesh in which the piezoelectric fan is located. The rest of the domain is fixed, includes the cylinder and the mesh does not change over time. These two domains are interconnected by an interface. The inlet is defined as pressure inlet; outlet is defined as pressure outlet and the ambient temperature is 295 K. Side walls are treated as pressure boundaries, permitting the airflow inward or outward with ambient temperature of 295 K.

By changing the distance between the cylinder and piezoelectric fan and the amplitude of the piezoelectric fan different cooling quantities are obtained. The governing equations used are discussed in Section 2.2.

An image and a schematic of the experimental setup of Lin's work [20] are shown in Figure 3.4.

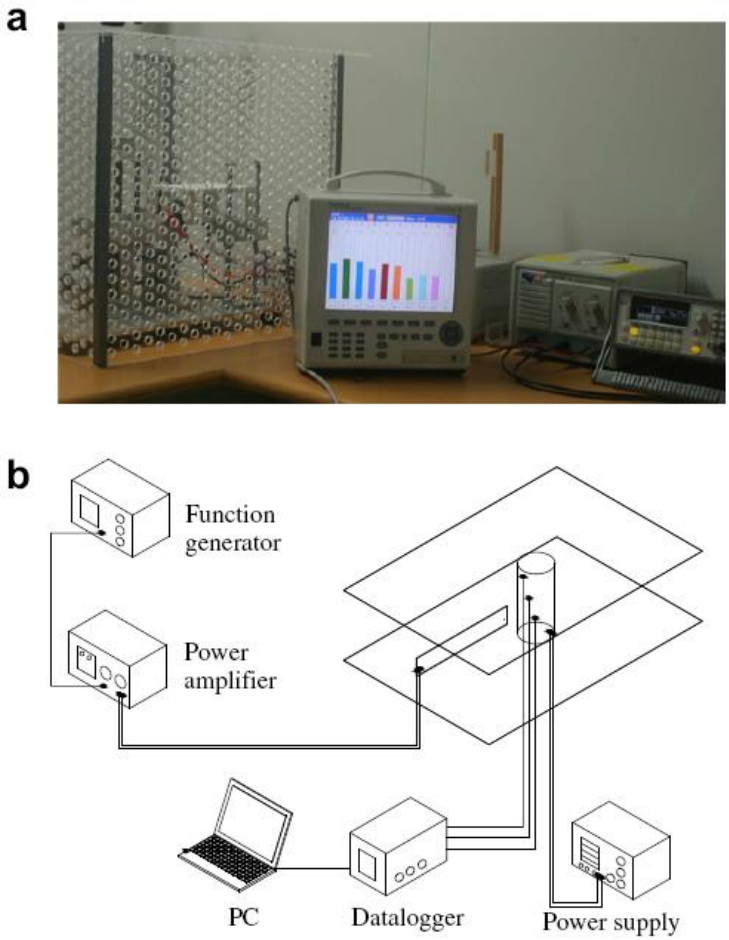

Figure 3.4 General view of experimental setup [20]

3.2 Study of Validation

Results were obtained by varying the dimensionless amplitude of piezoelectric fan (α = a / w) and the dimensionless distance between piezoelectric fan tip and heated surface (δ = d / w). In the reference study, the α value was taken as 1, 2, and 3, and the δ value was taken as 0.5, 1, and 1.5. In the validation study, α value was taken constant as 2 as in the thesis study and δ value was changed to 0.5, 1, and 1.5. A general view of the computational domain is given in Figure 3.5.

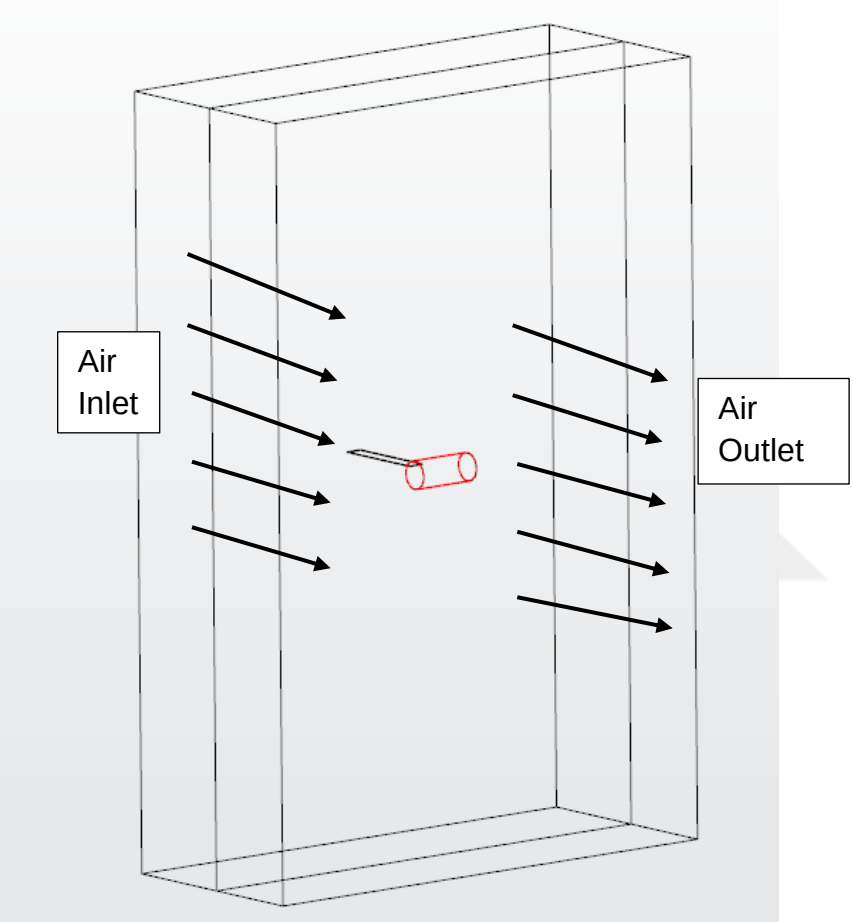

Figure 3.5 General view of the CFD domain with δ=1.5

The results were compared by heat transfer coefficient augmentation ratio (ξ). The formulation of these parameters is given in Eq. (10):

$$\xi = \frac{h_{pf}}{h_n} = \frac{\frac{q_s}{T_{s,pf} - T_a}}{\frac{q_s}{T_{s,n} - T_a}} = \frac{T_{s,n} - T_a}{T_{s,pf} - T_a} \qquad (10)$$

As has been explained earlier, CFD model was created and Ansys Fluent 17.2 is used for simulations. The movement function of this particular piezoelectric fan is defined by a UDF and given in Appendix F. Each period of the fan is divided into 400 parts and $7x10^{-5}$ s time step is used.

After establishing the CFD model, natural convection solution was obtained. Then, piezoelectric fan is vibrated and the forced convection solution is found. The tabulated natural and forced average temperatures and the number of time steps for different δ values are given in Table 3-1.

Table 3-1 Average surface temperature for natural and forced convection

	δ = 1.5	δ = 1.0	δ = 0.5
Number of Time Steps	7400	3300	3300
Average Surface Temperature after Natural Convection (K)	362	362	362
Average Surface Temperature after Forced Convection (K)	340	335	330.2

The heat transfer augmentation ratio as dimensionless distance between the piezoelectric fan tip and the heated cylinder is given in Figure 3.6.

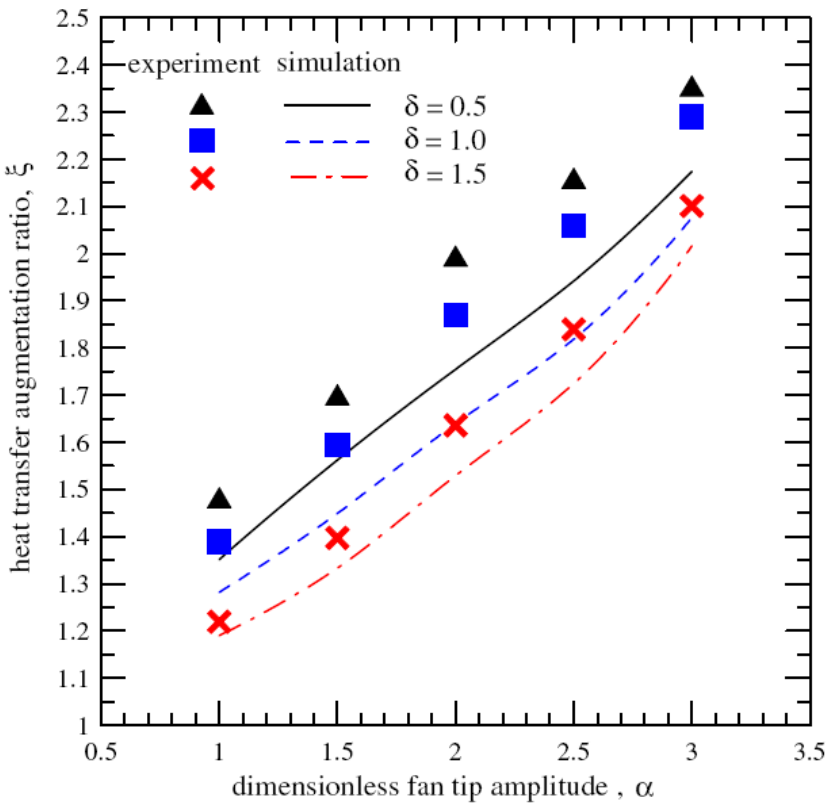

Figure 3.6 Variations of heat transfer augmentation ratio as function of dimensionless distance between piezoelectric fan tip and heated surface [20]

As a boundary condition, 1000 W/m^2 is defined at the inner wall of the cylinder. In the steady state of natural convection, the average temperature of the cylinder surface was fixed at 362 K while the outside was 295 K. Then the piezoelectric fan started to vibrate.

The solution for δ = 1.5 after ~0.5 s flow time, the average temperature of the cylinder surface was fixed at 340 K. In this case heat transfer augmentation ratio becomes;

$$\xi = \frac{h_{pf}}{h_n} = \frac{\dfrac{q_s}{T_{s,pf} - T_a}}{\dfrac{q_s}{T_{s,n} - T_a}} = \frac{T_{s,n} - T_a}{T_{s,pf} - T_a} = \frac{363 - 295}{340 - 295} = 1.51 \qquad (11)$$

The corresponding value for this result is 1.64 for the experimental result and the numerical one is 1.52 as shown in Figure 3.6. The heat transfer augmentation ratio results for δ = 1.5, 1.0 and 0.5 are given in Table 3-2.

Table 3-2 Heat transfer augmentation ratio results

	δ = 1.5	δ = 1.0	δ = 0.5
Lin's Study [20] (Exp.) ξ	1.64	1.88	2.00
Lin's Study [20] (Num.) ξ	1.52	1.64	1.75
Validation Study ξ	1.51	1.67	1.90

3.3 Results of Validation

The results obtained for the heat transfer augmentation ratio is calculated for different δ values and α = 2 are compared against experimental and numerical ones obtained by Lin [20] and presented in Table 3-3.

Table 3-3 Heat transfer augmentation ratio comparison

		Error of Validation Study Compared to Experimental Results	Error of Validation Study Compared to Numeric Results
Heat Transfer Augmentation Ratio	δ=1.5	$\frac{1.64-1.51}{1.64}\times 100 = 8\%$	$\frac{1.52-1.51}{1.52}\times 100 = 0.6\%$
	δ=1.0	$\frac{1.88-1.67}{1.88}\times 100 = 11\%$	$\frac{1.64-1.67}{1.64}\times 100 = 1.8\%$
	δ=0.5	$\frac{2.0-1.90}{2.0}\times 100 = 5\%$	$\frac{1.75-1.90}{1.75}\times 100 = 8.5\%$

It is worth to note that, the Lin's [20] results show about 10% difference in between experimental and numeric results. In the corresponding work, it is suggested that the main reason of this difference is the lack of radiation however experimental uncertainties and the turbulence modelling could also be the other reasons. When the Table 1-1 is examined, the maximum of 11% difference is found between the validation study and the Lin's [20] experimental results for δ=1.0. On the other hand, the maximum difference of 8.5% is found between the validation study and Lin's [20] numerical results for δ=0.5. In cases with δ=1.0 and δ=1.5, these variations are even lower than 2%.

The error rate for δ = 1.0 and α = 2, which is the case with the same parameters as the work done in the thesis, is 1.8%. As a result, considering the specific error margin, it can be concluded that the results of the study with the results of the article are compatible with each other and the presented method and the solution are successful.

CHAPTER 4
RESULTS AND DISCUSSION

In the solution procedure, a steady state solution is achieved first under natural convection. After reaching the steady solution, it is as initial conditions then a pseudo steady state is reached by using the transient solver with dynamic mesh. Two different types of boundary conditions are defined at the base of the fin block arrangements. As a first type of boundary condition, the total amount of heat applied to the base of fin blocks is kept constant for all fin block configurations. Second type of boundary condition applied to the base of fin blocks is the constant heat flux for all fin block configurations. These two kind of boundary conditions are implemented for both horizontal and vertical piezoelectric fan arrangement. With these boundary conditions, simulations were performed separately by changing the number of fins in a fin block from 1 to 10, and the total of 20 different solutions were obtained for horizontal fan arrangement. For vertical fan arrangement 2, 5 and 10-fin-block configurations have been solved in order to compare the results against the ones achieved with horizontal fan arrangement. The solutions are discussed in terms of the applied boundary conditions, i.e., the constant heat flux and the constant total heat.

Horizontal and vertical fan arrangements are shown in Figure 4.1 and Figure 4.2.

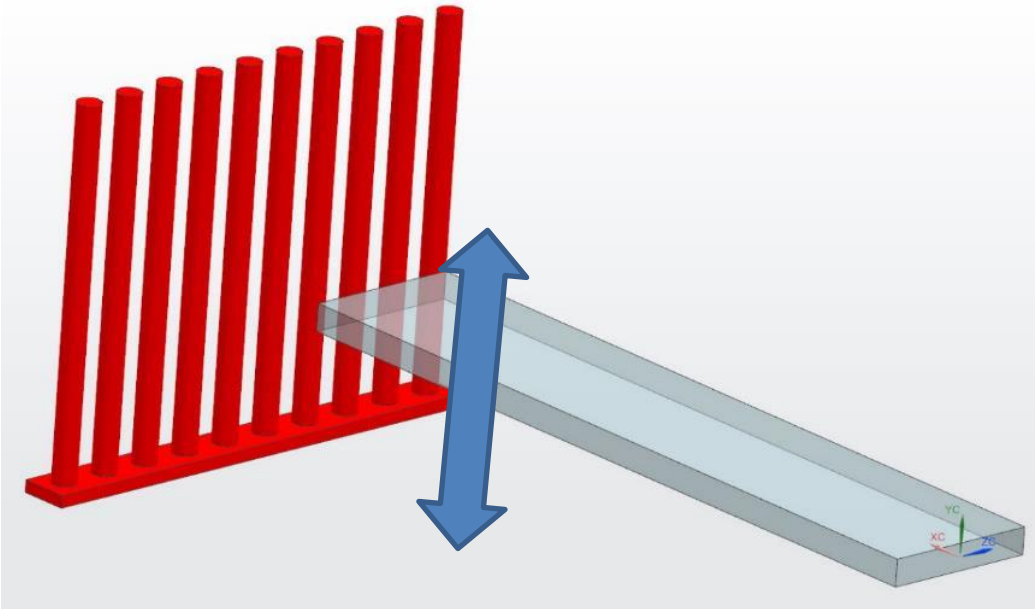

Figure 4.1 Horizontal fan arrangement with 10-fin-block configuration

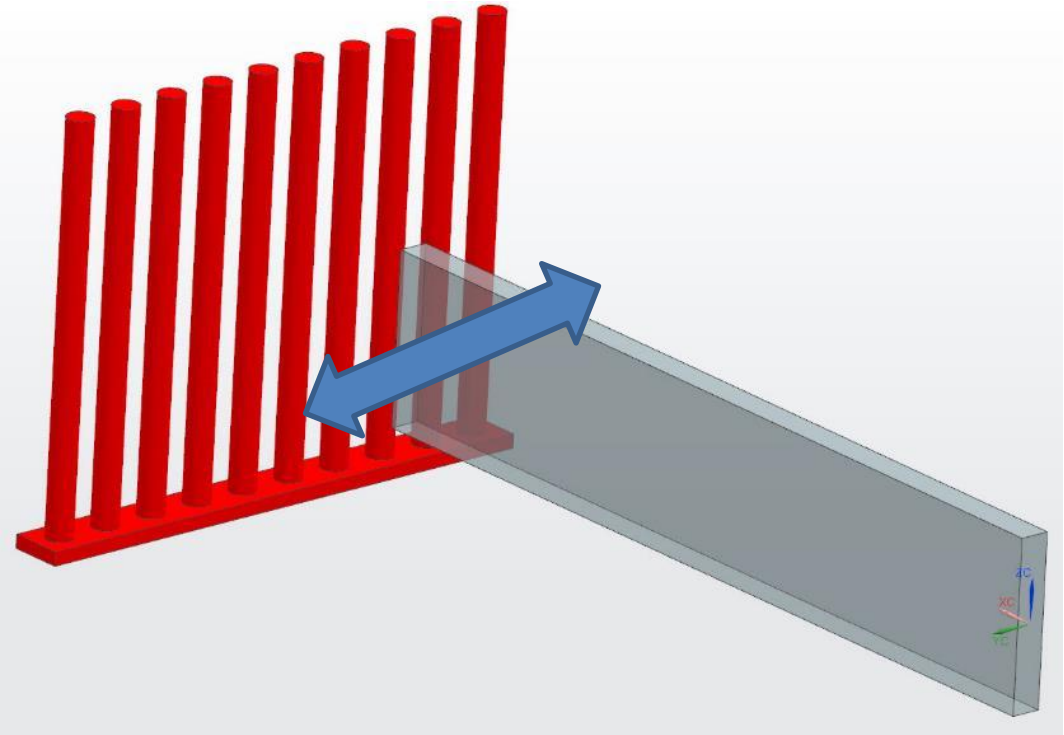

Figure 4.2 Vertical fan arrangement with 10-fin-block configuration

The studies which include experimental setups in the literature, the experiments last for minutes to reach pseudo state equilibrium. In the transient solution, the time step was used as $5x10^{-5}$ seconds so that the model could operate without showing any numerical instabilities due to dynamic mesh operation. When real-time CFD solution is implemented, at least 10 million time step will be needed to obtain the pseudo steady state solution. In this case, even if the CFD code runs without any problems, it will require an excessive amount of time in the order of years. In order to reduce the computational time to reasonable duration without facing any numerical errors, the density and the heat capacity of the material of the fin block have been reduced to 1/1000 of their original values. This reduction affects only the time constant of the problem without changing the obtained temperature distribution since the pseudo state solutions are used in this study. That can be seen in the Eqs. (12) and (13). Although density and heat capacity are important for transient solution, they do not affect the result of steady state solution. The only property that affects the steady state solution for temperature distribution is thermal conductivity.

$$k\frac{\partial T}{\partial z} = q_s \qquad (12)$$

$$\pm k \frac{\partial T}{\partial x_i} = h(T - T_\infty) \qquad (13)$$

In the transient solution pseudo steady state is obtained in between 3500 and 5000 time steps. This corresponds to the real time values of 0.15 to 0.25 s. In each fin configuration simulations, these results were achieved in about 1 week by running in parallel processors on a computer which have 2.3 GHz processors with 24 GB ram.

4.1 Flow Field Analysis

The velocity vectors, velocity and temperature fields of the flow created by the horizontal and vertical piezoelectric fan arrangements for the 5-fin-block geometry configuration are given below. Figures are belonged to the time when piezoelectric fans are moving from their neutral positions.

Figure 4.3 and Figure 4.4 clearly show how the airflow changes for horizontal and vertical fan arrangements. In horizontal fan arrangement, air flow created by upward and downward motion sweeps the whole fin height while in the vertical fan arrangement air flow created by right and left motion sweeps the whole fin block width at different strengths. In other words, central fins are most affected in the horizontal and upper section of complete fin height is most affected in the vertical fan configurations. Top views at z=15 mm plane (middle height of the fin block) are presented in Figures 4.5 and 4.6.

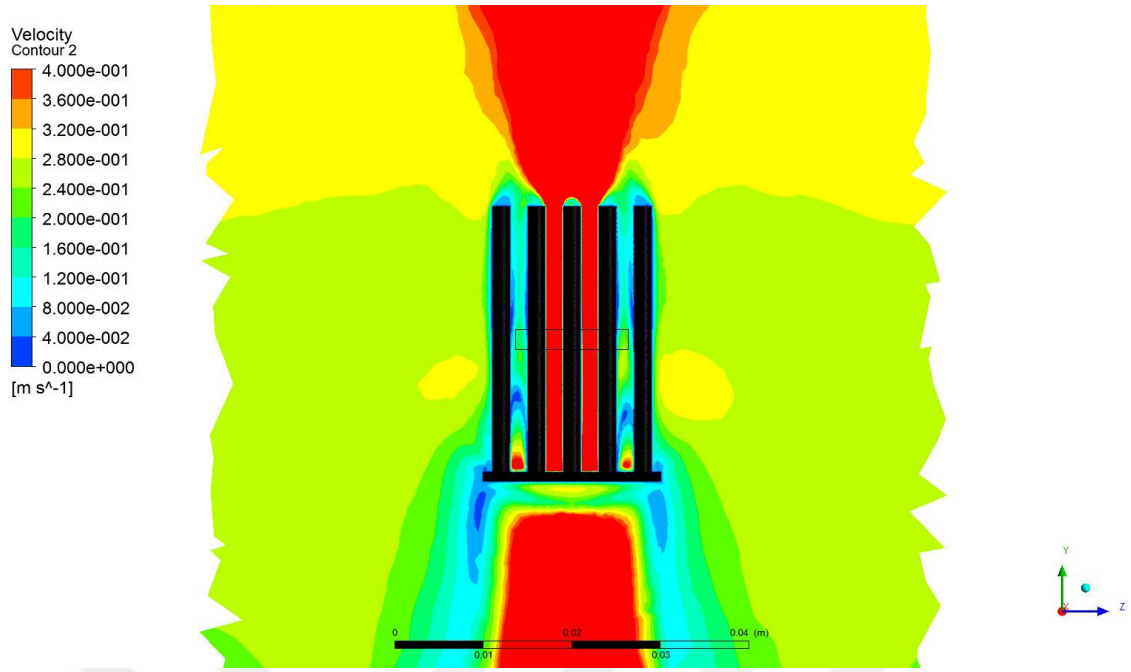

Figure 4.3 Velocity distribution of the airflow for horizontal fan arrangement front view

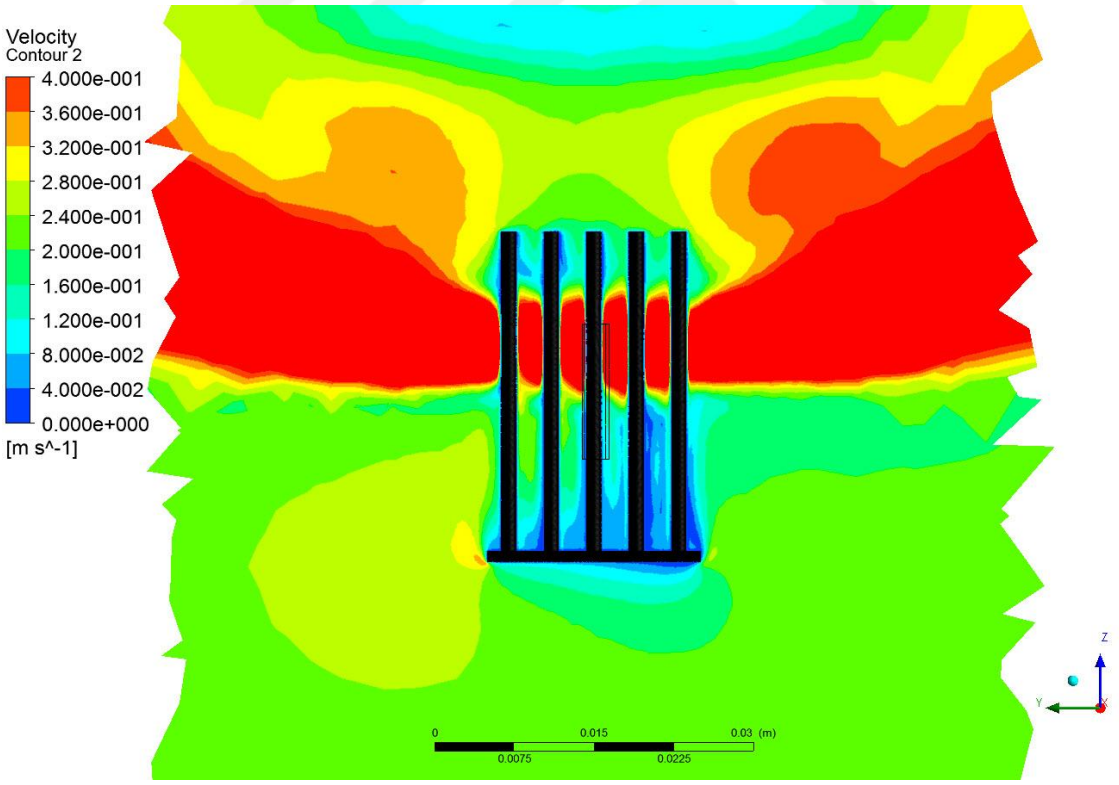

Figure 4.4 Velocity distribution of the airflow for vertical fan arrangement front view

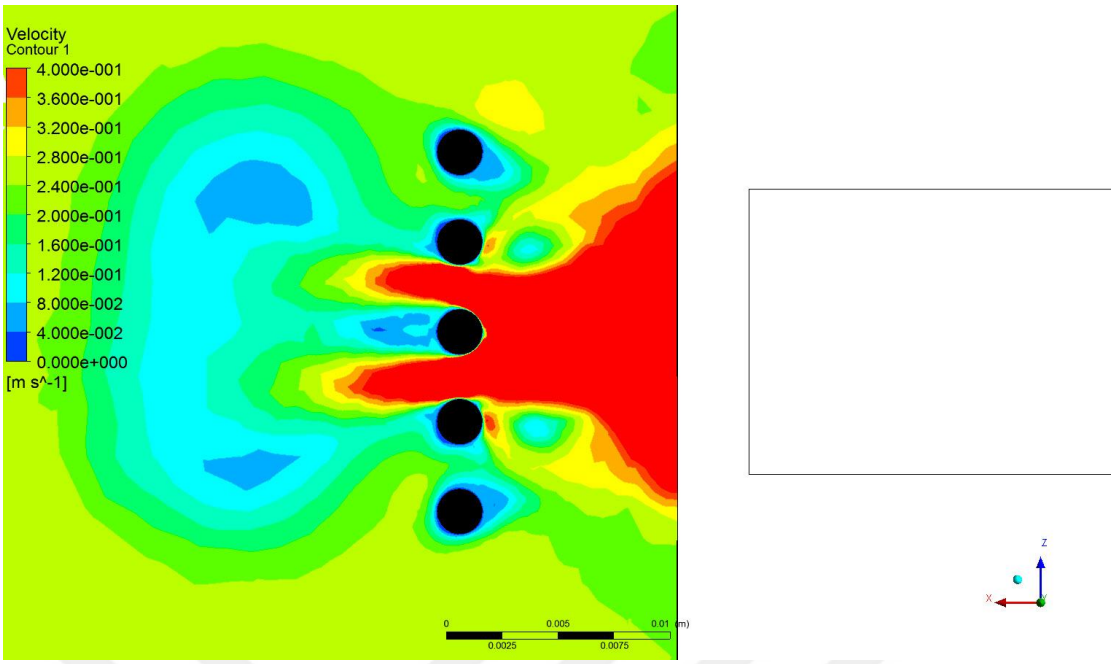

Figure 4.5 Velocity distribution of the airflow for horizontal fan arrangement top view

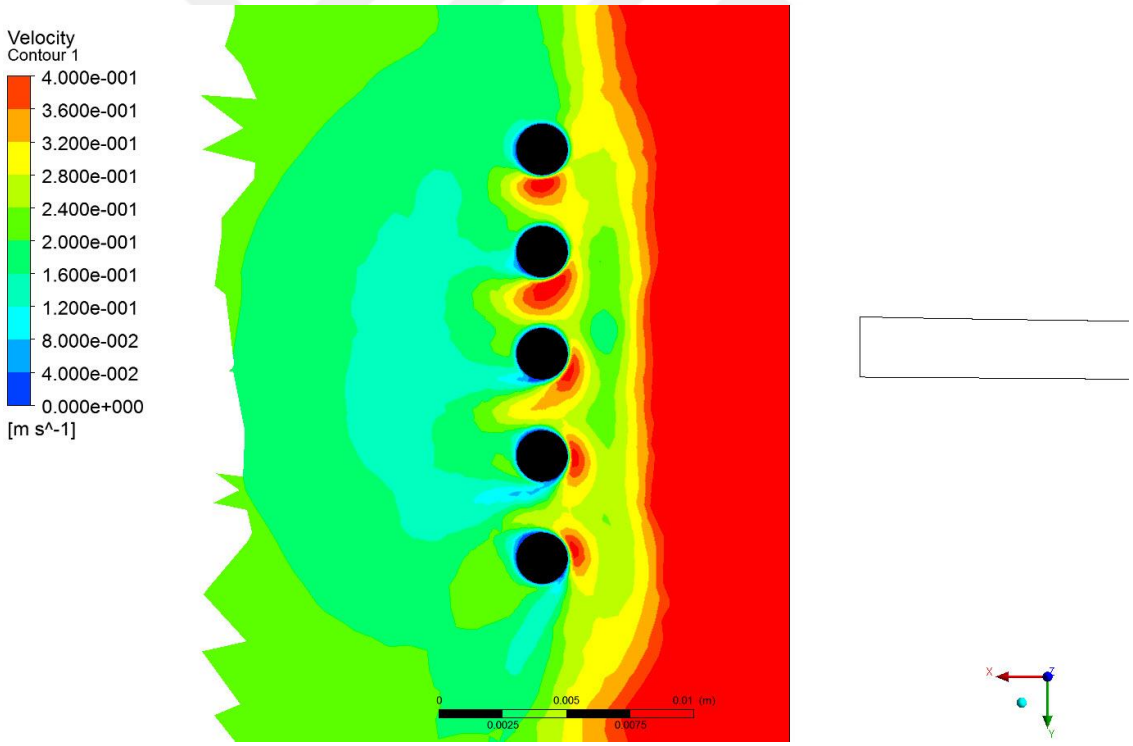

Figure 4.6 Velocity distribution of the airflow for vertical fan arrangement top view

Figure 4.7, Figure 4.8, Figure 4.9, Figure 4.10, Figure 4.11 and Figure 4.12 show the velocity vectors of the airflow. In these figures vortices and separation regions in the flow created by two different fan configurations can be seen clearly.

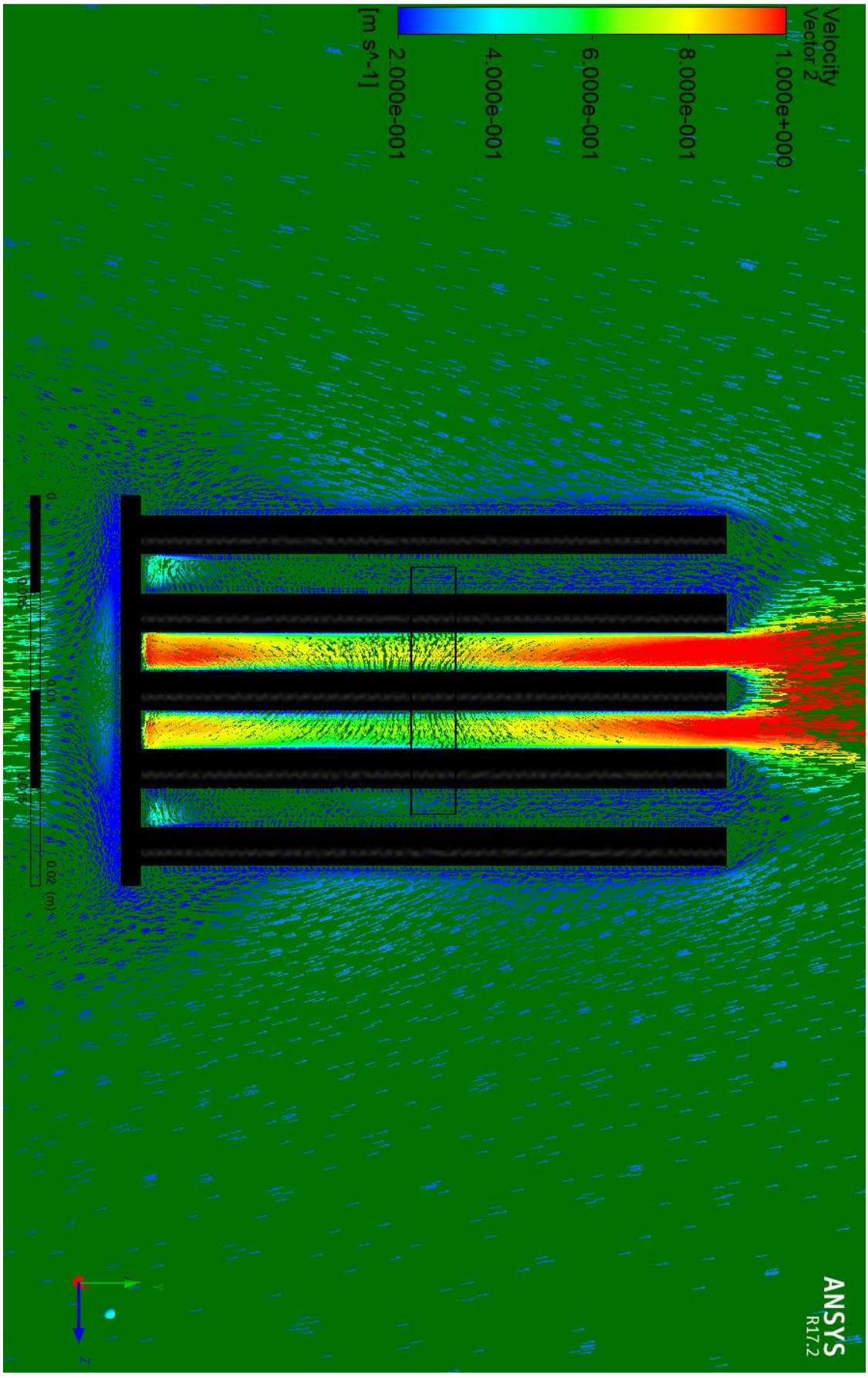

Figure 4.7 Velocity vectors of the airflow for horizontal fan arrangement front view

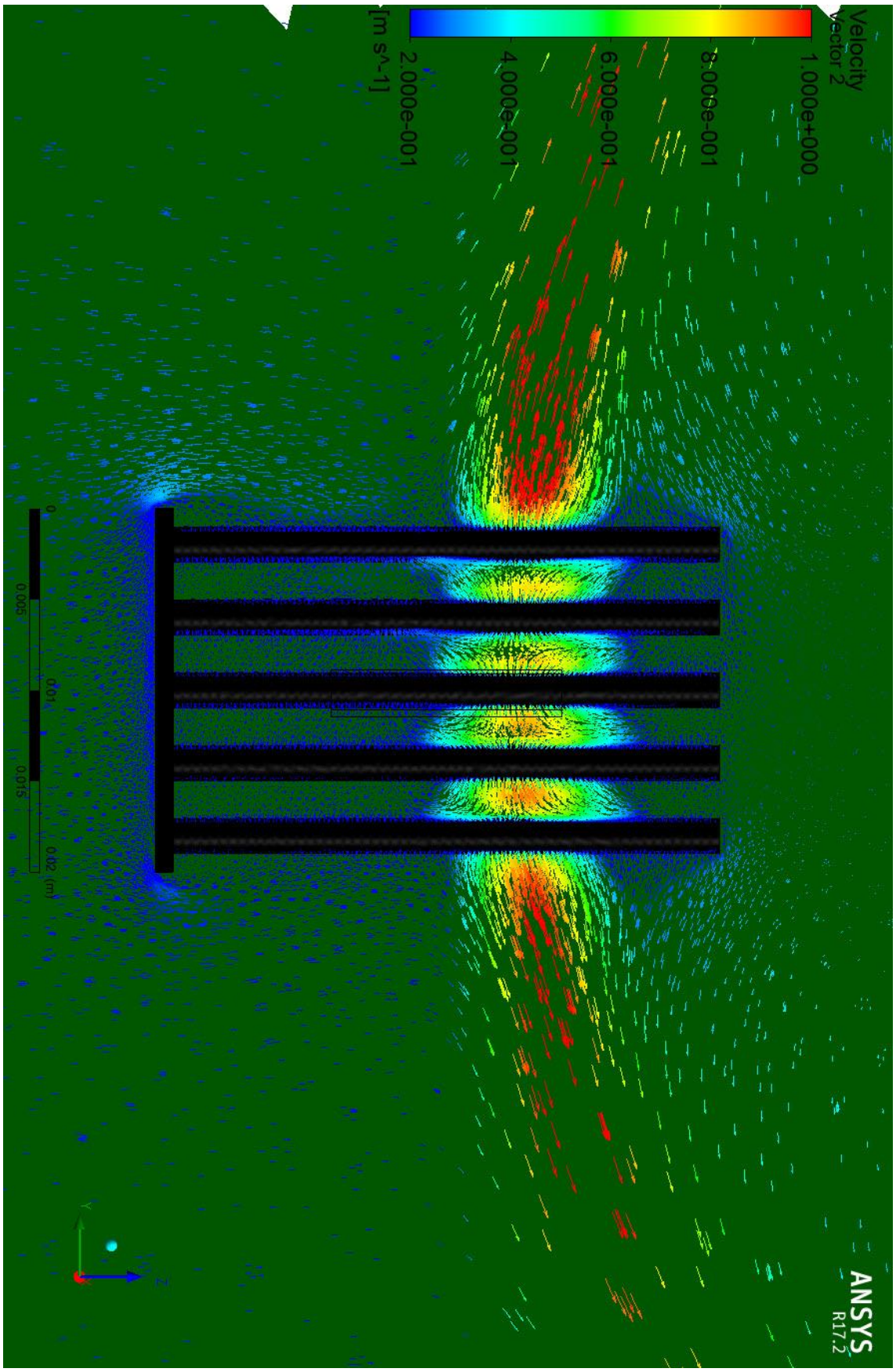

Figure 4.8 Velocity vectors of the airflow for vertical fan arrangement front view

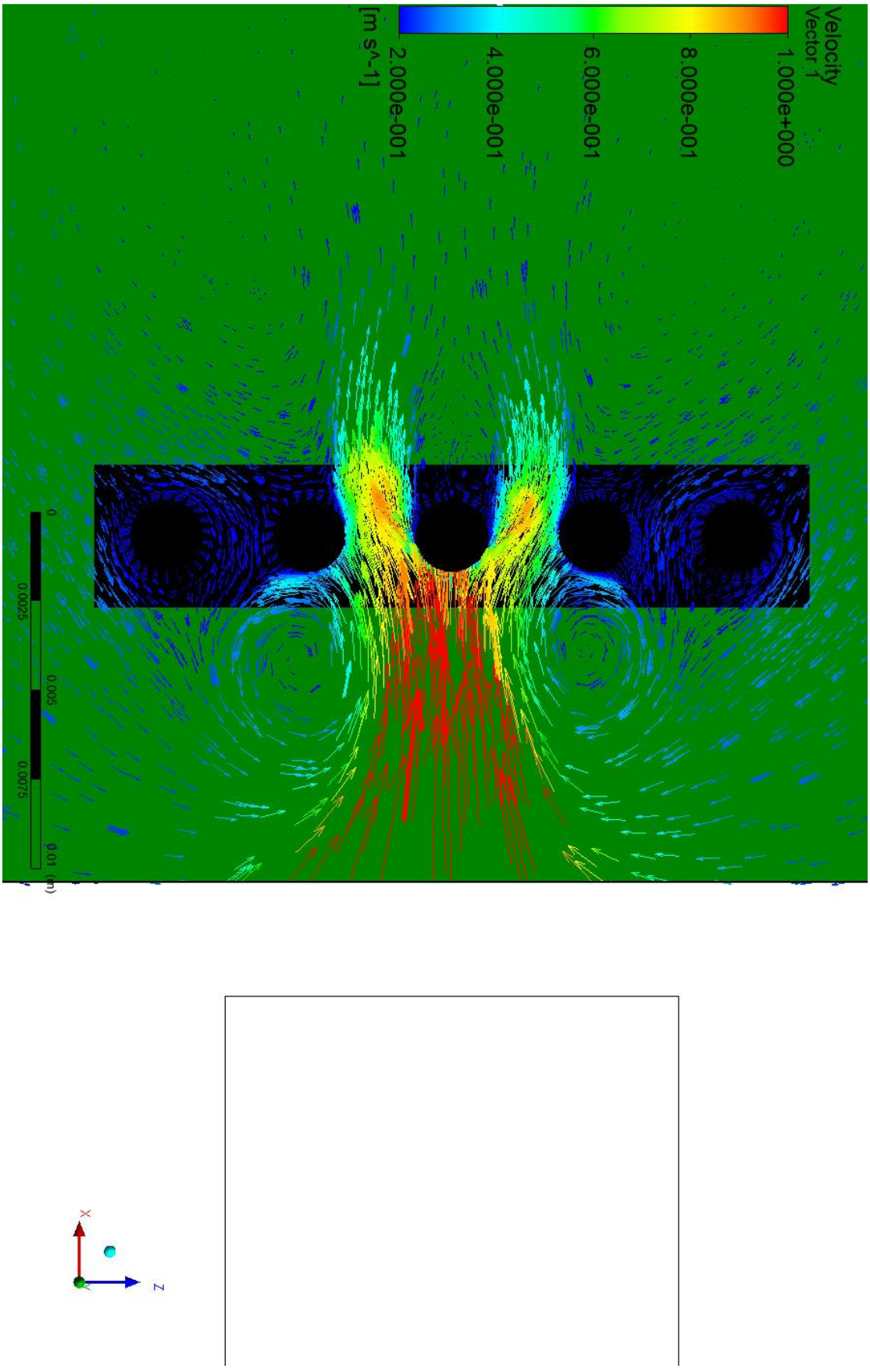

Figure 4.9 Velocity vectors of the airflow for horizontal fan arrangement top view-1

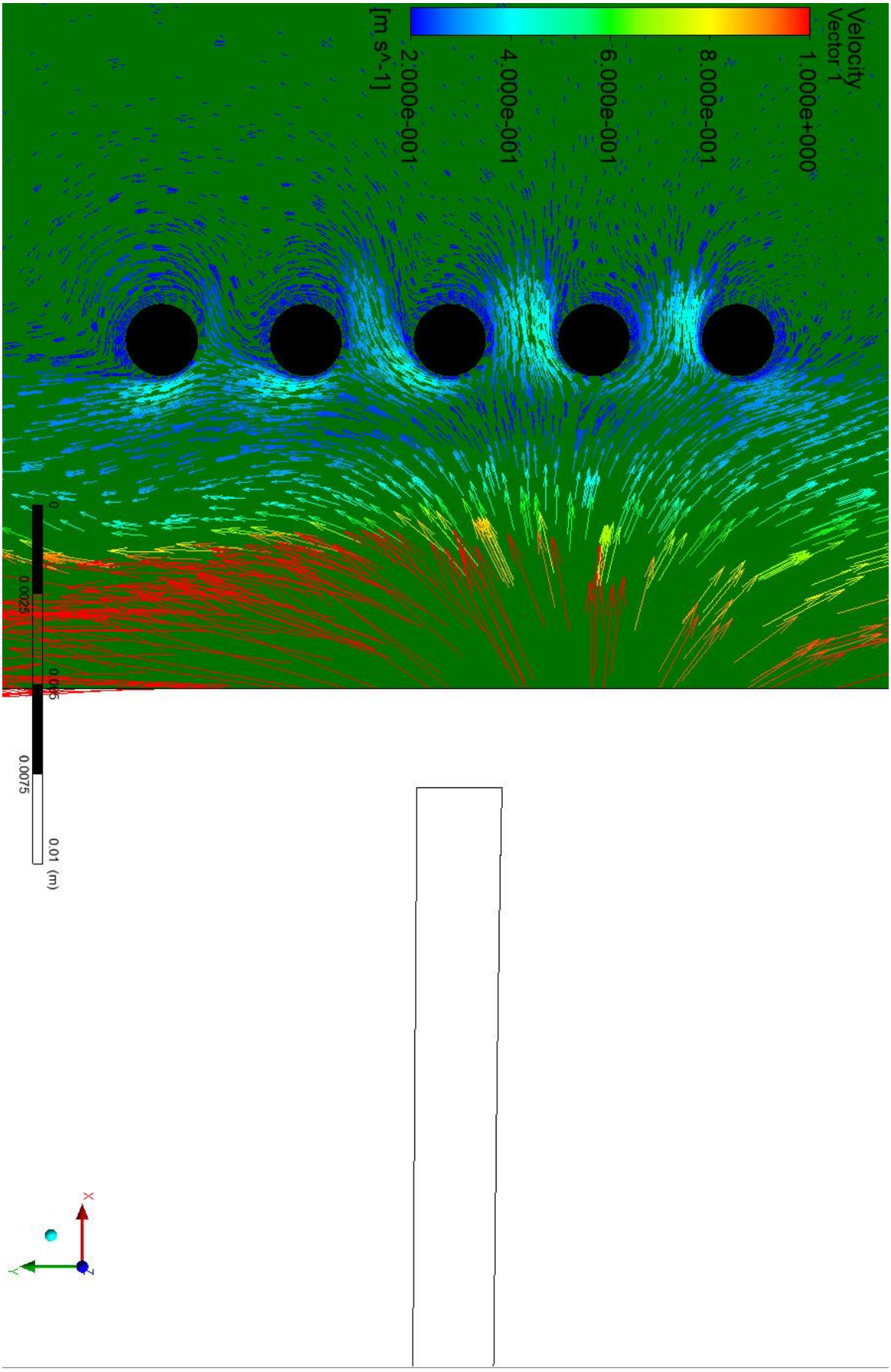

Figure 4.10 Velocity vectors of the airflow for vertical fan arrangement top view-1

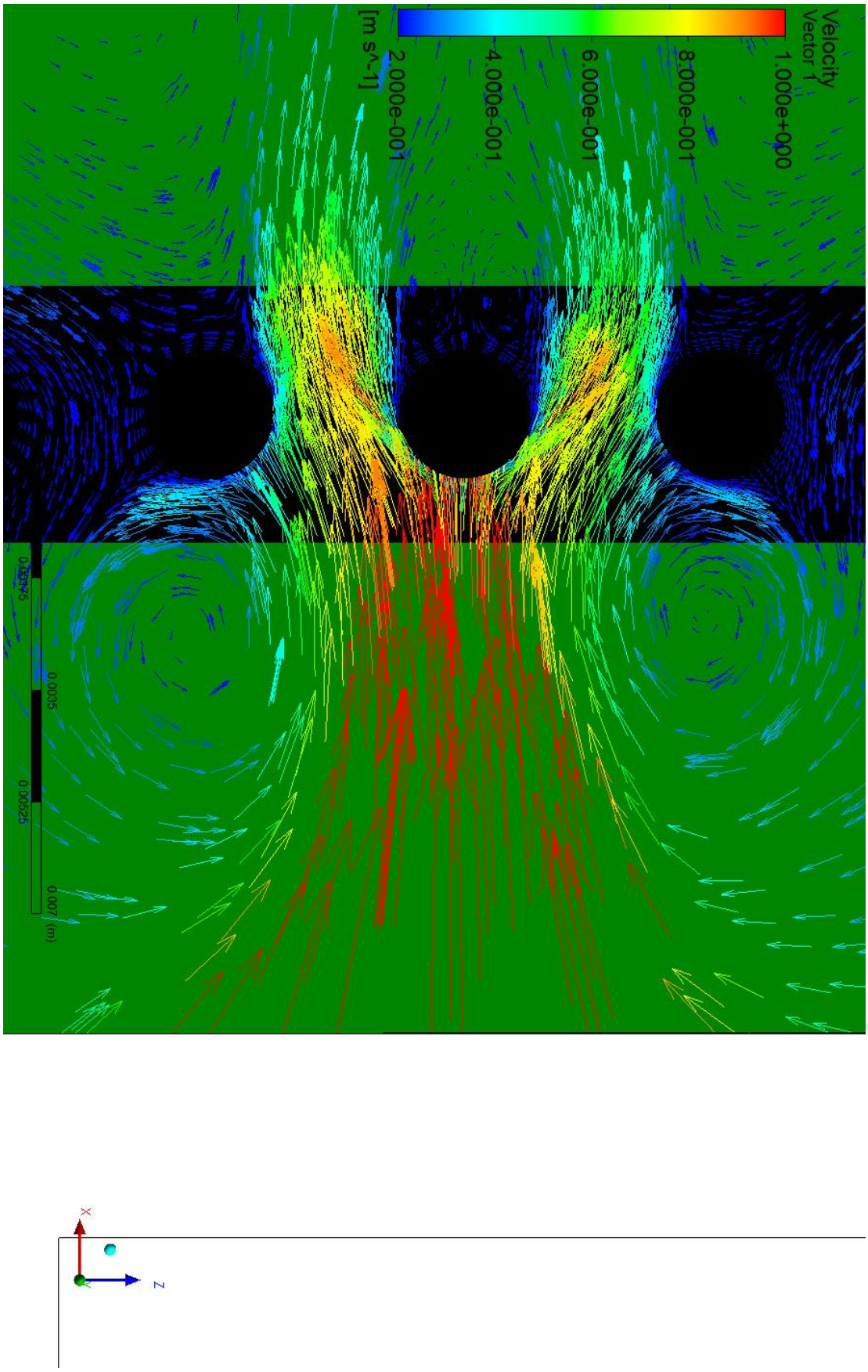

Figure 4.11 Velocity vectors of the airflow for horizontal fan arrangement top view-2

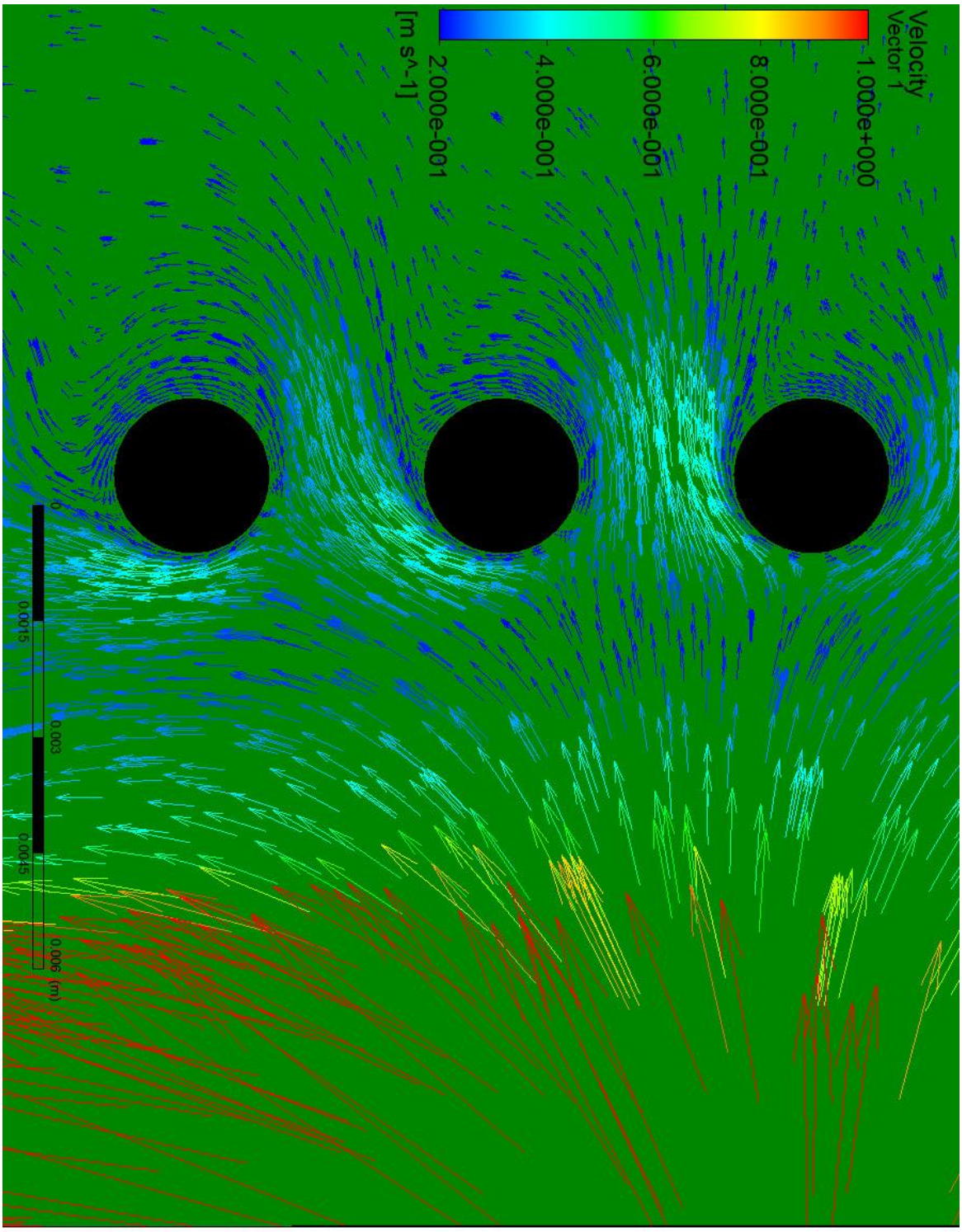

Figure 4.12 Velocity vectors of the airflow for vertical fan arrangement top view-2

Figure 4.13, Figure 4.14 Figure 4.15 and Figure 4.16 show temperature distributions in the domain for two different fan configurations. In the horizontal fan arrangement, the temperature distribution is more uniform from bottom to top while it shows more variation in temperature distribution in the vertical fan arrangement. Temperature values in the upper middle height of fin block is lower than the top and bottom regions since the air flow is directed to the slightly upper middle height of the fin block in the vertical fan arrangement.

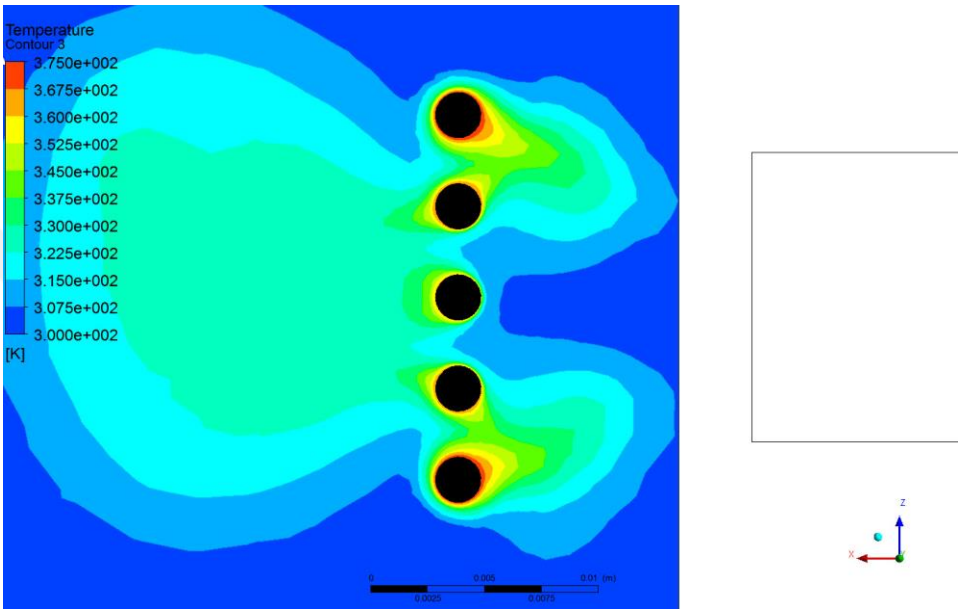

Figure 4.13 Temperature distribution of the airflow for horizontal fan arrangement top view

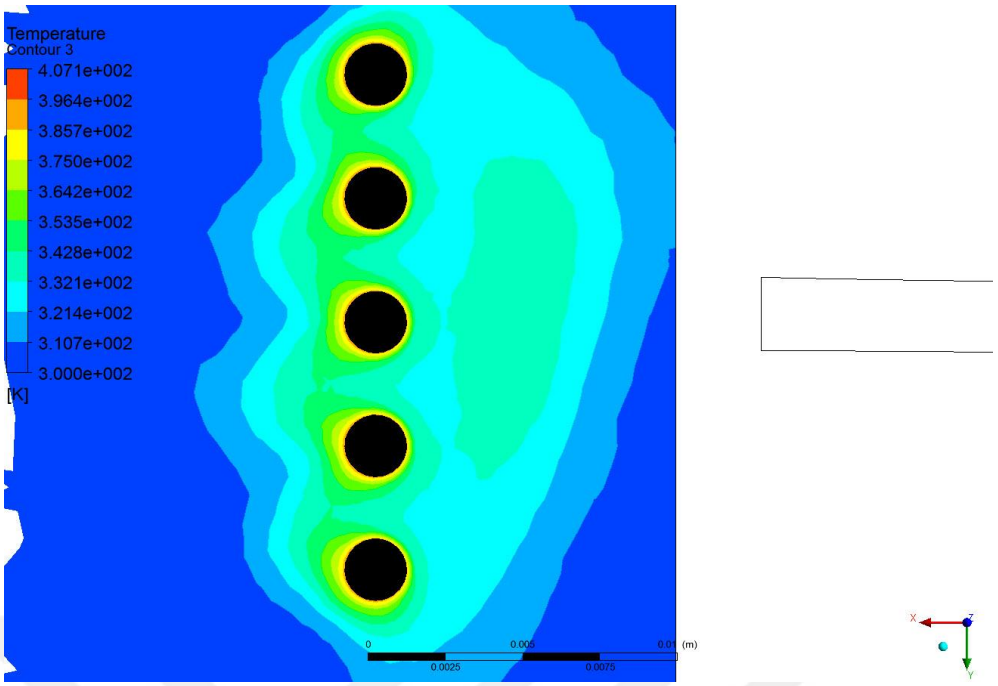

Figure 4.14 Temperature distribution of the airflow for vertical fan arrangement top view

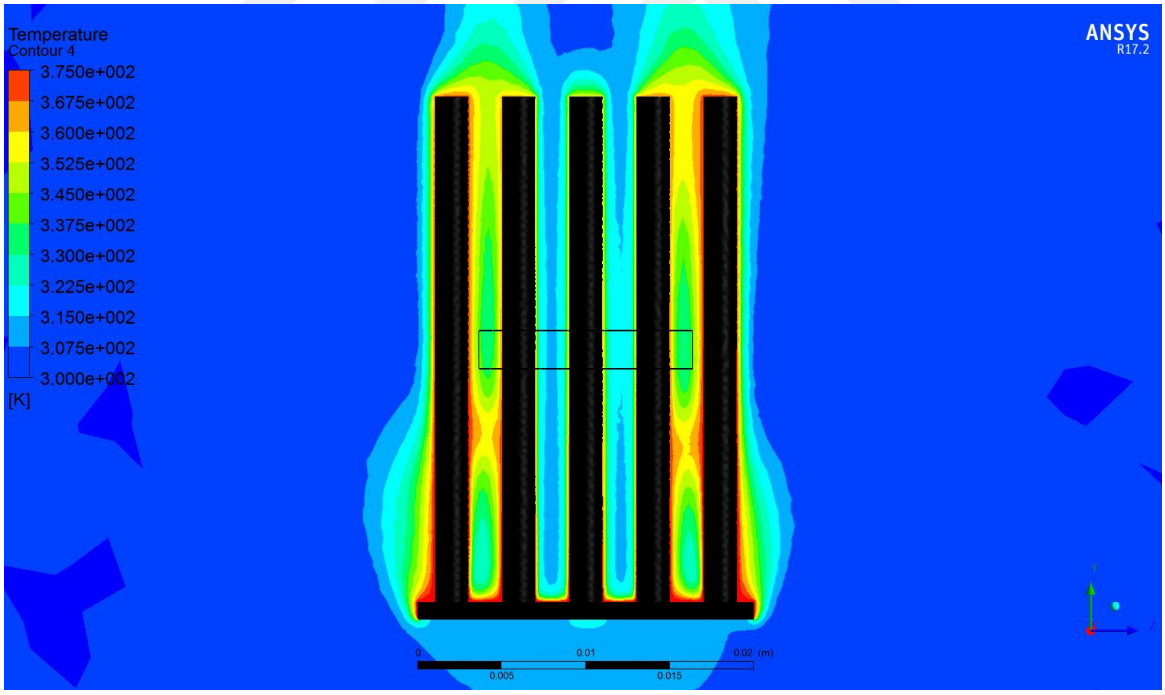

Figure 4.15 Temperature distribution of the airflow for horizontal fan arrangement front view

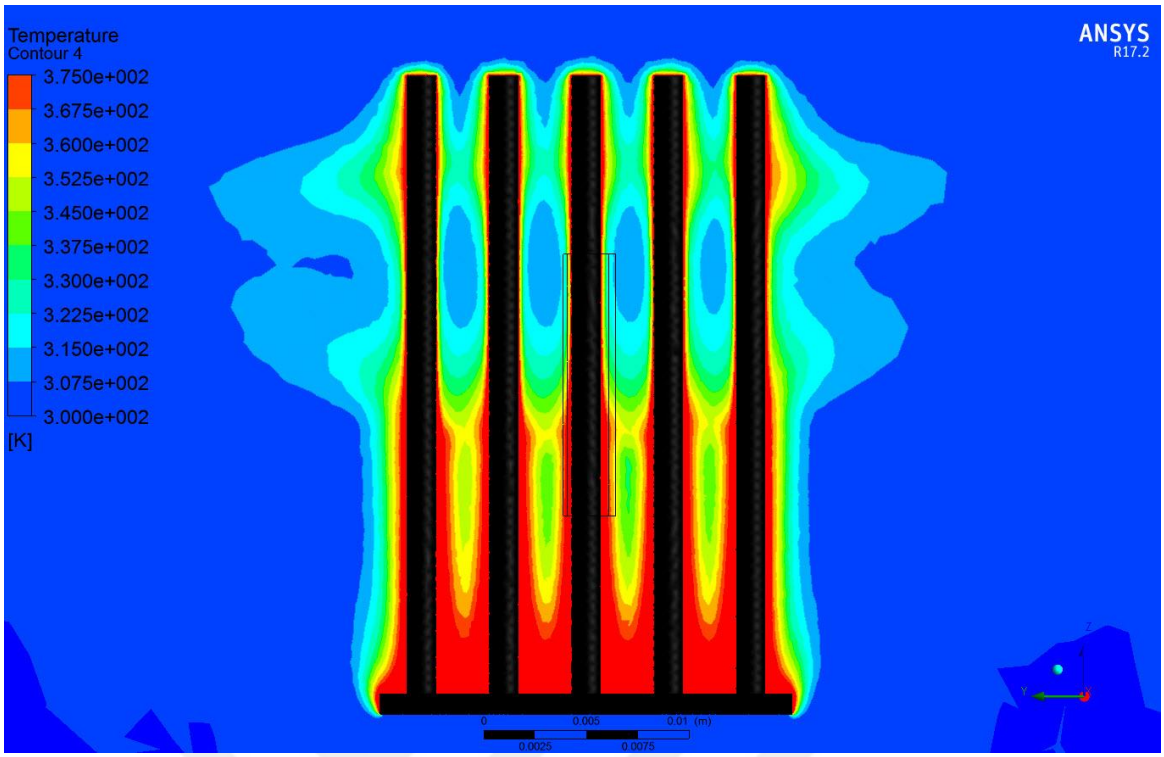

Figure 4.16 Temperature distribution of the airflow for vertical fan arrangement front view

4.2 Results for Constant Total Heat Boundary Condition with Horizontal Fan Arrangement

In the simulations, first, the fin block is cooled down by natural convection only, keeping the piezoelectric fan off. The solution was repeated by giving a fixed amount of heat instead of a constant heat flux as a boundary condition to the base of the fin block. Since the number of fins in fin blocks are increased from 1 to 10, a finite number that can be divided by the numbers 1 to 10 is found. The least common multiple for 1 to 10 is 5040. In order to see temperature differences occur during forced convection clearly, 5040 is multiplied by 10. So the chosen heat flux is 50400 W/m^2 for 1 fin configuration and 1/10th of that value for 10 fin configuration. For example, the heat applied for constant total heat (q_a) boundary condition is calculated by multiplying 50400 W/m^2 by the base area of 1, 5 and 10-fin-block configuration.

q_a (W) = applied heat flux (w/m^2) x width of base (m) x length of base (m)

$q_{a,1}$ = 50400 X 0.004 X 0.004 = 0.8064 W

$q_{a,5}$ = 10080 X 0.004 X 0.020 = 0.8064 W

$q_{a,10}$ = 5040 X 0.004 X 0.040 = 0.8064 W

This is the total heat provided at the base of the fin block regardless of the number of fins. After steady solution was achieved, piezoelectric fan started to vibrate with horizontal fan arrangement. Then pseudo-steady state solution was achieved. This procedure was repeated with 1 to 10 fins added side by side across the piezoelectric fan.

For the 1-fin-block, the average surface temperature of the fin block was 451.98 K for the steady state solution for natural convection. After the natural convection is reached a steady state, transient simulation is turned on. With the vibrating piezoelectric fan, the average surface temperature of the fin block was found to be 339.56 K after the pseudo steady state solution. In this case heat transfer augmentation ratio becomes;

$$\xi = \frac{h_{pf}}{h_n} = \frac{\frac{q_s}{T_{s,pf} - T_a}}{\frac{q_s}{T_{s,n} - T_a}} = \frac{T_{s,n} - T_a}{T_{s,pf} - T_a} = \frac{451.98 - 300}{339.56 - 300} = 3.84 \qquad (14)$$

For the 1-fin-block, the result is 3.84 times better cooling performance than the natural convection under the flow generated by the piezoelectric fan.

The change in the average surface temperature of the fin block with time in the transient solution is shown in Figure 4.17, in which the initial temperature is obtained from the natural convection solution.

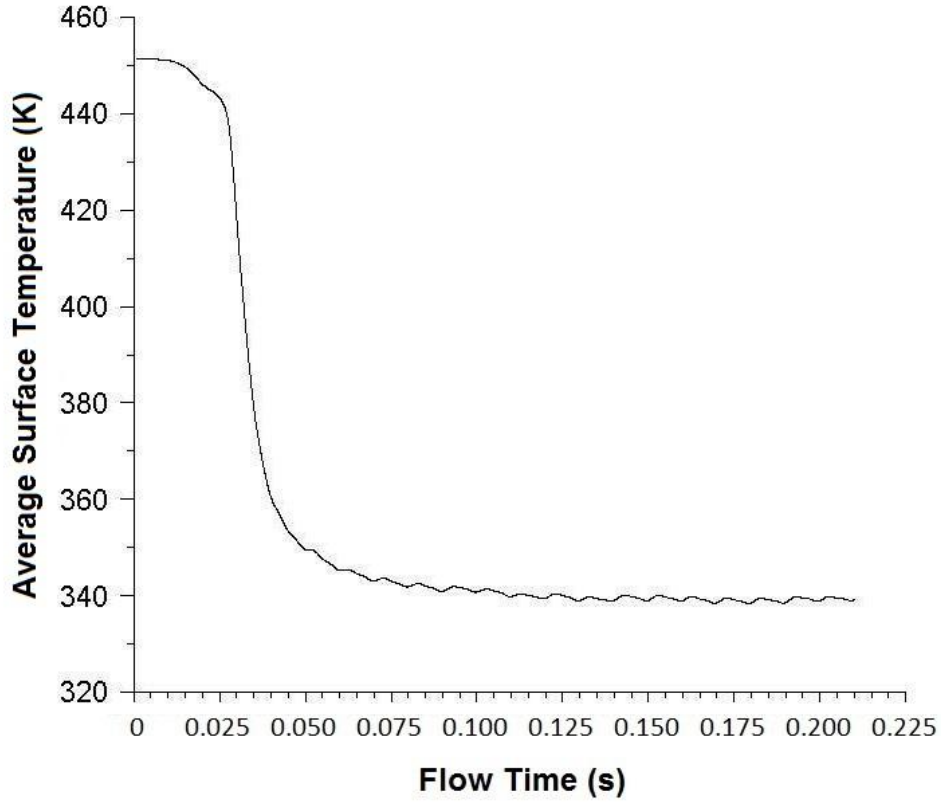

Figure 4.17 Average surface temperature of 1-fin-block for constant total heat

The temperature distribution for 1-fin-block is shown in Figure 4.18. The temperature distribution for the other fin block configurations are given in Appendix A.

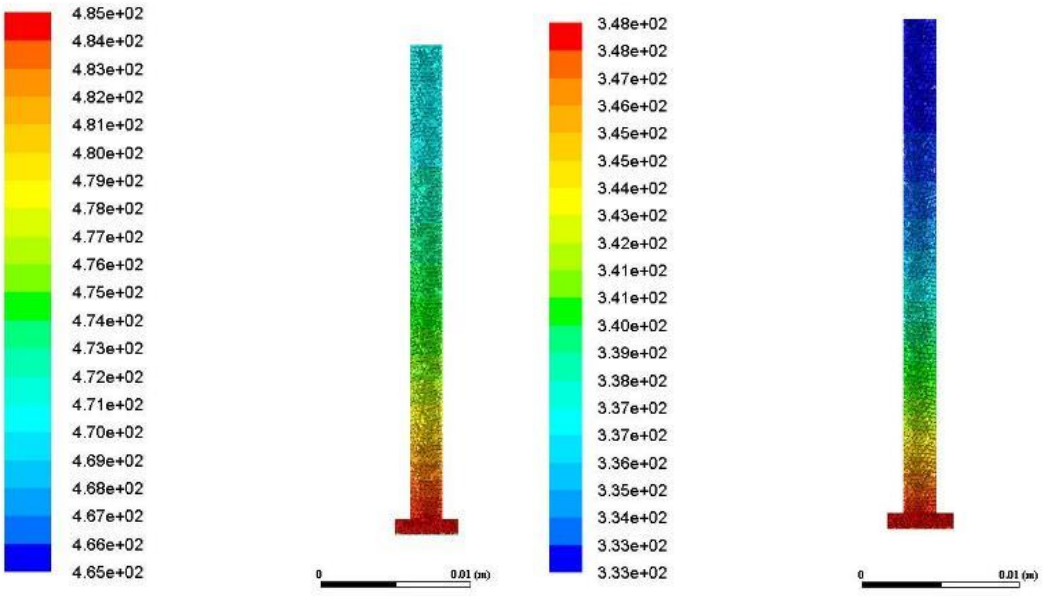

(a) (b)

Figure 4.18 Temperature distribution (in K) of 1-fin-block after natural convection (a) and piezoelectric fan cooling (b)

Table 4-1 shows the tabulated results for the heat transfer augmentation ratio values and the average temperatures of the surface of the fin blocks consisting of fins of 1 to 10. The results in the table are obtained after the steady state solution is reached under natural convection and then after the pseudo-steady state solution is reached under forced convection by the flow created by the piezoelectric fan.

Table 4-1 Heat transfer augmentation ratio and the average surface temperatures of fin blocks for the constant total heat of 0.8064 W

Boundary Condition = 0.8064 W	Temperature After Natural Convection Cooling (K)	Temperature After Piezoelectric Fan Cool Down the Fin Block (K)	Heat Transfer Augmentation Ratio
1 Fin	451.98	339.56	3.84
2 Fins	393.20	323.05	4.04
3 Fins	368.08	318.65	3.65
4 Fins	354.00	315.79	3.42
5 Fins	344.91	314.42	3.11
6 Fins	338.46	313.15	2.92
7 Fins	333.76	312.39	2.72
8 Fins	330.07	311.69	2.57
9 Fins	327.16	310.81	2.49
10 Fins	324.54	309.87	2.51

The average surface temperature results for different number of fins are given in Figure 4.19.

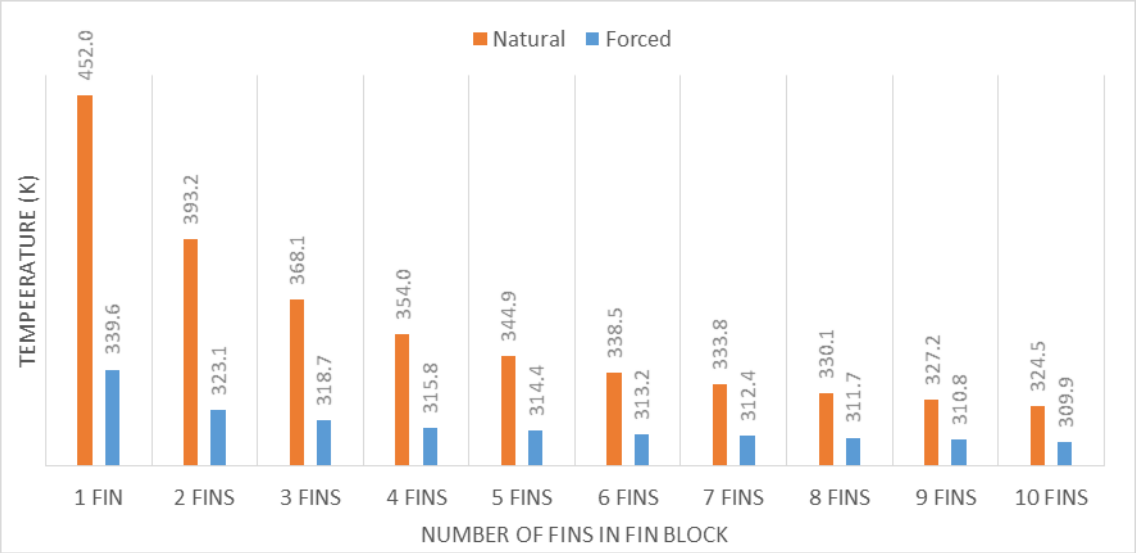

Figure 4.19 Average surface temperatures of fin blocks for constant total heat boundary condition for natural and forced convection cooling

The heat transfer augmentation ratio results for different number of fins are shown in Figure 4.20.

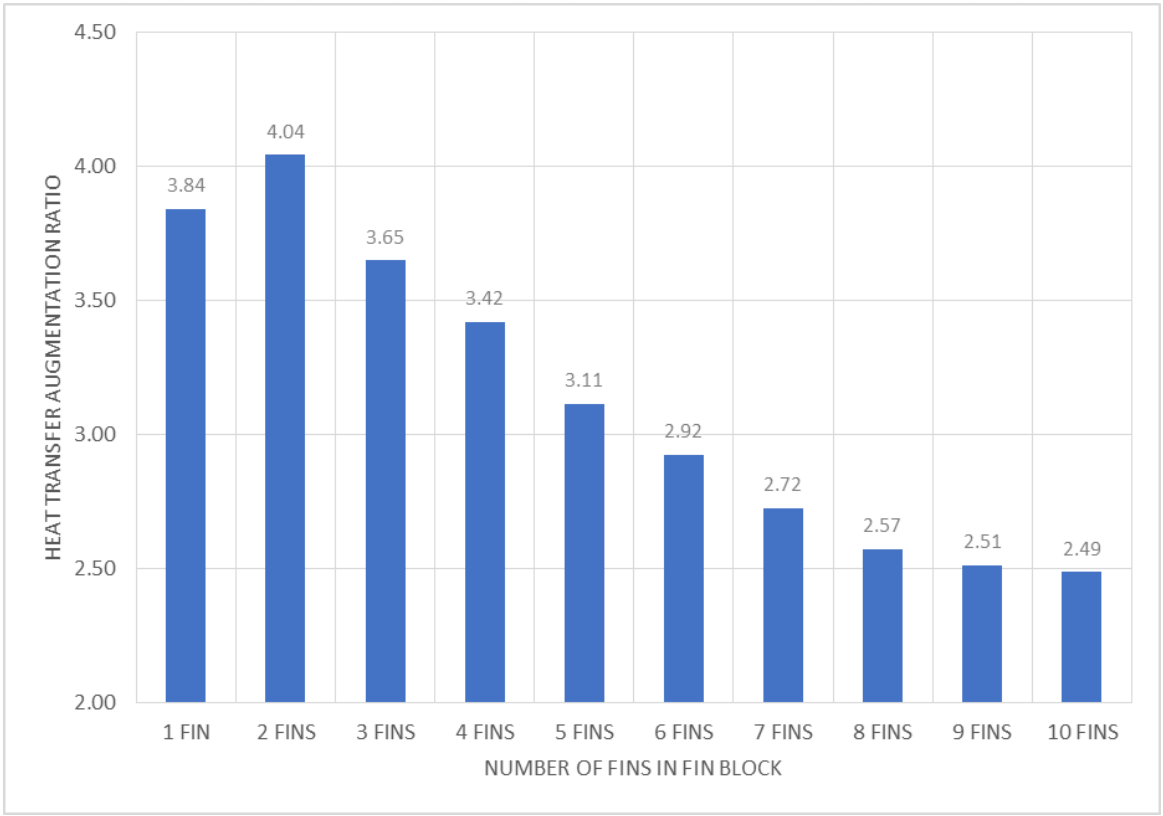

Figure 4.20 Heat transfer augmentation ratio for constant total heat

According to these results, the highest heat transfer augmentation ratio is seen in the 2-fin-block case. Then the value of the heat transfer augmentation ratio continues to decrease with increasing number of fins. When examined as a percentage, it is steadily decreasing by 7.5% on average from 2-fin-block to 8-fin-block.

The differences between the average surface temperatures of fins obtained under the natural convection and obtained under the forced convection created by the piezoelectric fan are given in Figure 4.21.

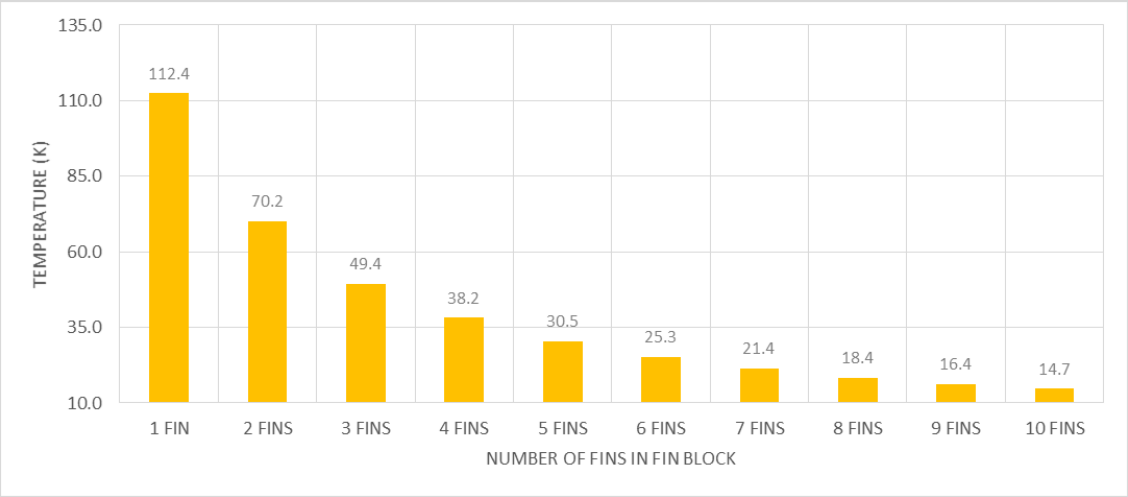

Figure 4.21 Temperature difference between natural and forced convection for constant total heat

As a result of the natural and forced convection solutions, when the average fin block temperatures are compared, the highest average temperature difference is 1-fin-block as expected because the total heat supplied remains constant. The resulting temperature differences were reduced regularly from 1 to 10-fin block.

The base temperatures of fin blocks cooled down under the forced convection generated by the piezoelectric fan is given in Figure 4.22.

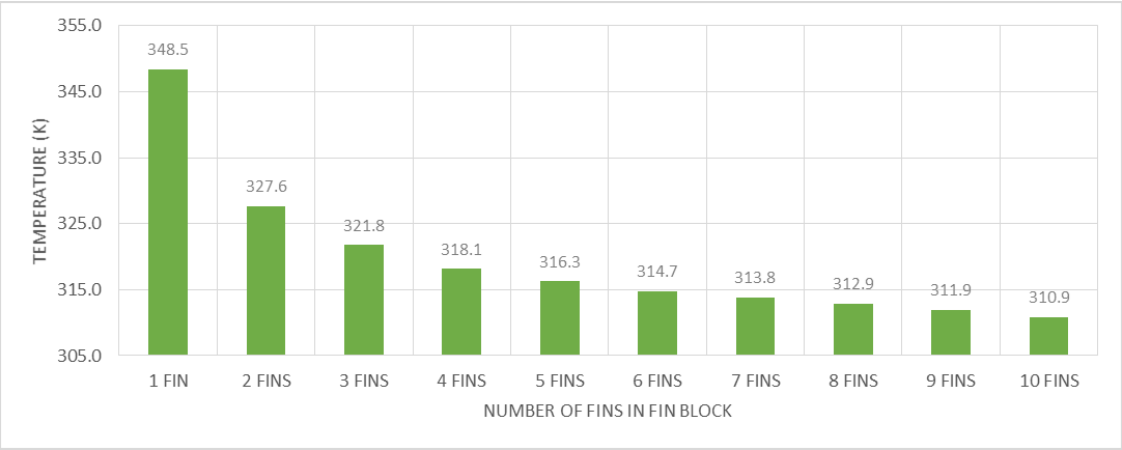

Figure 4.22 Base temperature of the fin blocks

Some electronic equipment requires a certain base temperature to operate when there is a constant total heat boundary condition. The maximum average temperature is defined on the specification sheet for the surface on which devices are mounted. This value is defined as the base temperature and the base temperature must be lower than that value for the electronic device to operate. If this value is exceeded, the device will not work because it is not cooled down enough. When the Figure 4.22 is examined, it is observed that the base temperature of the fin block decreases with increasing number of fins. This change is sharp between 1 and 2-fin-block, then decreases with a constant slope of approximately 3%. The number of fins in a fin block can be chosen from the Figure 4.22 according to desired base temperature criterion.

4.3 Results for Constant Heat Flux Boundary Condition with Horizontal Fan Arrangement

As has been explained in the previous section, after the computational model is built, first the simulation is performed under natural convection condition while keeping the piezoelectric fan off. A fixed 50400 W/m^2 heat flux was applied to the base of each fin in a fin block as a boundary condition. The transient solution with the forced convection was started after a steady solution with natural convection is reached. A pseudo steady state was obtained for the average surface temperature of the fin block under the flow generated by the piezoelectric fan vibration with horizontal fan arrangement. This simulation was repeated for 1 to 10 fins attached side by side.

When a constant heat flux of 50400 W/m^2 was given for each fin, the heat transfer augmentation ratio was achieved with the following results. As an example, the average surface temperature of the 2-fin-block was obtained as 347.35 K after the piezoelectric fan was vibrated while the temperature value for the natural convection steady-state solution was 476.67 K. In this case, heat transfer augmentation ratio;

$$\xi = \frac{h_{pf}}{h_n} = \frac{\dfrac{q_s}{T_{s,pf} - T_a}}{\dfrac{q_s}{T_{s,n} - T_a}} = \frac{T_{s,n} - T_a}{T_{s,pf} - T_a} = \frac{476.67 - 300}{347.35 - 300} = 3.73 \qquad (15)$$

For the 2-fin-block, according to heat transfer augmentation ratio calculation, the result is 3.73 times better cooling performance than the natural convection under the flow generated by the piezoelectric fan.

The change in the average surface temperature of the fin block with time in the transient solution is shown in Figure 4.23, again it is worth noting that the initial temperature value is obtained by the natural convection solution.

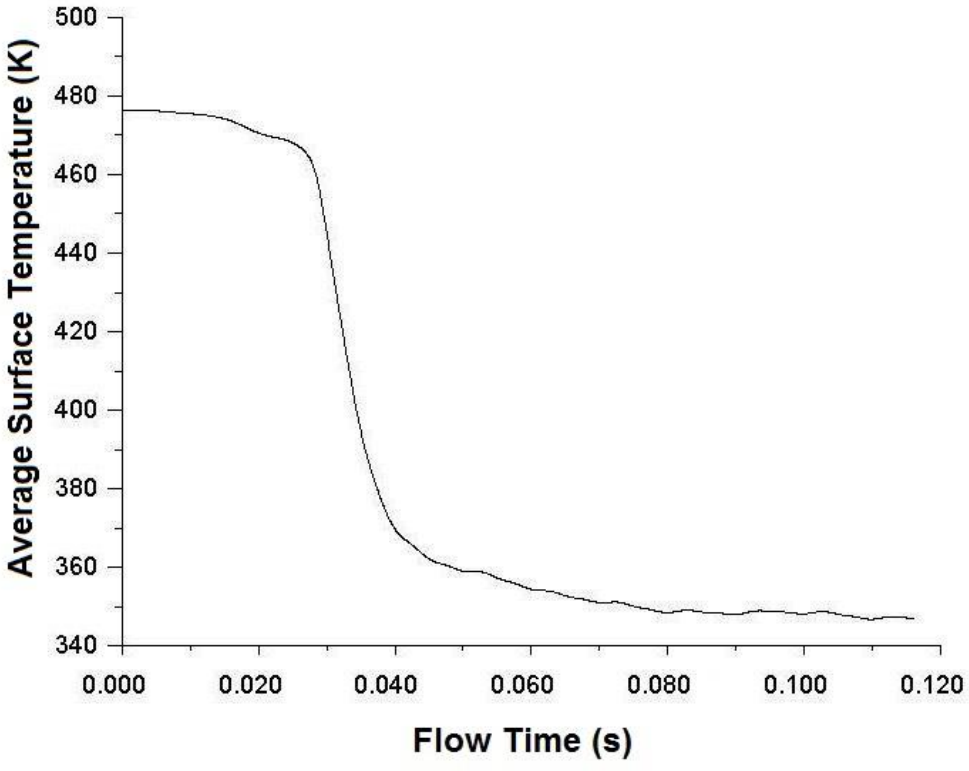

Figure 4.23 Average surface temperature of 2-fin-block for constant heat flux

The temperature distributions for the 2-fin-block with and without piezoelectric fan vibration are shown in Figure 4.24. The temperature distribution for the other fin block configurations are given in Appendix B.

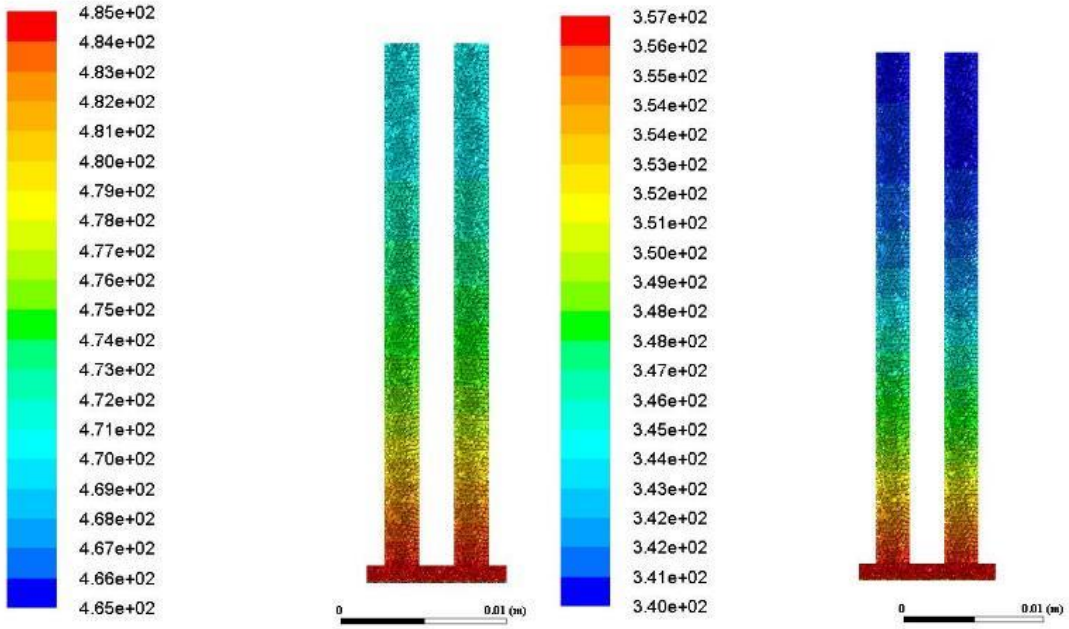

(a) (b)

Figure 4.24 Temperature distribution (in K) of 2-fin-block after natural convection (a) and piezoelectric fan cooling (b)

Table 4-2 shows the tabulated results for the heat transfer augmentation ratio and the average temperatures of the surface of the fin blocks consisting of fins of 1 to 10. The results in the table are given after the steady state solution under natural convection and after the pseudo steady state solution under forced convection by the flow created by the piezoelectric fan.

Table 4-2 Heat transfer augmentation ratio and the average surface temperatures of fin blocks for constant heat flux of 50400 W/m^2

Boundary Condition = 50400 W/m2	Temperature of the Fin Block After Natural Convection Cooling	Temperature of the Fin Block After Piezoelectric Fan Cool Down	Heat Transfer Augmentation Ratio
1 Fin	451.98	339.56	3.84
2 Fins	476.67	347.35	3.73
3 Fins	485.73	353.63	3.46
4 Fins	490.51	364.75	2.94
5 Fins	493.67	373.63	2.63
6 Fins	495.60	378.12	2.50
7 Fins	497.55	385.04	2.32
8 Fins	498.92	387.35	2.28
9 Fins	499.92	393.14	2.15
10 Fins	500.90	399.09	2.03

The average surface temperature results for different number of fins are given in Figure 4.25.

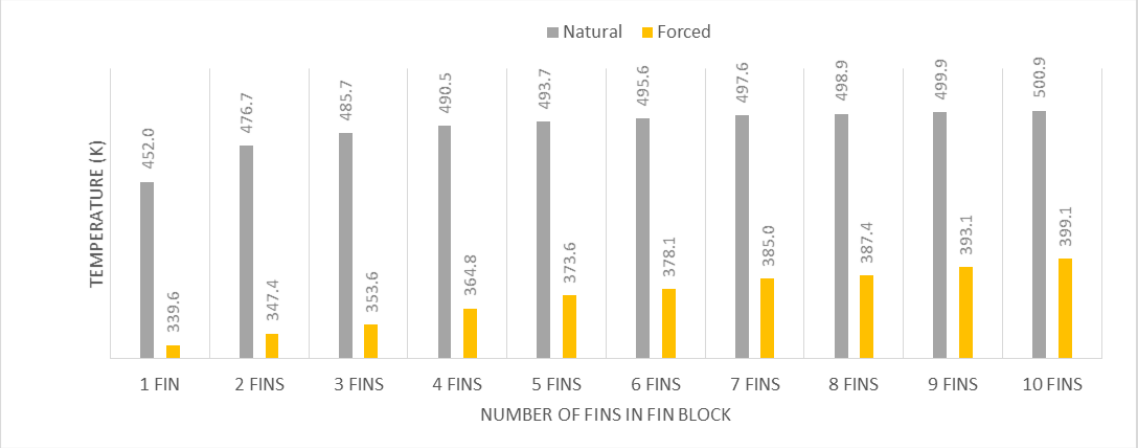

Figure 4.25 Average surface temperatures of fin blocks for constant heat flux for natural and forced convection cooling

The heat transfer augmentation ratio results for different number of fins are shown in Figure 4.26.

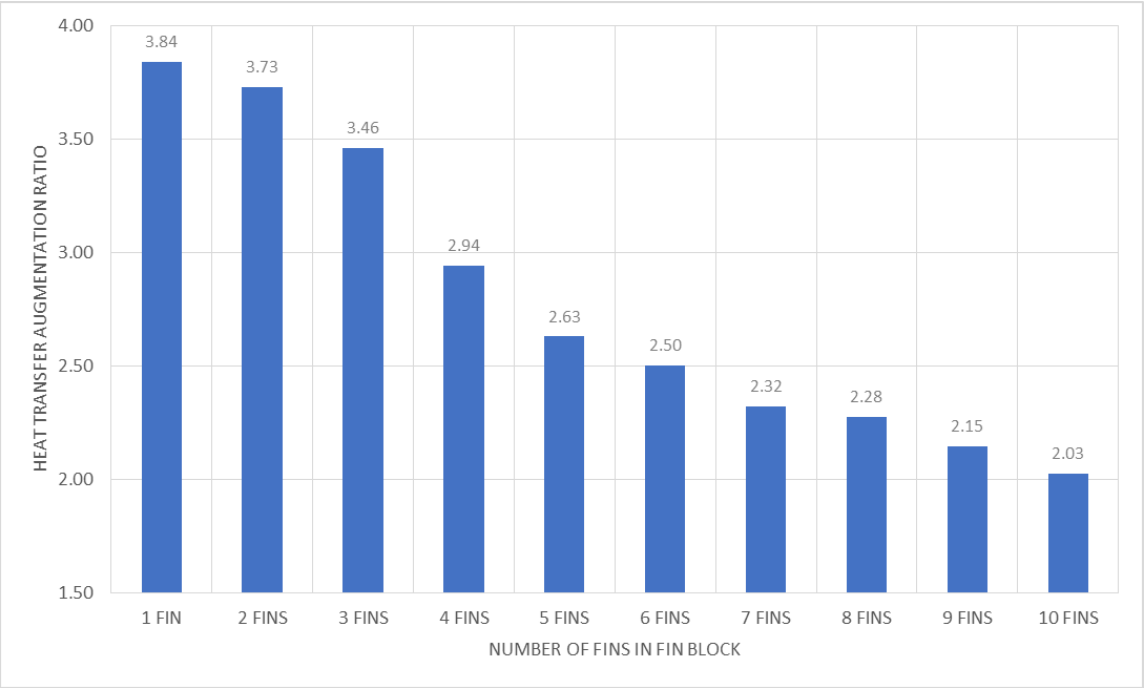

Figure 4.26 Heat transfer augmentation ratio for constant heat flux

According to these results, the highest heat transfer augmentation ratio is obtained for 1-fin-block. Then as in the constant total heat boundary condition solution, the value of the heat transfer augmentation ratio decreases as the number of fins increase. When examined as a percentage, a decline in augmentation ratio is relatively sharper from 3-fin-block to 5-fin-block then it becomes smoother.

The differences between the average surface temperatures of fins obtained under natural convection and obtained under the forced convection created by the piezoelectric fan are given in Figure 4.27.

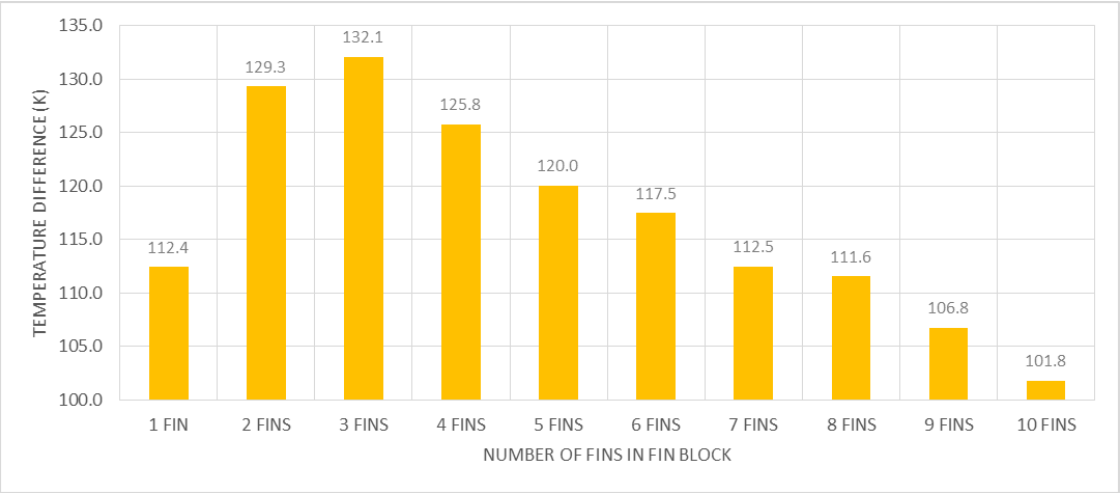

Figure 4.27 Temperature difference between natural and forced convection for constant heat flux

As a result of the natural and forced convection solutions, when the average fin block temperatures are compared, the highest average temperature difference is found to be in the 3-fin-block case contradictorily to the results in Section 4.2. Then the resulting differences decrease with an increasing number of fins and the minimum value was reached for the 10-fin-block case. When these results are examined, the 1-fin-block and the 7-fin-block perform approximately the same amount of average surface temperature difference, although the heat transfer augmentation ratio is the highest in 1-fin-block. 2-fin-block and 4-fin-block have seen similar total average surface temperature difference.

The base temperatures of fin blocks cooled down under the forced convection generated by the piezoelectric fan is given in Figure 4.28.

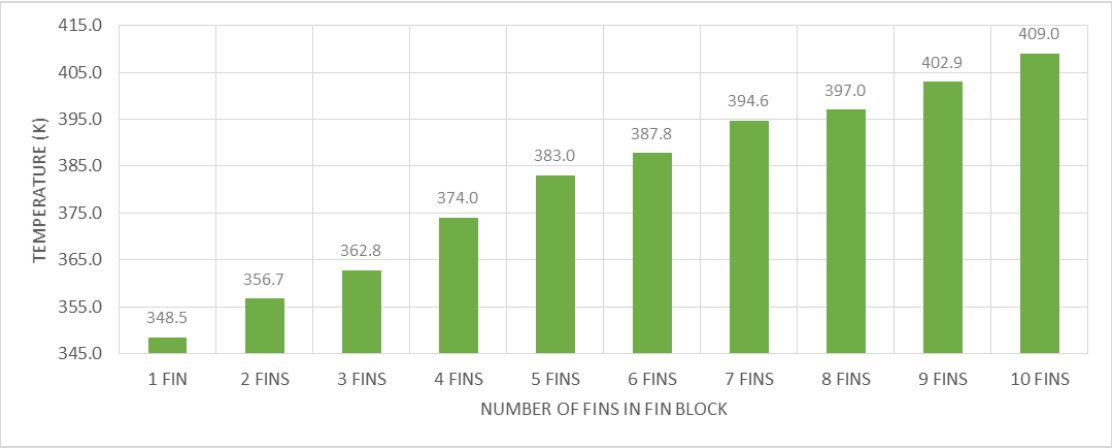

Figure 4.28 Base temperature of the fin blocks

As explained in Section 4.2 the base temperature is important for electronic equipment. When Figure 4.28 is examined, it is observed that the base temperature of the fin block increases constantly with increasing number of fins from 1-fin-block to 10-fin-block configuration. For constant heat flux boundary condition, it is seen that 10-fin-block configuration has the highest average base temperature. In real applications, the number of fins in a fin block can be chosen form a similar figure to the one presented with Figure 4.28 according to desired base temperature criterion.

4.4 Results for Constant Total Heat Boundary Condition with Vertical Fan Arrangement

In this section, the effects of the orientation of the piezoelectric fan on cooling performance are investigated by rotating the fan by 90 degrees. For this case, a constant 0.8064 W heat was applied to the base of the each fin block as a boundary condition as explained in Section 4.2. The transient solution with the forced convection, i.e., with fan movement, was started after cooling simulation with natural convection condition. A pseudo-steady state was obtained for the average surface temperature of the fin block under the flow generated by the piezoelectric fan vibration with vertical fan arrangement. This solution was repeated for 2, 5 and 10-fin-block configurations.

The average surface temperature of the 2-fin-block was fixed at 344.36 K after the piezoelectric fan was vibrated while the natural convection steady-state solution was 394.04 K. In this case, heat transfer augmentation ratio;

$$\xi = \frac{h_{pf}}{h_n} = \frac{\frac{q_s}{T_{s,pf} - T_a}}{\frac{q_s}{T_{s,n} - T_a}} = \frac{T_{s,n} - T_a}{T_{s,pf} - T_a} = \frac{394.04 - 300}{344.36 - 300} = 2.12 \qquad (16)$$

For the 2-fin-block, the result is 2.12 times better cooling performance than the natural convection under the flow generated by the piezoelectric fan.

The change in the average surface temperature values of the fin block for both horizontal and vertical fan arrangements as a function of time of transient solution after the natural convection solution are shown in Figure 4.29. It is seen that the horizontal arrangement provides a more effective cooling for the same fin configuration.

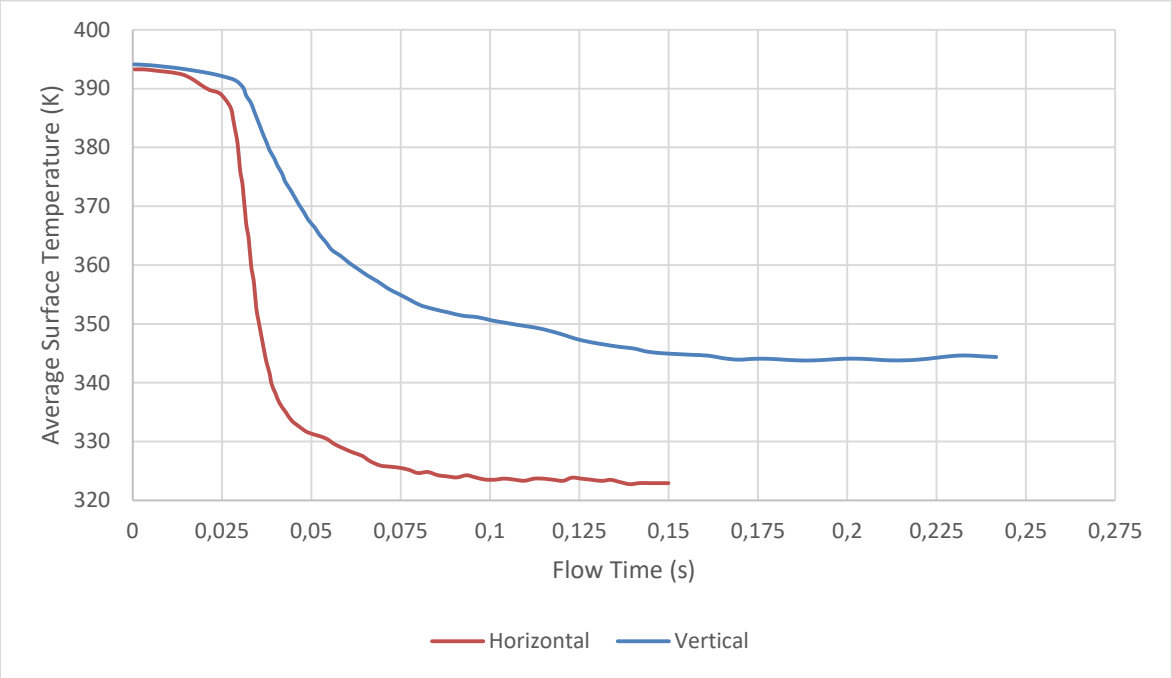

Figure 4.29 Average surface temperature of 2-fin-block for constant total heat

The temperature distributions with and without a piezoelectric fan for the 2-fin-block are shown in Figure 4.30. The temperature distribution for the other fin block configurations are given in Appendix C.

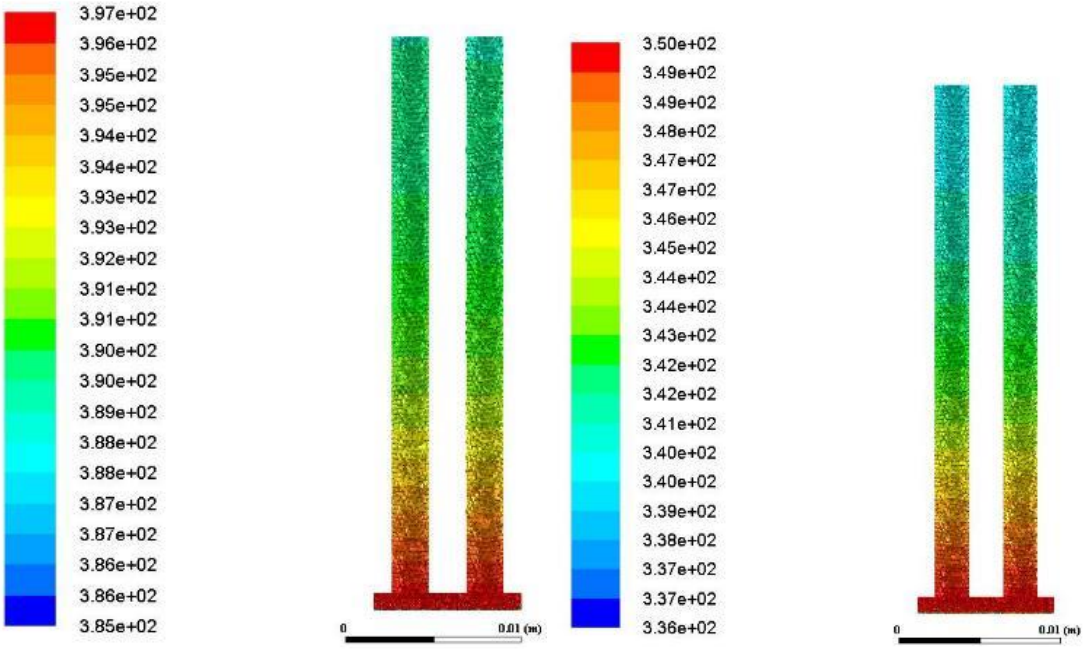

(a) (b)

Figure 4.30 Temperature distribution (in K) of 2-fin-block after natural convection (a) and piezoelectric fan cooling (b)

Table 4-3 shows the tabulated results for the average temperatures of the surface of the fin blocks consisting of fins of 2, 5 and 10. The results in the table are given after the steady state solution under natural convection and after the pseudo-steady state solution under forced convection by the flow created by the piezoelectric fan.

Table 4-3 Average surface temperatures of fin blocks for constant total heat

Boundary Condition 50400 W/m2	Average Surface Temperature of the Fin Block After Natural Convection Cooling	Average Surface Temperature of the Fin Block After Piezoelectric Fan Cool Down	Heat Transfer Augmentation Ratio
2 Fins	394.04	344.36	2.12
5 Fins	345.34	319.46	2.33
10 Fins	324.66	310.29	2.40

The average surface temperature results are given in Figure 4.31.

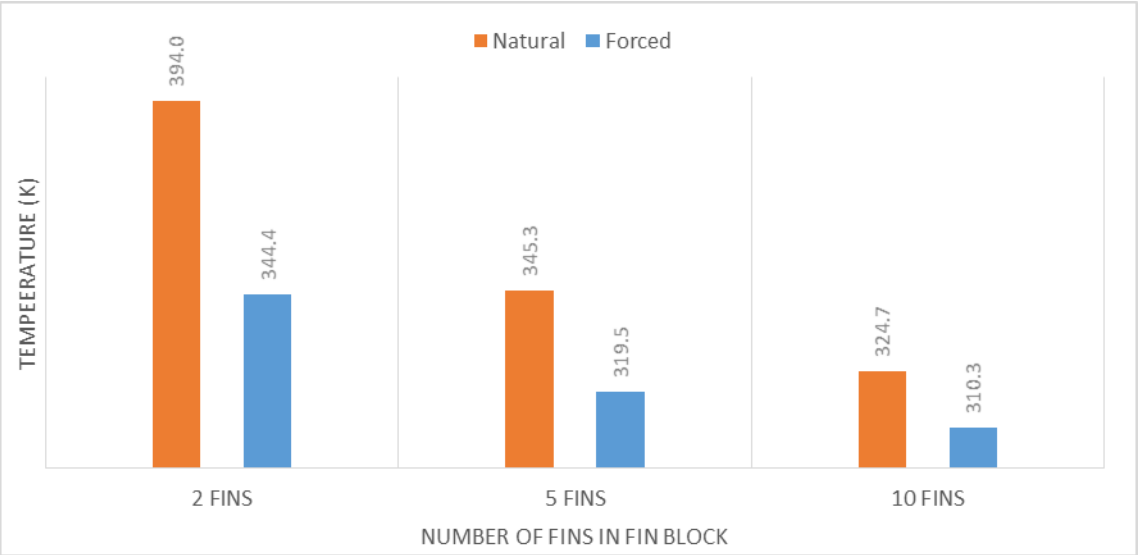

Figure 4.31 Average surface temperatures of fin blocks for constant total heat

The heat transfer augmentation ratio results are given in Figure 4.32.

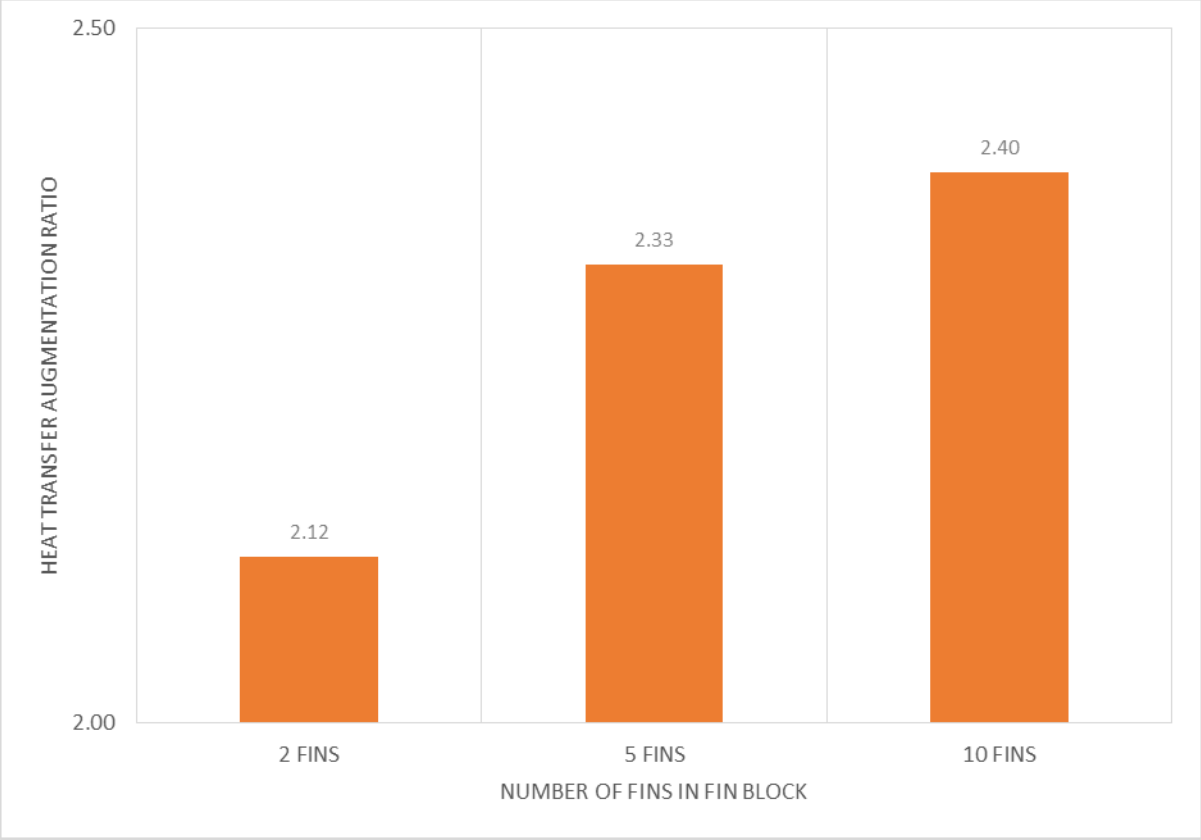

Figure 4.32 Heat transfer augmentation ratio for constant total heat

According to these results, the heat transfer augmentation ratio for 10-fin-block configuration is higher than 2 and 5-fin-block configuration and contradicting the results discussed in Section 4.2. When compared with horizontal fan arrangement, these values are lower than the horizontal fan configurations. Also average surface temperatures for vertical fan arrangement is higher than horizontal fan arrangement. So it can be concluded that, for this fin geometry, for all fin configurations vertical fan arrangement could provide a lower heat transfer performance. According to the fin geometry studied in the thesis, the horizontal arrangement shows better thermal cooling results. The reason is that the height of the fin is 30 mm and the width of the fan is 12.7 mm.

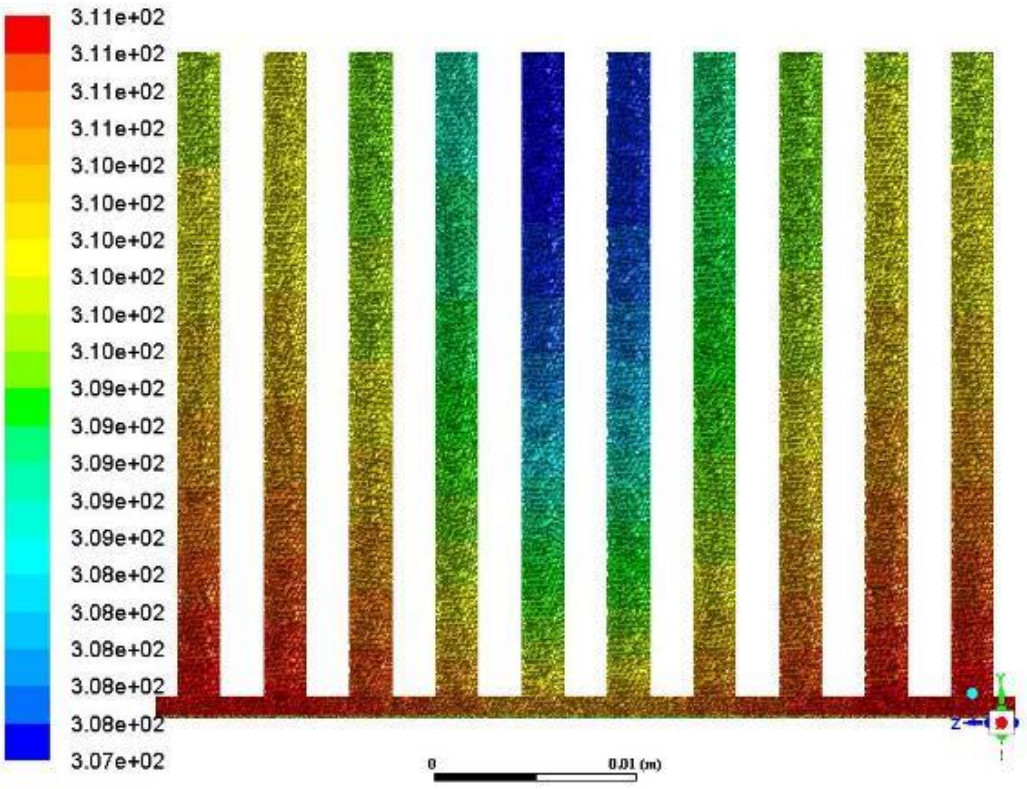

(a)

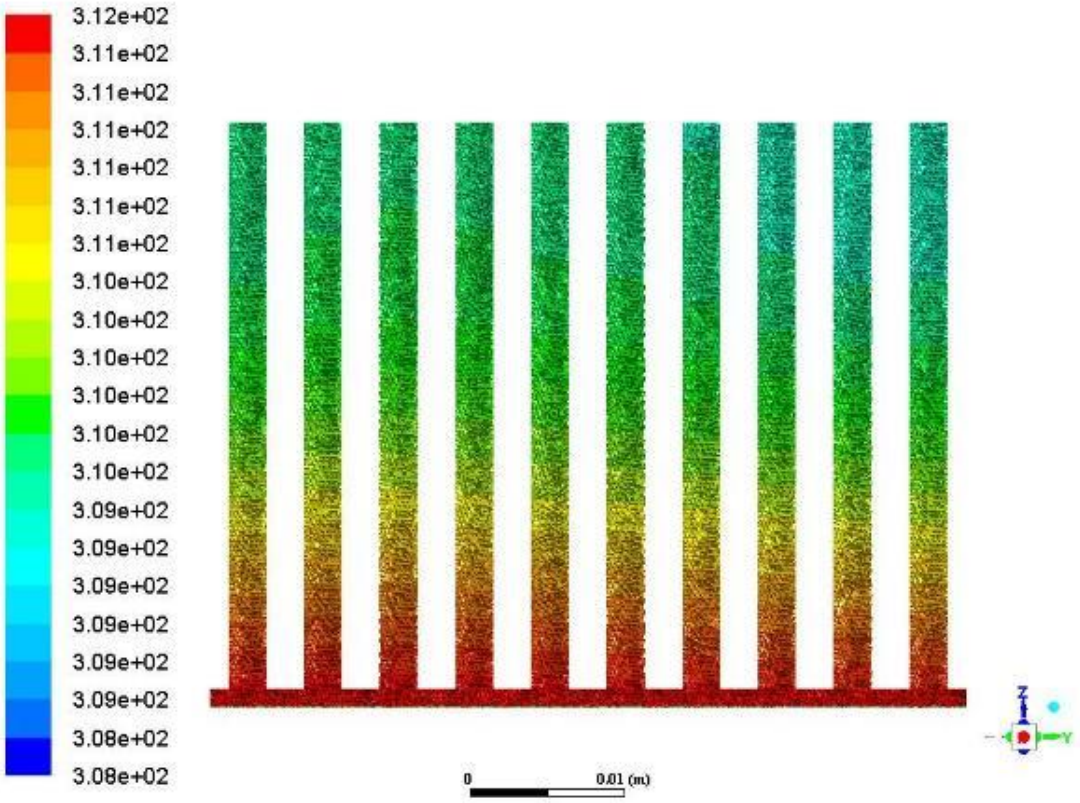

(b)

Figure 4.33 Temperature distribution (in K) of 10-fin-block for constant total heat boundary condition with (a) horizontal and (b) vertical fan arrangement

As shown in Figure 4.33, only the middle part of the fin block can be cooled, and the top and bottom parts are not sufficiently cooled for vertical fan arrangement. In the horizontal fan arrangement, the middle fins in the fin block are found to be having lower temperature values compared to the values of outside fins, however in the vertical fan arrangement it is hard to distinguish the fins from each other by referring their temperature values. Although the temperature distributions are different for 10-fin-block, the heat transfer augmentation ratio is same since the average surface temperature is same for both vertical and horizontal fan arrangement. The heat transfer augmentation ratio values which are given in Table 4-4 show that the difference between horizontal and vertical fan arrangements, while it is substantial for 2-fin-block, the difference decreases for 5-fin-block and 10-fin-block. In addition, in 10-fin-block configuration there is almost no difference is achieved between cooling performances. This means the

performance of vertical fan arrangement is getting closer to the one of horizontal fan arrangement when the number of fins in a fin block is increasing.

Table 4-4 Heat transfer augmentation ratio comparison between horizontal and vertical fan arrangement

Boundary Condition 50400 W/m^2	Heat Transfer Augmentation Ratio for Horizontal Fan Arrangement	Heat Transfer Augmentation Ratio for Vertical Fan Arrangement
2 Fins	4.04	2.12
5 Fins	3.11	2.33
10 Fins	2.51	2.40

4.5 Results for Constant Heat Flux Boundary Condition with Vertical Fan Arrangement

In this section, the orientation of the piezoelectric fan is changed by rotating it by 90 degrees to investigate its effects on cooling performance with constant heat flux boundary condition. For this case a fixed 50400 W/m^2 heat flux was applied to the base of the each fin block as a boundary condition as explained in Section 4.3. The transient solution with the forced convection was started after cooling with natural convection. A pseudo-steady state was obtained for the average surface temperature of the fin block under the flow generated by the piezoelectric fan vibration with vertical fan arrangement. This solution was repeated for 2, 5 and 10-fin-block configurations similarly in Section 4.4.

The average surface temperature of the 2-fin-block was fixed at 387.4K after the piezoelectric fan was vibrated while the natural convection steady-state solution was 477.2K. In this case, heat transfer augmentation ratio;

$$\xi = \frac{h_{pf}}{h_n} = \frac{\dfrac{q_s}{T_{s,pf} - T_a}}{\dfrac{q_s}{T_{s,n} - T_a}} = \frac{T_{s,n} - T_a}{T_{s,pf} - T_a} = \frac{477.2 - 300}{387.4 - 300} = 2.03 \qquad (17)$$

For the 2-fin-block, the result is 2.03 times better cooling than the natural convection under the flow generated by the piezoelectric fan.

The change in the transient average surface temperature values of the fin block for horizontal and vertical fan arrangements are shown in Figure 4.34 in which the initial values show the natural convection solution. It is seen that the horizontal fan arrangement delivers faster and more effective cooling for the condition under investigation.

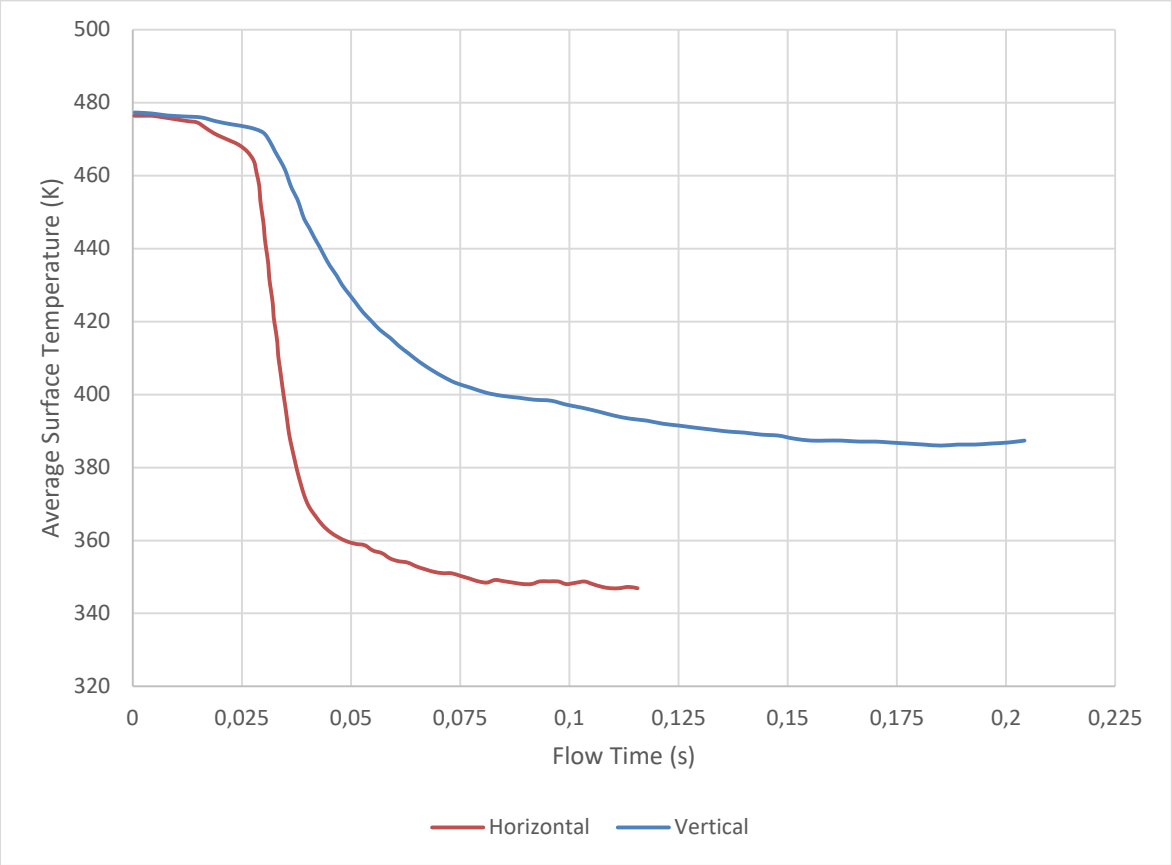

Figure 4.34 Average surface temperature of 2-fin-block for constant heat flux for horizontal and vertical fan arrangement

The temperature distributions with and without a piezoelectric fan for the 2-fin-block is shown in Figure 4.35. The temperature distribution for the other fin block configurations are given in Appendix D.

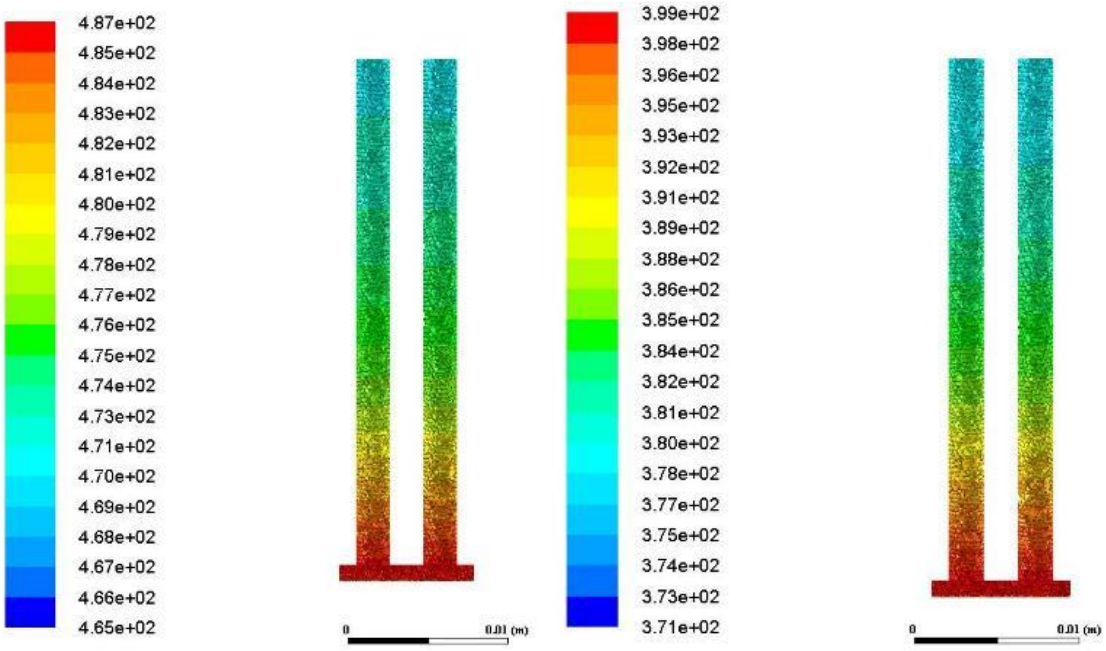

(a) (b)

Figure 4.35 Temperature distribution (in K) of 2-fin-block after natural convection (a) and piezoelectric fan cooling (b)

Table 4-5 shows the tabulated results for the average temperatures of the surface of the fin blocks consisting of fins of 2, 5 and 10. The results in the table are given after the steady state solution under natural convection and after the pseudo-steady state solution under forced convection by the flow created by the piezoelectric fan.

Table 4-5 Average surface temperatures of fin blocks for constant heat flux

Boundary Condition 50400 W/m2	Average Surface Temperature of the Fin Block After Natural Convection Cooling	Average Surface Temperature of the Fin Block After Piezoelectric Fan Cool Down	Heat Transfer Augmentation Ratio
2 Fins	477.20	387.40	2.03
5 Fins	493.60	395.22	2.03
10 Fins	495.96	402.47	1.91

The average surface temperature results are given in Figure 4.36.

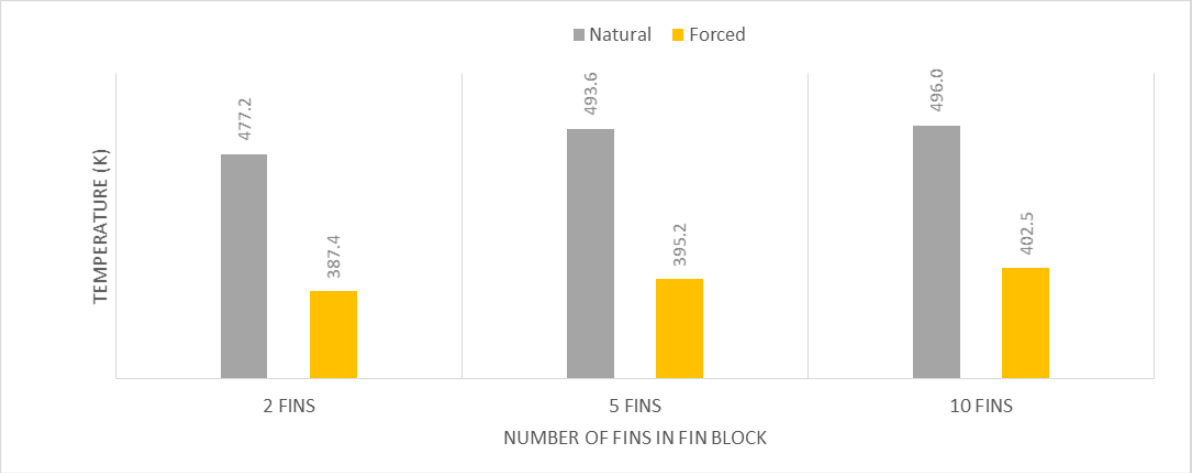

Figure 4.36 Average surface temperatures of fin blocks for constant heat flux

The heat transfer augmentation ratio results are given in Figure 4.37.

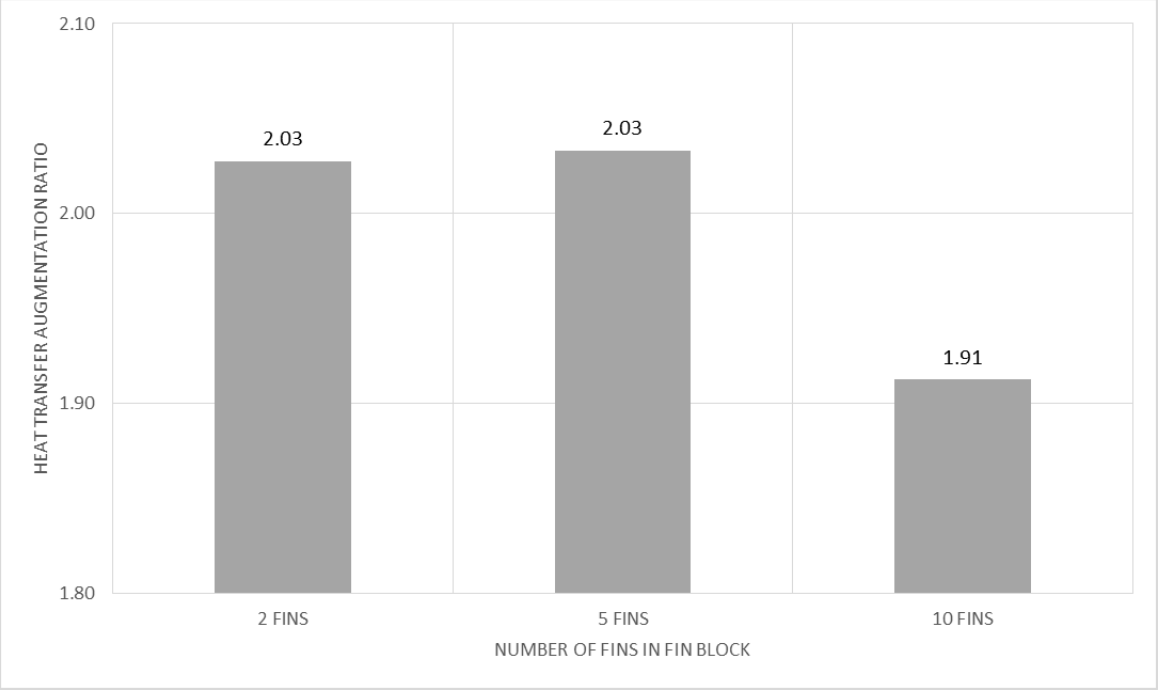

Figure 4.37 Heat transfer augmentation ratio for constant heat flux

According to these results, there is no difference in heat transfer augmentation ratio for 2 and 5-fin-block configurations. The heat transfer augmentation ratio for 10-fin-block configuration is lower than 2 and 5-fin-block configuration. When compared with horizontal fan arrangement, these values are lower than the

horizontal fan configurations. Also the average surface temperatures for vertical fan arrangement are higher than the ones with horizontal fan arrangement. So it can be concluded that, for this fin geometry, for all fin configurations vertical fan arrangement have worse heat transfer performance as in Section 4.4. According to the fin geometry studied in the thesis, the horizontal arrangement shows better thermal cooling results. The reason is that the height of the fin is 30 mm and the width of the fan is 12.7 mm.

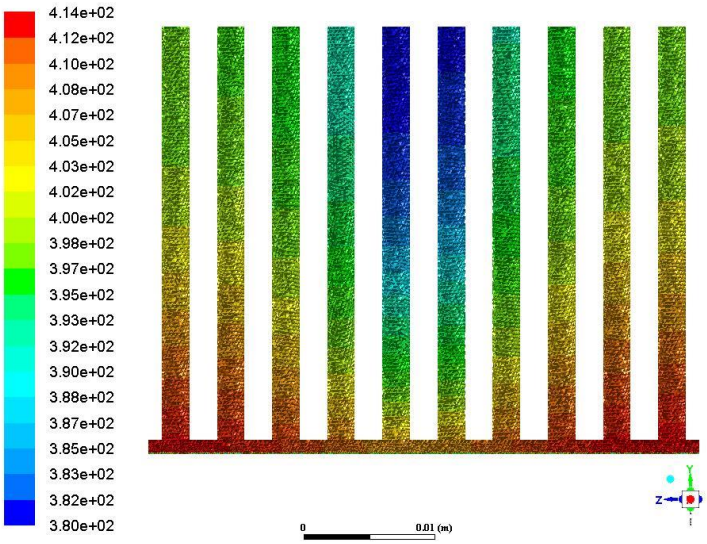

(a)

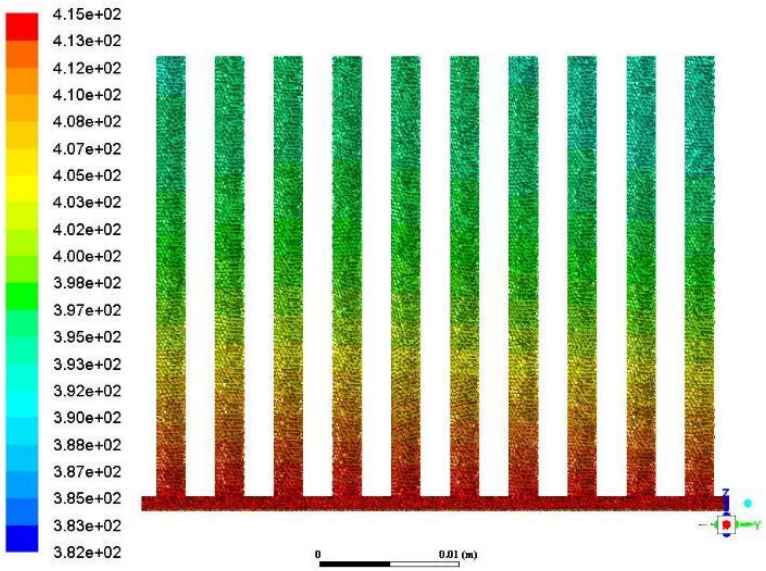

(b)

Figure 4.38 Temperature distribution (in K) of 10-fin-block for constant heat flux boundary condition with (a) horizontal and (b) vertical fan arrangement

As shown in Figure 4.38, the lower temperature values in the middle part of the fin block are seen for the horizontal fan orientation while it is visually hard to distinguish the temperature differences amongst fins in the vertical fan orientation. Although the temperature distributions are different for 10-fin-block, the heat transfer augmentation ratio is same since the average surface temperature is same for both vertical and horizontal fan arrangement. The heat transfer augmentation ratio values are given in Table 4-6 show that the difference between horizontal and vertical fan arrangement significant for 2-fin-block and 5-fin-block cases, whereas it is relatively low for the case with 10-fin-block. Additionally, it can be concluded that there is almost no difference between cooling performances for different fan orientations in 10-fin-block configuration. This suggests that the performance of vertical fan arrangement is getting closer to the one of horizontal fan arrangement when the number of fins in fin blocks is increasing similarly as in the Section 4.4.

Table 4-6 Heat transfer augmentation ratio comparison between horizontal and vertical fan arrangement

Boundary Condition 50400 W/m^2	Heat Transfer Augmentation Ratio for Horizontal Fan Arrangement	Heat Transfer Augmentation Ratio for Vertical Fan Arrangement
2 Fins	3.73	2.03
5 Fins	3.63	2.03
10 Fins	2.03	1.91

CHAPTER 5
CONCLUSIONS AND FUTURE WORK

In this study, forced convection, which occurs under the influence of a commercial piezoelectric fan, is computationally investigated for the fin blocks with changing number of fins.

Two different types of boundary conditions have been applied during this work. First, a total fixed heat load of 0.8064 W was applied to the fin base for each fin configuration. In the second case, 50400 W/m^2 constant heat flux is applied to the fin base for each fin configuration.

As the result of the first boundary condition application, the heat transfer augmentation ratio was the highest in the 2-fin-block at 4.04. This value decreased to 2.48 as the number of fins increased. The maximum temperature difference between the natural and the forced convection conditions is found to be 112.42 K for 1-fin-block. It then drops with a decreasing slope towards the case of 10-fin-block with increasing number of fins. For the average base temperature, the lowest temperature is obtained as 348.45 K for the 1-fin-block. This value increases uniformly as the number of fins increased and found to be 408.98 K for the 10-fin-block.

As a result of the application of the second type of boundary condition, the maximum heat transfer augmentation ratio was found to be 3.84 for the 1-fin-block. This value decreased to 2.27 as the number of fins increased. Another criterion, the difference between the average surface temperature values for the natural convection and the forced convection condition simulations, is obtained as 132.1 K as the highest of all for 3-fin-block case. Based on this criterion, the best cooling occurs in 3-fin-block and the corresponding temperature difference for the natural and forced convection conditions has a lower value for increasing and decreasing number of fins. For this criterion, the 1-fin result and the 7-fin-block show almost the same result as around 112 K. Another critical criterion for electronic unit cooling is that the base temperature of a fin block. The lowest average base temperature value is found as 348.45 K for the 1-fin-block case. This value then increased by an average of 2.5% with each fin as the number of fins increased. For the 10-fin-block this value is predicted as 101.8 K.

For constant total heat boundary condition with the vertical fan arrangement, the heat transfer augmentation ratio is obtained lower than the one in the horizontal fan arrangement. For example, in 2-fin-block configuration, the heat transfer augmentation ratio is predicted as 4.04 for the horizontal fan arrangement, and 2.12 for the vertical fan arrangement. Similarly, for constant heat flux boundary condition with the vertical fan arrangement, the heat transfer augmentation ratio is shown to be lower than the one in the horizontal fan arrangement. For example, in 2-fin-block configuration, while the heat transfer augmentation ratio is found as 3.73 for the horizontal fan arrangement, it is decreased to 2.03 for the vertical fan arrangement.

The cooling performance of vertical fan arrangement with constant total heat boundary condition is increasing with the increasing number of fins in a fin block, on the contrary the result of horizontal fan arrangement. The cooling performance of vertical fan arrangement with constant heat flux condition is nearly same for all fin configuration. Additionally, there is almost no difference observed in cooling performance for 10-fin-block configuration for two different fan orientations. As a result, horizontal fan arrangement has better cooling performance than vertical fan arrangement for the fin geometries in this study.

For the future work, it is concluded that 3 basic studies can be done in the future.

- Working with a multi-piezoelectric fan structure with different orientations to be used as a prime source
- Creation of different piezoelectric fan geometries depending on fin structure
- Complicated and nested piezoelectric fan and fin design such as given in Figure 5.1

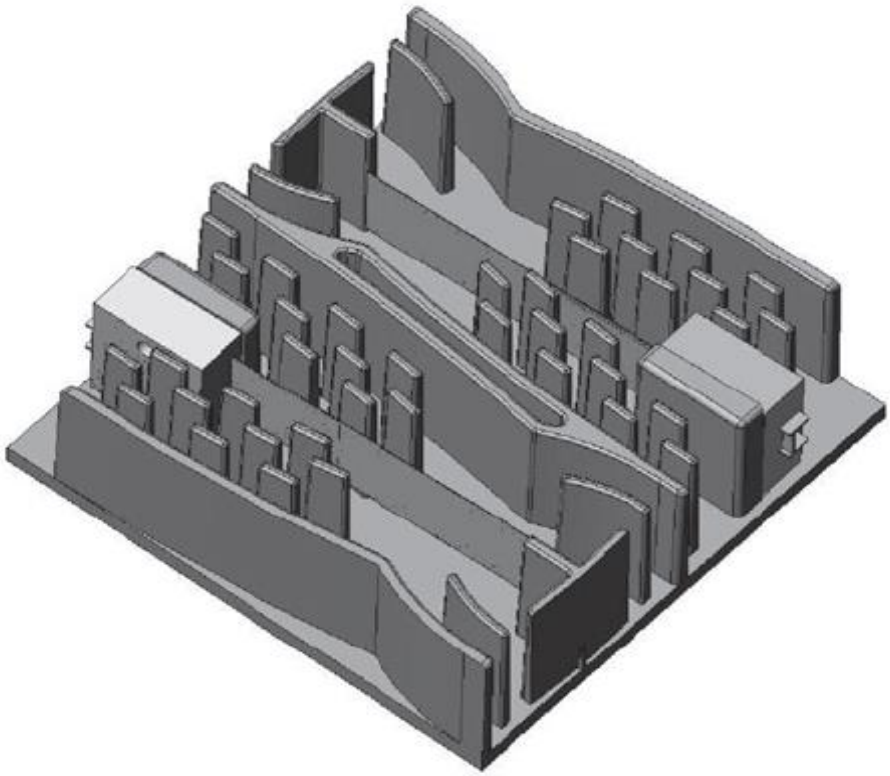

Figure 5.1 Nested fin and piezoelectric fan arrangement example [4]

REFERENCES

[1] R. Hannemann, J. Marsala, and M. Pitasi, “Pumped Liquid Multiphase Cooling,” in *Electronic and Photonic Packaging, Electrical Systems Design and Photonics, and Nanotechnology*, 2004, vol. 2004, pp. 469–473.

[2] X. Zhang *et al.*, “Combined giant inverse and normal magnetocaloric effect for room-temperature magnetic cooling,” *Phys. Rev. B*, vol. 76, no. 13, p. 132403, Oct. 2007.

[3] T. Açikalin, S. V. Garimella, A. Raman, and J. Petroski, “Characterization and optimization of the thermal performance of miniature piezoelectric fans,” *Int. J. Heat Fluid Flow*, vol. 28, no. 4, pp. 806–820, 2007.

[4] J. Petroski, M. Arik, and M. Gursoy, “Optimization of piezoelectric oscillating fan-cooled heat sinks for electronics cooling,” *IEEE Trans. Components Packag. Technol.*, vol. 33, no. 1, pp. 25–31, 2010.

[5] H. K. Ma, H. C. Su, C. L. Liu, and W. H. Ho, “Investigation of a piezoelectric fan embedded in a heat sink,” *Int. Commun. Heat Mass Transf.*, vol. 39, no. 5, pp. 603–609, 2012.

[6] S. F. Liu, R. T. Huang, W. J. Sheu, and C. C. Wang, “Heat transfer by a piezoelectric fan on a flat surface subject to the influence of horizontal/vertical arrangement,” *Int. J. Heat Mass Transf.*, vol. 52, no. 11–12, pp. 2565–2570, 2009.

[7] M. A. Bidakhvidi, S. Vanlanduit, R. Shirzadeh, and D. Vucinic, “Experimental and computational analysis of the flow induced by a piezoelectric fan,” 2012.

[8] M. Kimber, K. Suzuki, N. Kitsunai, K. Seki, and S. V. Garimella, “Pressure and Flow Rate Performance of Piezoelectric Fans,” *IEEE Trans. Components Packag. Technol.*, vol. 32, no. 4, pp. 766–775, 2009.

[9] www.piezo.com, “Fans & resonators 65,” p. 1801, 2011.

[10] M. Toda and S. Osaka, “Vibrational Fan Using the Piezoelectric Polymer Pvf2.,” *Proc. IEEE*, vol. 67, no. 8, pp. 1171–1173, 1979.

[11] T. AÇikalin, S. M. Wait, S. V. Garimella, and A. Raman, “Experimental investigation of the thermal performance of piezoelectric fans,” *Heat Transf. Eng.*, vol. 25, no. 1, pp. 4–14, 2004.

[12] C. H. Huang, Y. F. Chen, and H. Ay, “An inverse problem in determining the optimal position for piezoelectric fan with experimental verification,” *Int. J. Heat Mass Transf.*, vol. 55, no. 19–20, pp. 5289–5301, 2012.

[13] C.-N. Lin, “Analysis of three-dimensional heat and fluid flow induced by piezoelectric fan,” *Int. J. Heat Mass Transf.*, vol. 55, no. 11–12, pp. 3043–3053, 2012.

[14] P. Bürmann, A. Raman, and S. V. Garimella, “Dynamics and topology optimization of piezoelectric fans,” *IEEE Trans. Components Packag. Technol.*, vol. 25, no. 4, pp. 592–600, 2002.

[15] S. F. Sufian, M. Z. Abdullah, M. K. Abdullah, and J. J. Mohamed, “Effect of side and tip gaps of a piezoelectric fan on microelectronic cooling,” *IEEE Trans. Components, Packag. Manuf. Technol.*, vol. 3, no. 9, pp. 1545–1553,

2013.

[16] S. F. Sufian, M. Z. Abdullah, and J. J. Mohamed, “Effect of synchronized piezoelectric fans on microelectronic cooling performance,” *Int. Commun. Heat Mass Transf.*, vol. 43, pp. 81–89, 2013.

[17] M. Choi, C. Cierpka, and Y. H. Kim, “Effects of the distance between a vibrating cantilever pair,” *Eur. J. Mech. B/Fluids*, vol. 43, pp. 154–165, 2014.

[18] M. Kimber, R. Lonergan, and S. V. Garimella, “Experimental study of aerodynamic damping in arrays of vibrating cantilevers,” *J. Fluids Struct.*, vol. 25, no. 8, pp. 1334–1347, 2009.

[19] H. Y. Li and Y. X. Wu, “Heat transfer characteristics of pin-fin heat sinks cooled by dual piezoelectric fans,” *Int. J. Therm. Sci.*, vol. 110, pp. 26–35, 2016.

[20] C. N. Lin, “Heat transfer enhancement analysis of a cylindrical surface by a piezoelectric fan,” *Appl. Therm. Eng.*, vol. 50, no. 1, pp. 693–703, 2013.

[21] H. K. Ma, L. K. Tan, and Y. T. Li, “Investigation of a multiple piezoelectric-magnetic fan system embedded in a heat sink,” *Int. Commun. Heat Mass Transf.*, vol. 59, pp. 166–173, 2014.

[22] H. C. Su, C. L. Liu, T. J. Pan, and H. K. Ma, “Investigation of a multiple-vibrating fan system for electronics cooling,” *Annu. IEEE Semicond. Therm. Meas. Manag. Symp.*, vol. 1, no. c, pp. 110–115, 2013.

[23] M. Kimber and S. V. Garimella, “Measurement and prediction of the cooling characteristics of a generalized vibrating piezoelectric fan,” *Int. J. Heat Mass Transf.*, vol. 52, no. 19–20, pp. 4470–4478, 2009.

[24] M. K. Abdullah *et al.*, “Numerical and experimental investigations on effect of fan height on the performance of piezoelectric fan in microelectronic cooling,” *Int. Commun. Heat Mass Transf.*, vol. 36, no. 1, pp. 51–58, 2009.

[25] M. Choi, S. Y. Lee, and Y. H. Kim, “On the flow around a vibrating cantilever pair with different phase angles,” *Eur. J. Mech. B/Fluids*, vol. 34, pp. 146–157, 2012.

[26] H. K. Ma, L. K. Tan, Y. T. Li, and C. L. Liu, “Optimum thermal resistance of the multiple piezoelectric-magnetic fan system,” *Int. Commun. Heat Mass Transf.*, vol. 55, pp. 77–83, 2014.

[27] M. K. Abdullah *et al.*, “Optimum tip gap and orientation of multi-piezofan for heat transfer enhancement of finned heat sink in microelectronic cooling,” *Int. J. Heat Mass Transf.*, vol. 55, no. 21–22, pp. 5514–5525, 2012.

[28] M. Kimber, K. Suzuki, N. Kitsunai, K. Seki, and S. V. Garimella, “Quantification of piezoelectric fan flow rate performance and experimental identification of installation effects,” *2008 11th IEEE Intersoc. Conf. Therm. Thermomechanical Phenom. Electron. Syst. I-THERM*, pp. 471–479, 2008.

[29] C. N. Lin and J. S. Leu, “Study of thermal and flow characteristics of a heated cylinder under dual piezoelectric fans actuation,” *Int. J. Heat Mass Transf.*, vol. 78, pp. 1008–1022, 2014.

[30] S. F. Sufian, Z. M. Fairuz, M. Zubair, M. Z. Abdullah, and J. J. Mohamed, “Thermal analysis of dual piezoelectric fans for cooling multi-LED packages,”

Microelectron. Reliab., vol. 54, no. 8, pp. 1534–1543, 2014.

[31] H. Y. Li, S. M. Chao, J. W. Chen, and J. T. Yang, “Thermal performance of plate-fin heat sinks with piezoelectric cooling fan,” *Int. J. Heat Mass Transf.*, vol. 57, no. 2, pp. 722–732, 2013.

[32] S. Basak, A. Raman, and S. V. Garimella, “Dynamic Response Optimization of Piezoelectrically Excited Thin Resonant Beams,” *J. Vib. Acoust.*, vol. 127, no. 1, p. 18, 2005.

[33] S. V Garimella, *Analysis and Prediction of the Thermal Performance of Piezoelectrically Actuated Fans Analysis and Prediction of the Thermal Performance of*, vol. 30. 2008.

[34] B. Adrian, *Convection Heat Transfer*, 4th ed. John Wiley & sons, 2013.

APPENDIX A

Constant Total Heat - Temperature Distribution in Transient Solution - Horizontal Fan Arrangement

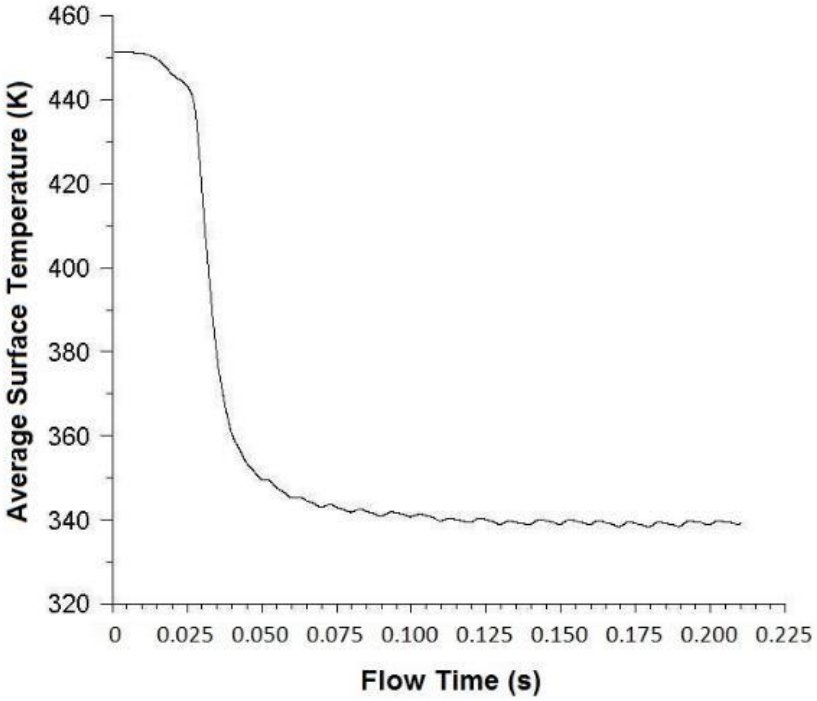

Figure 7.1 Average surface temperature of 1-fin-block

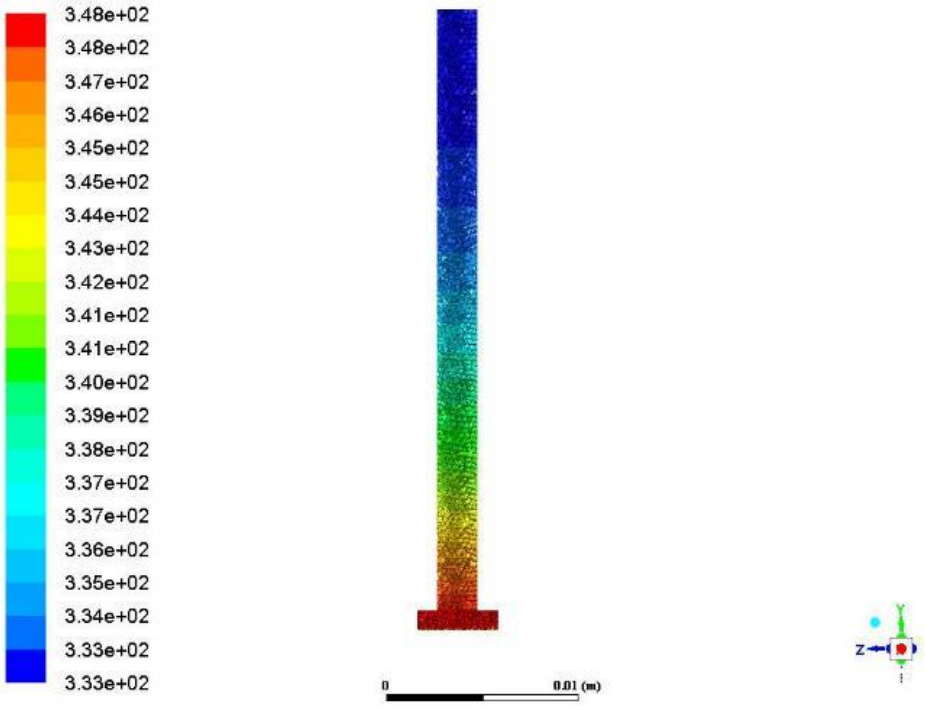

Figure 7.2 Temperature distribution (in K) of 1-fin-block

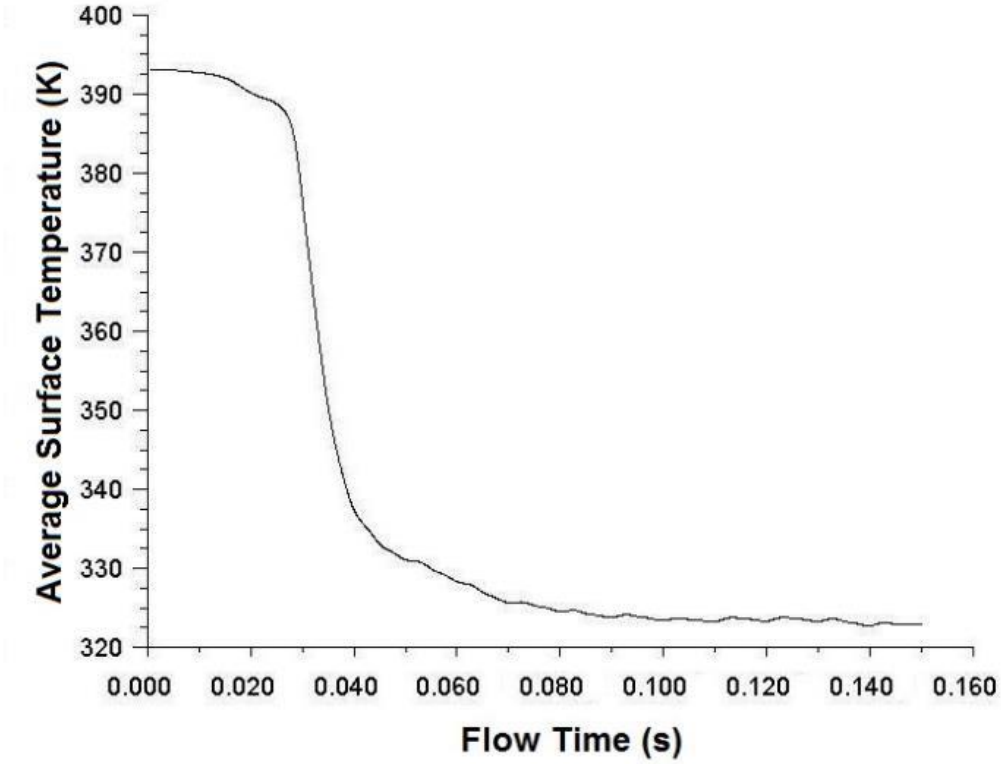

Figure 7.3 Average surface temperature of 2-fin-block

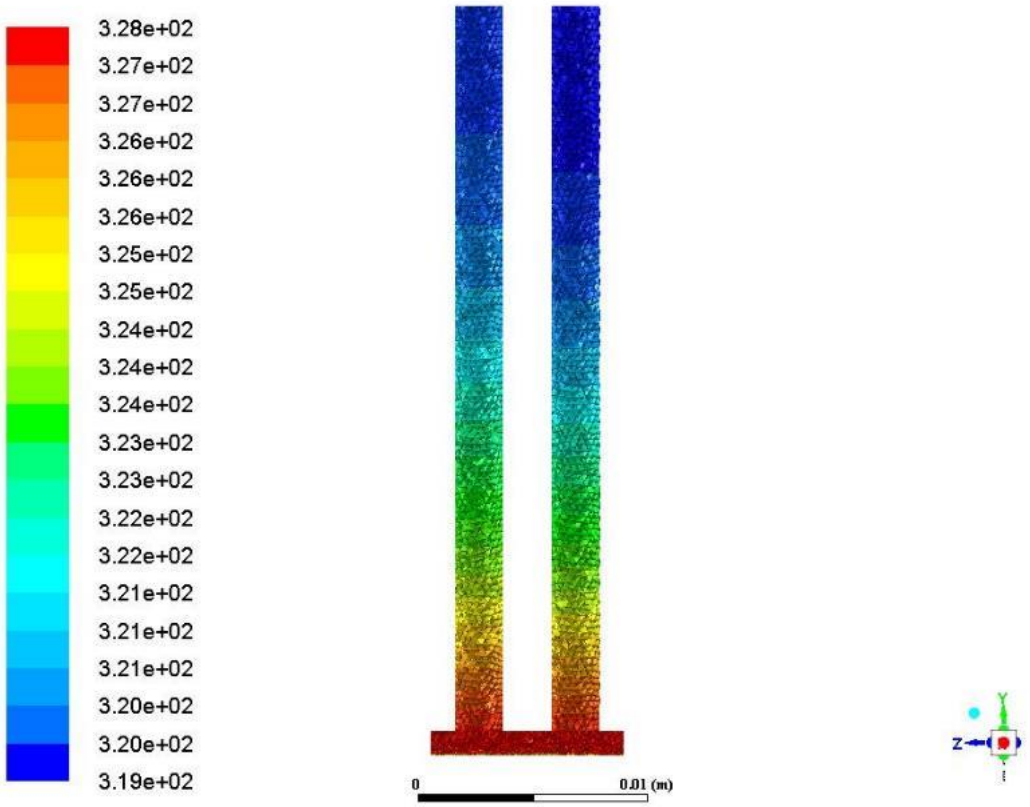

Figure 7.4 Temperature distribution (in K) of 2-fin-block

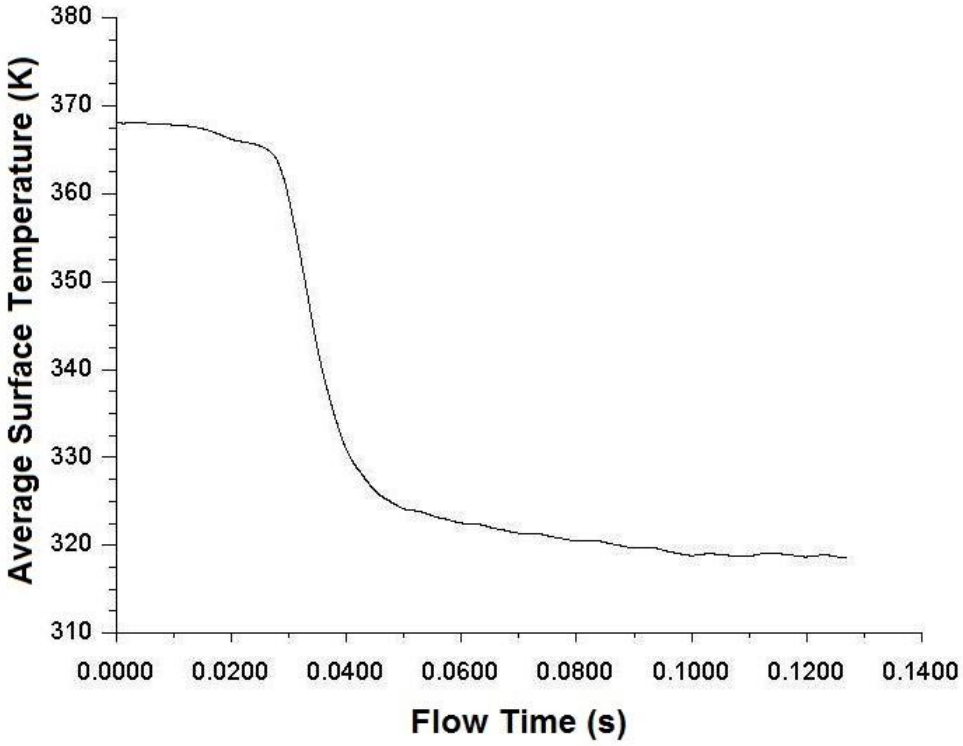

Figure 7.5 Average surface temperature of 3-fin-block

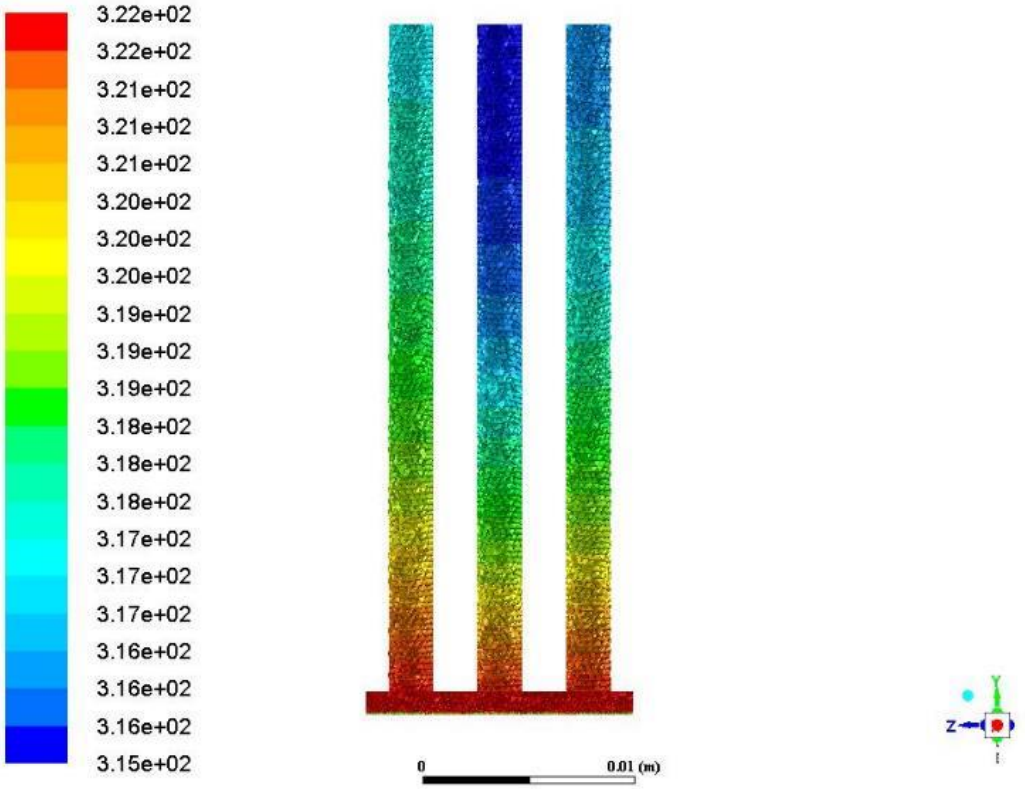

Figure 7.6 Temperature distribution (in K) of 3-fin-block

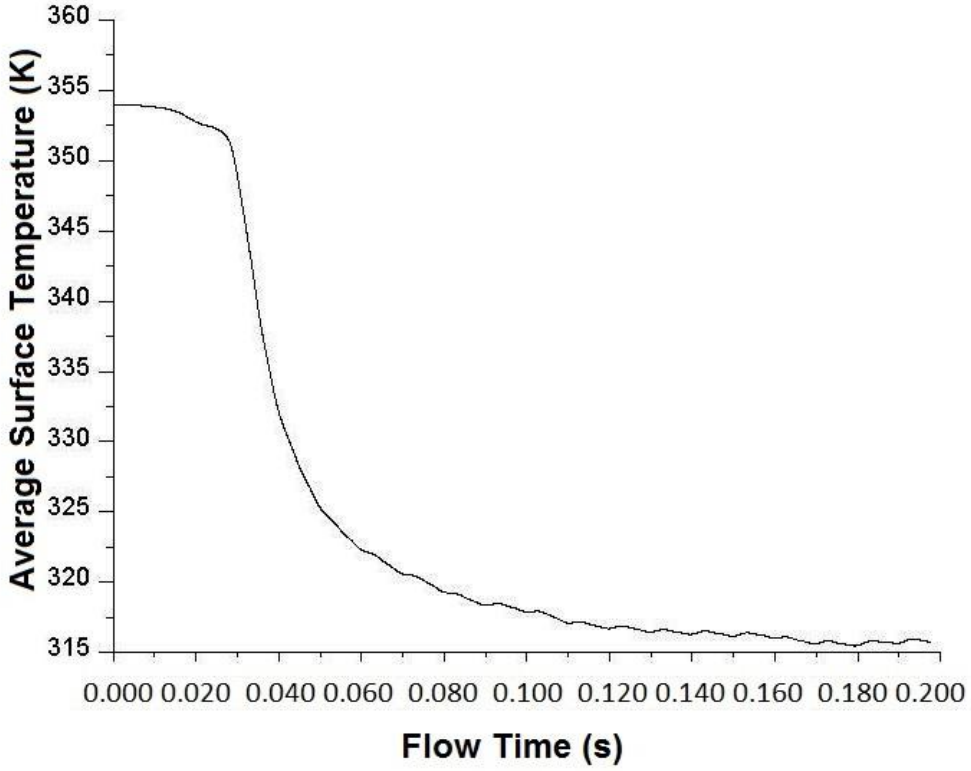

Figure 7.7 Average surface temperature of 4-fin-block

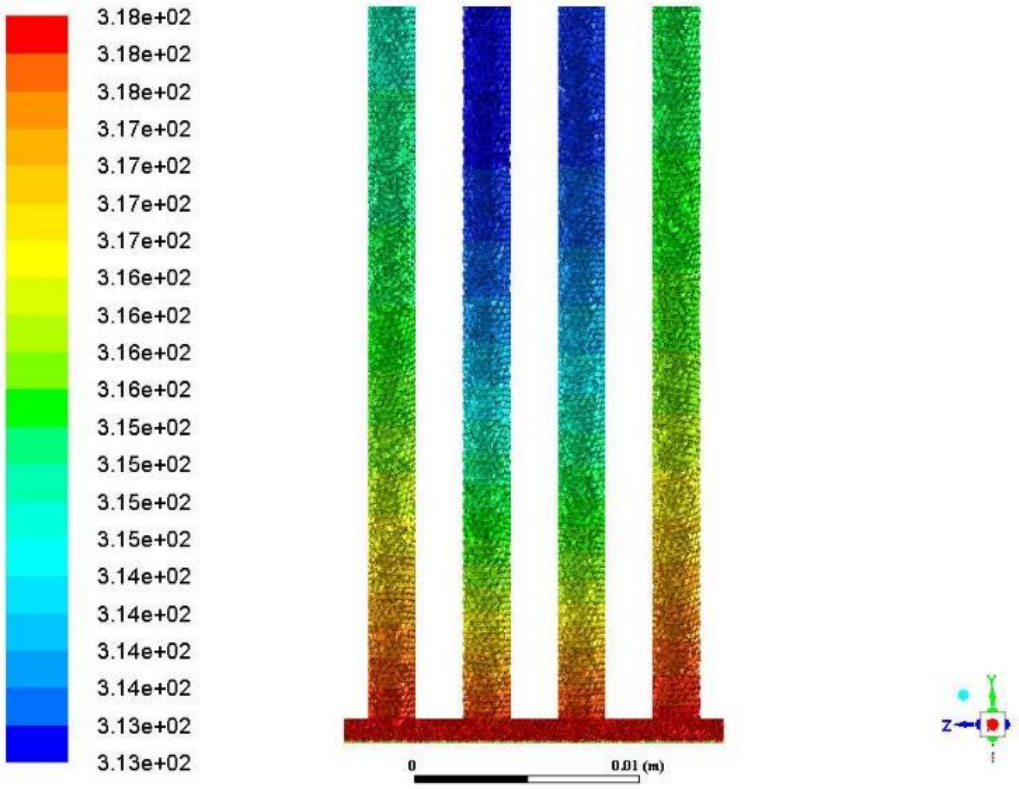

Figure 7.8 Temperature distribution (in K) of 4-fin-block

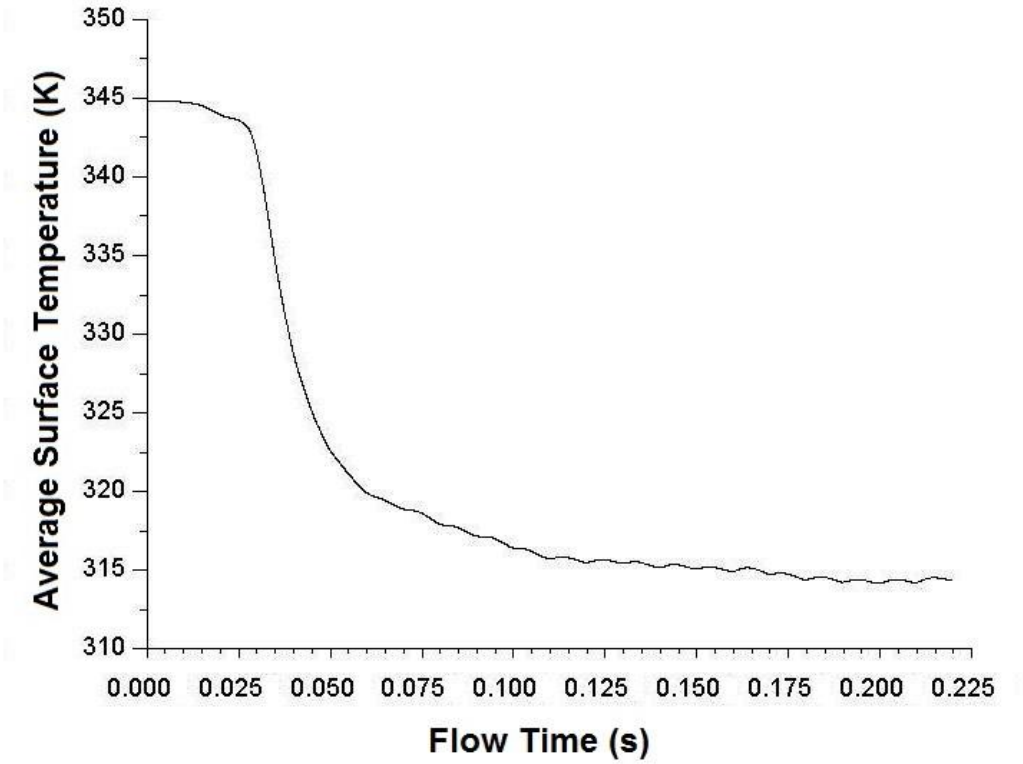

Figure 7.9 Average surface temperature of 5-fin-block

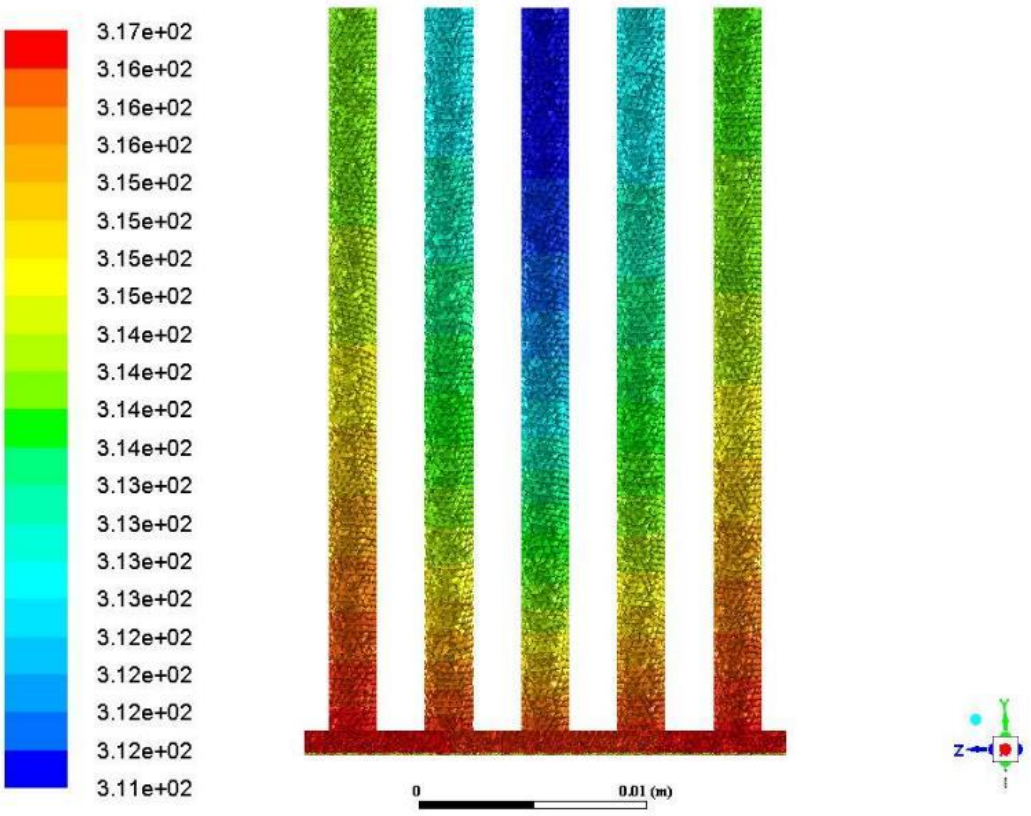

Figure 7.10 Temperature distribution (in K) of 5-fin-block

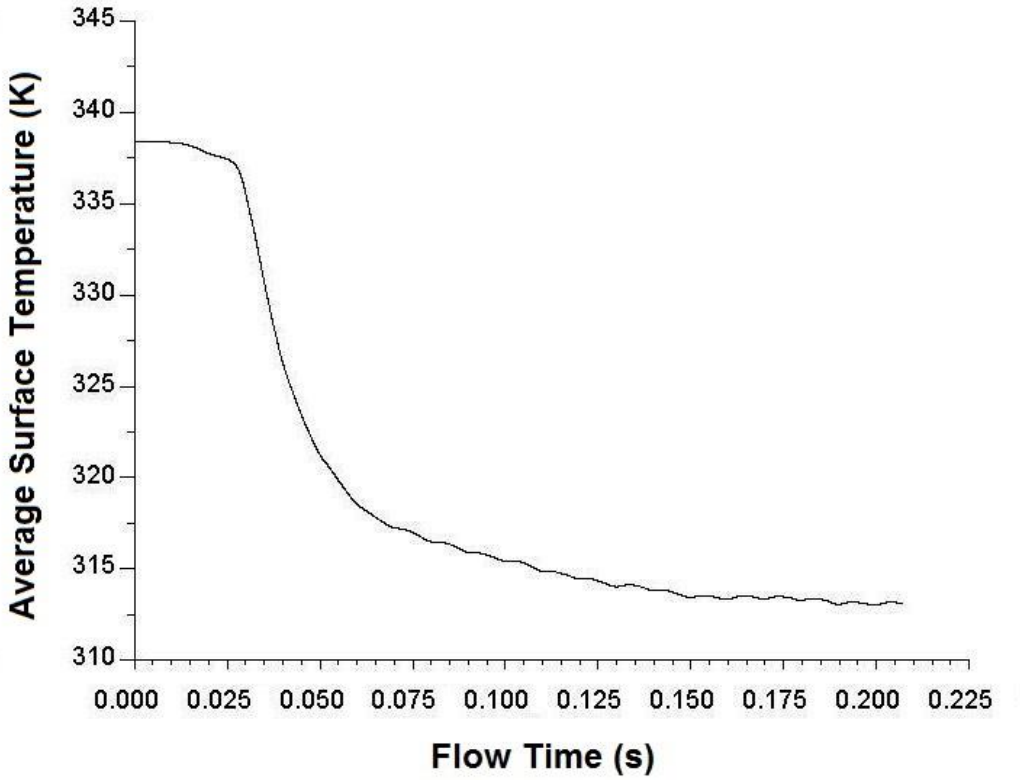

Figure 7.11 Average surface temperature of 6-fin-block

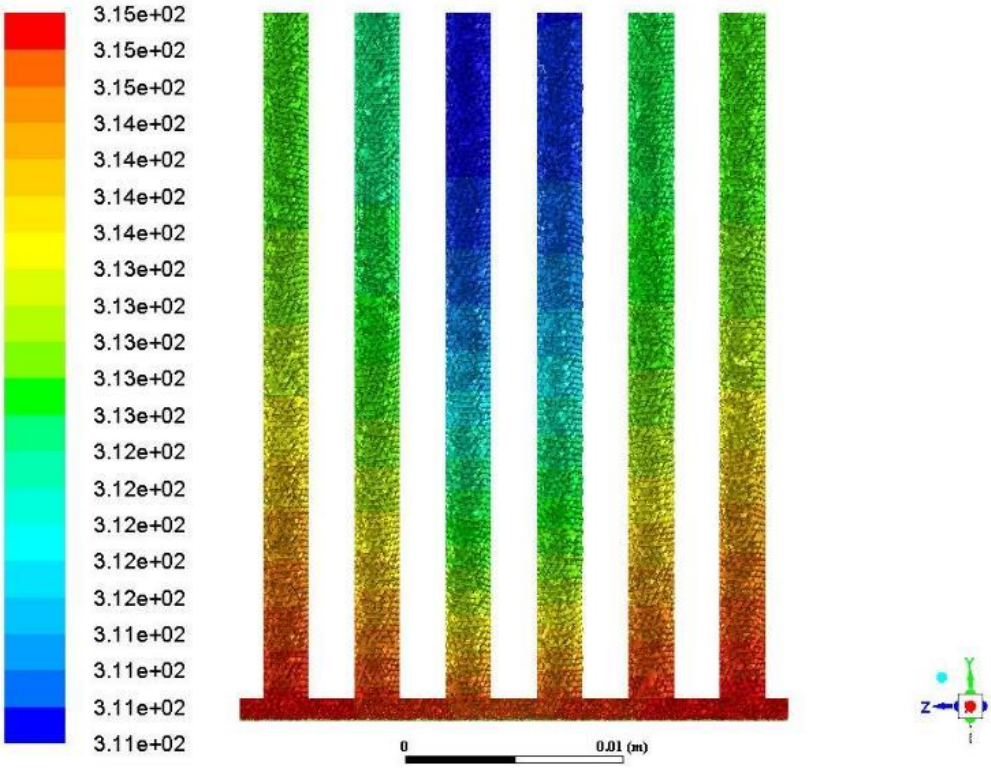

Figure 7.12 Temperature distribution (in K) of 6-fin-block

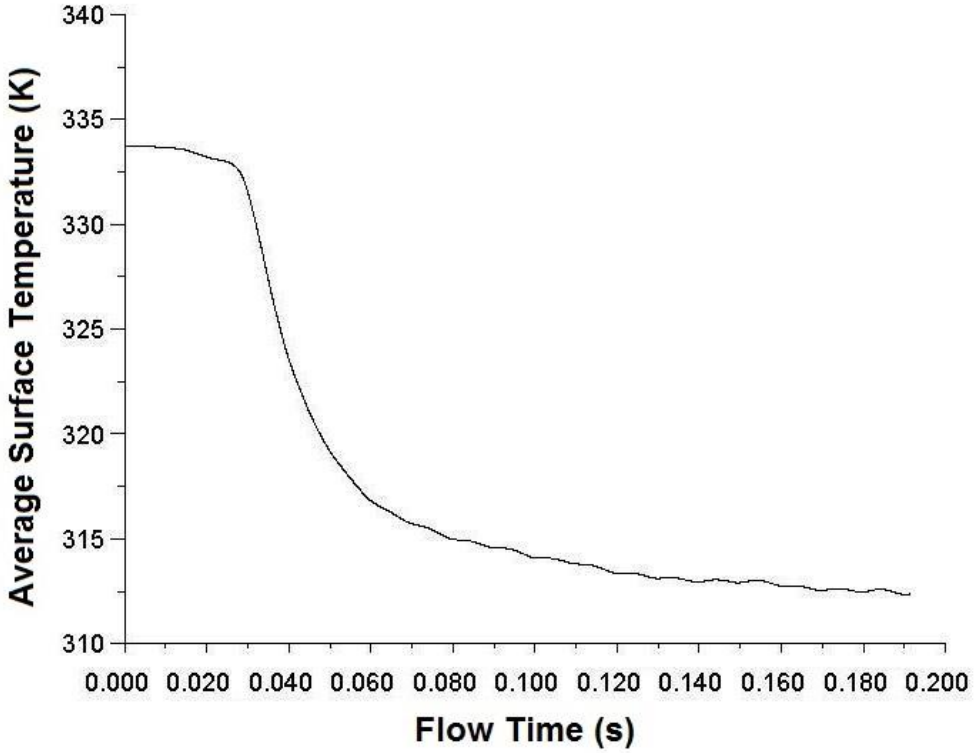

Figure 7.13 Average surface temperature of 7-fin-block

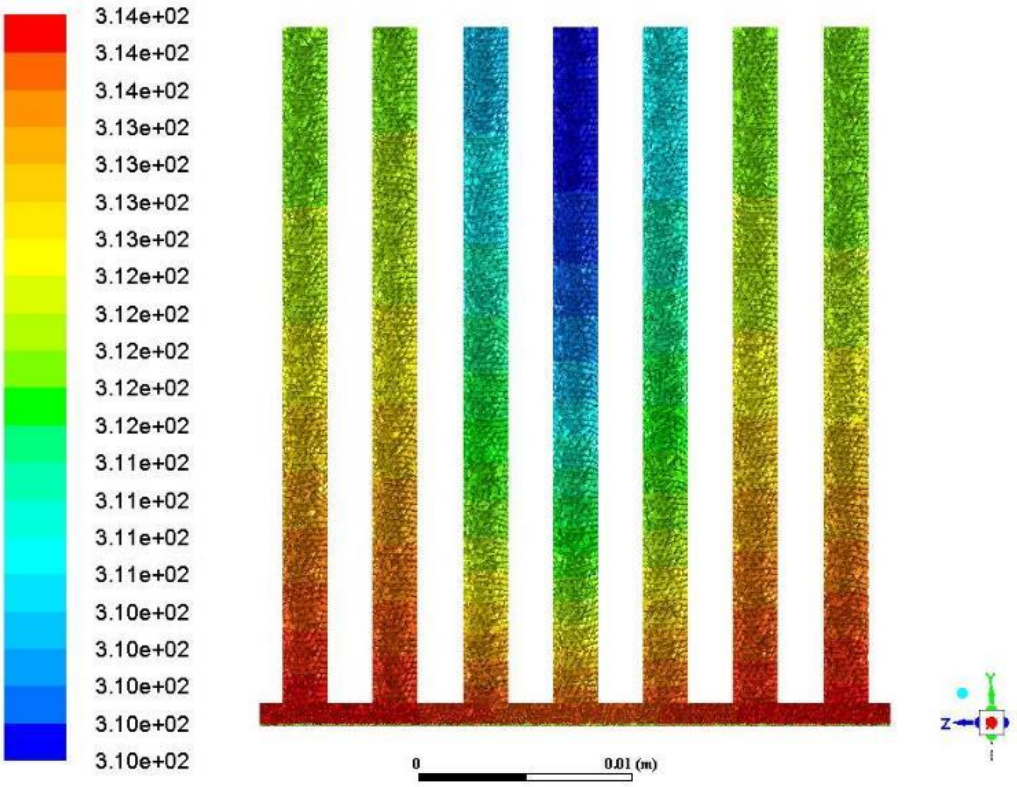

Figure 7.14 Temperature distribution (in K) of 7-fin-block

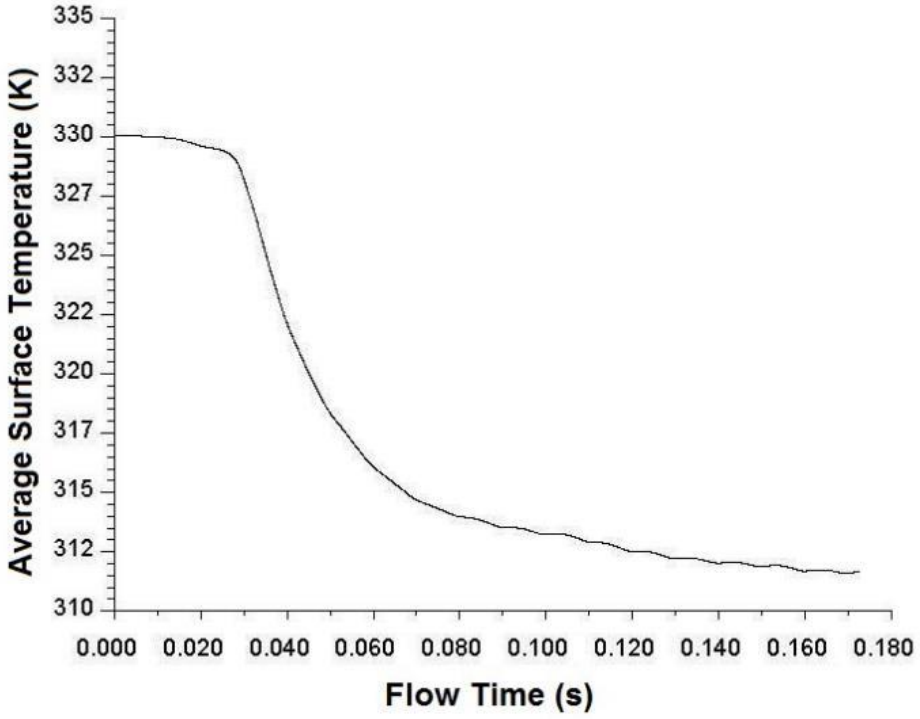

Figure 7.15 Average surface temperature of 8-fin-block

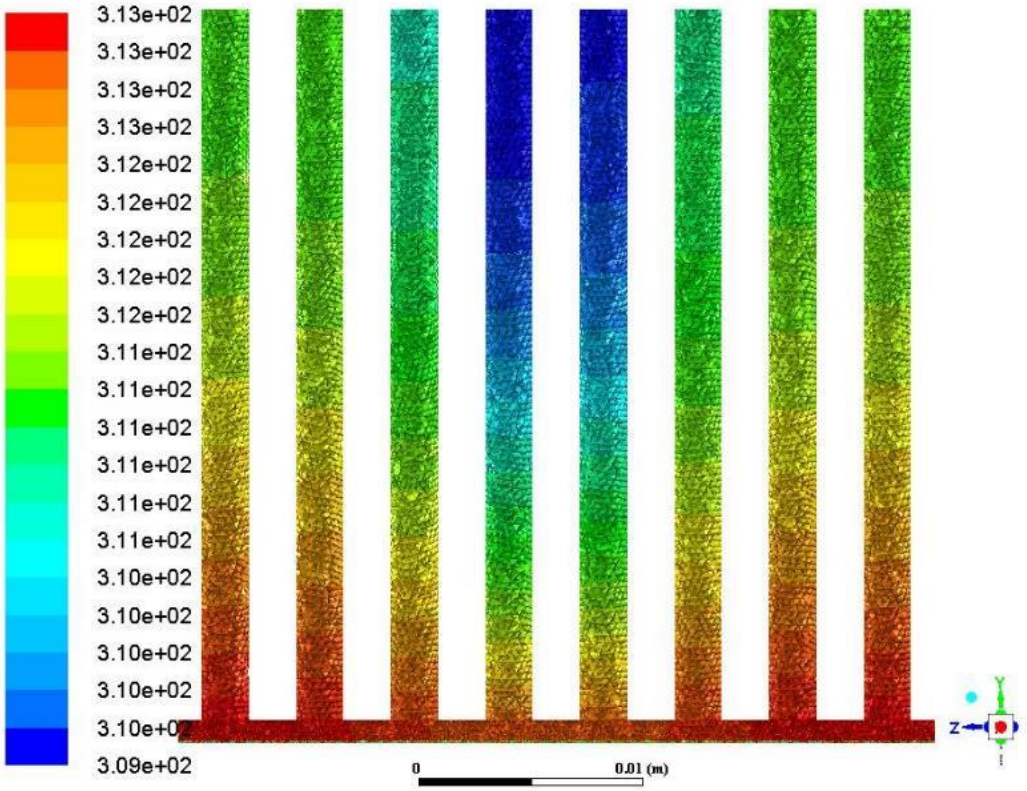

Figure 7.16 Temperature distribution (in K) of 8-fin-block

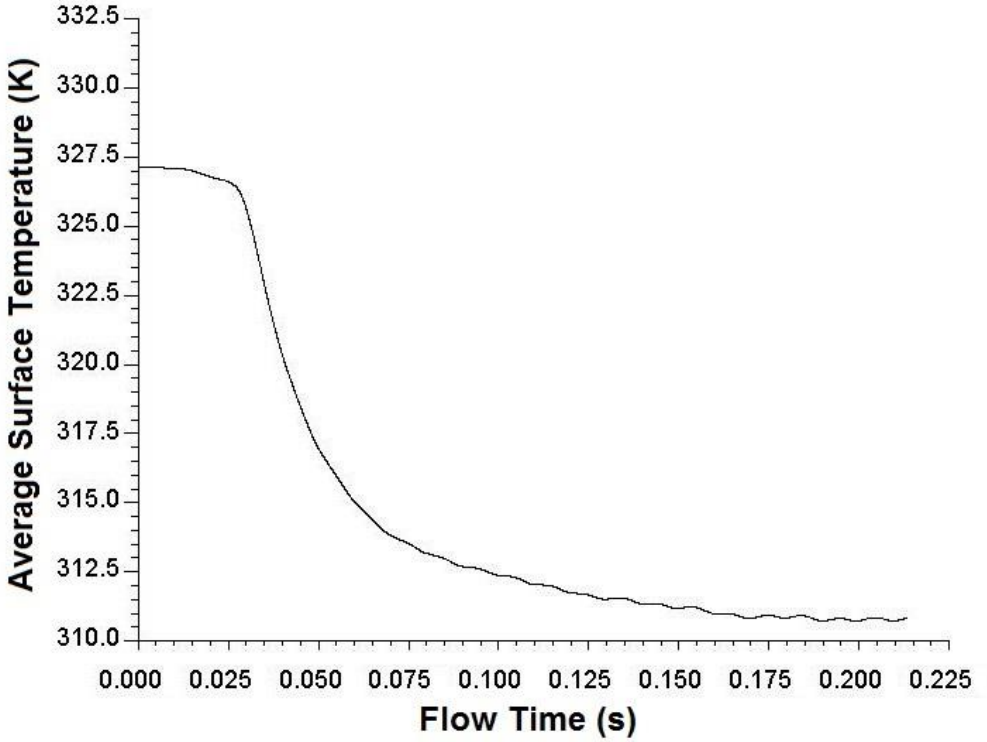

Figure 7.17 Average surface temperature of 9-fin-block

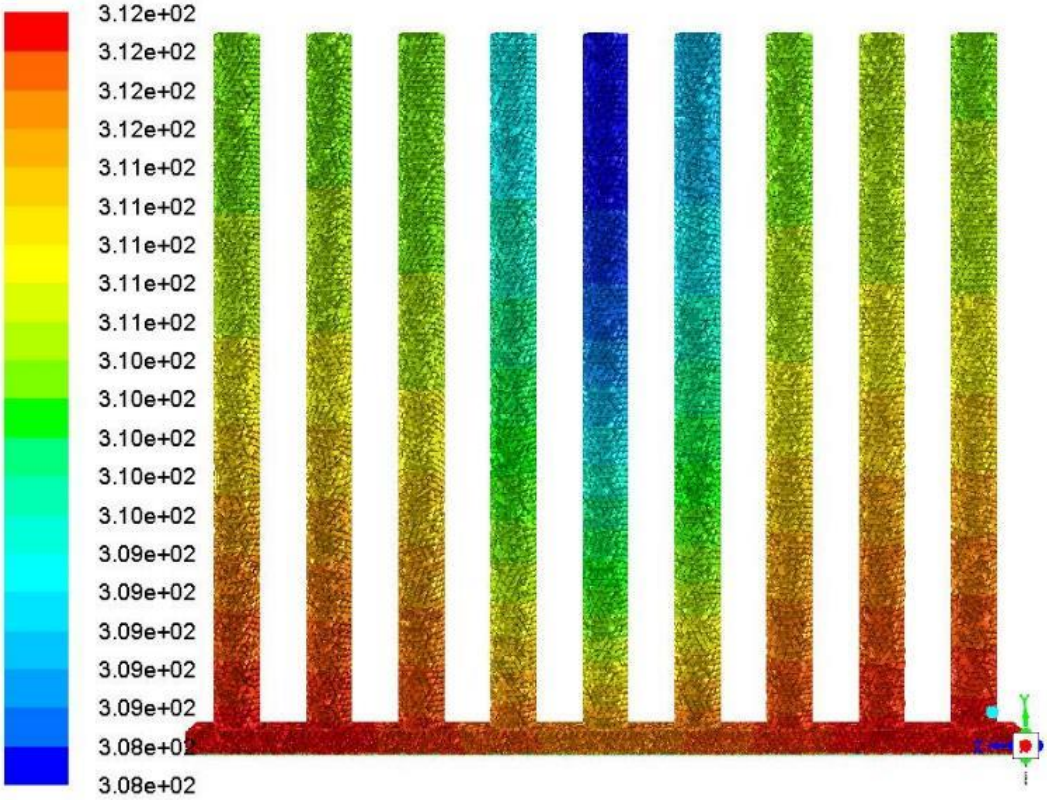

Figure 7.18 Temperature distribution (in K) of 9-fin-block

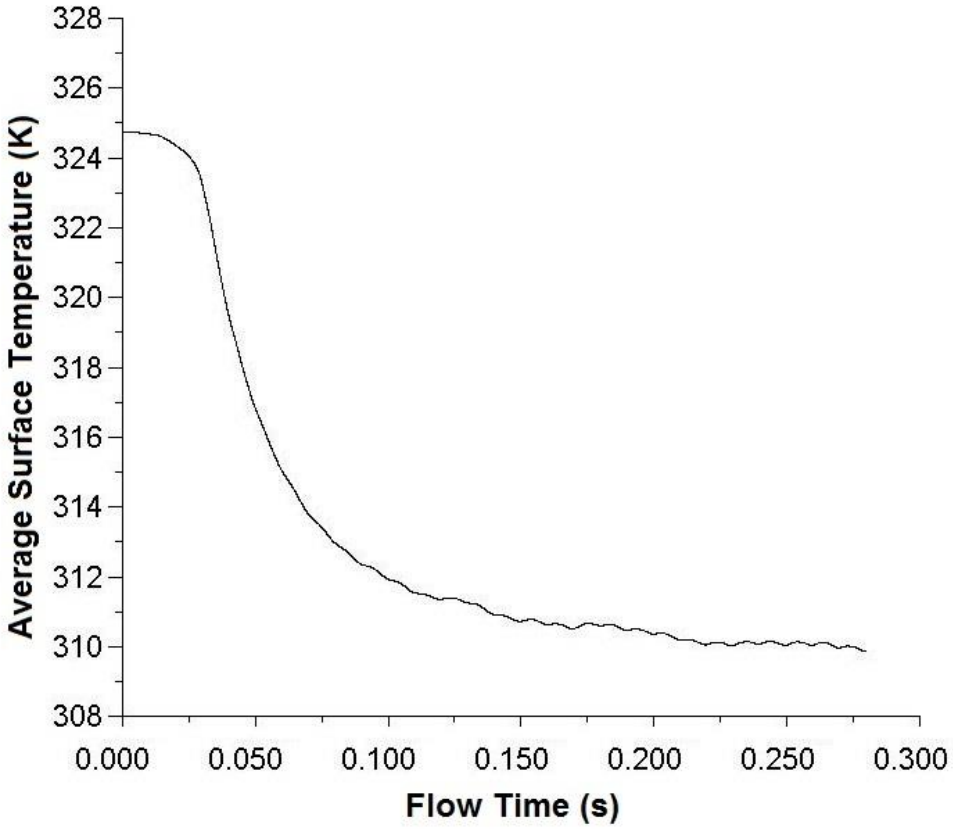

Figure 7.19 Average surface temperature of 10-fin-block

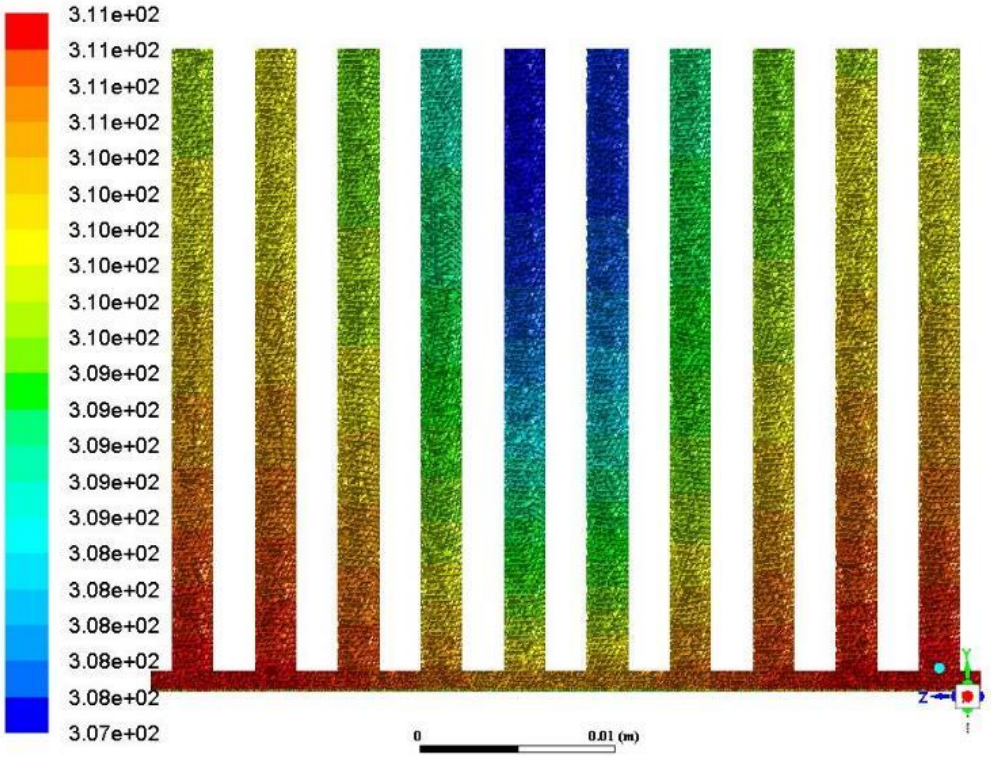

Figure 7.20 Temperature distribution (in K) of 10-fin-block

APPENDIX B

Constant Heat Flux - Temperature Distribution in Transient Solution – Horizontal Fan Arrangement

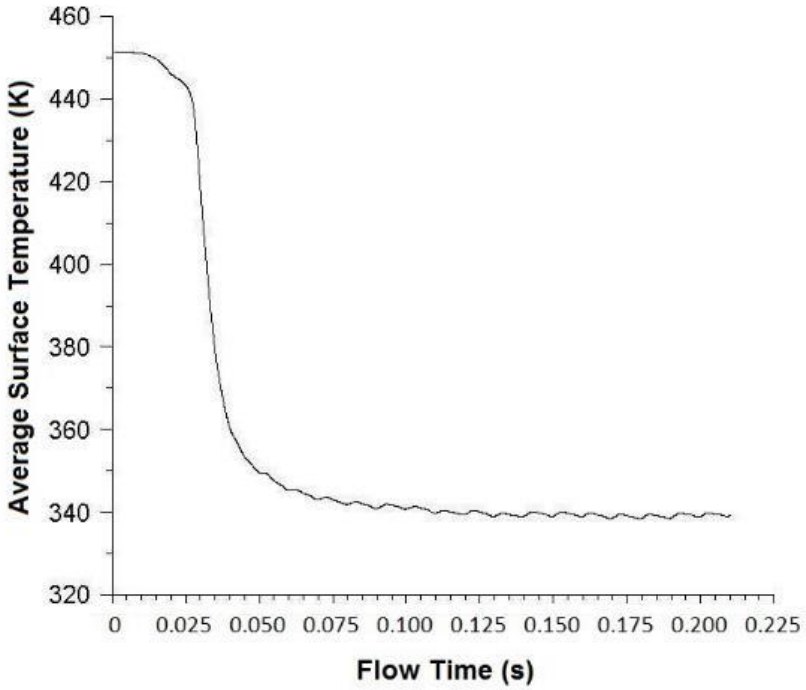

Figure 8.1 Average surface temperature of 1-fin-block

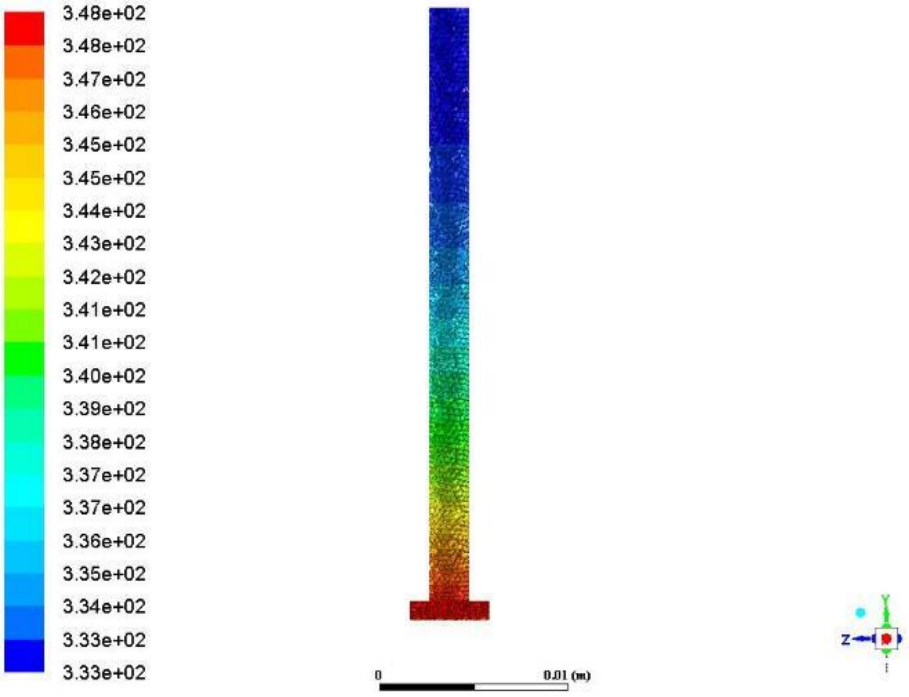

Figure 8.2 Temperature distribution (in K) of 1-fin-block

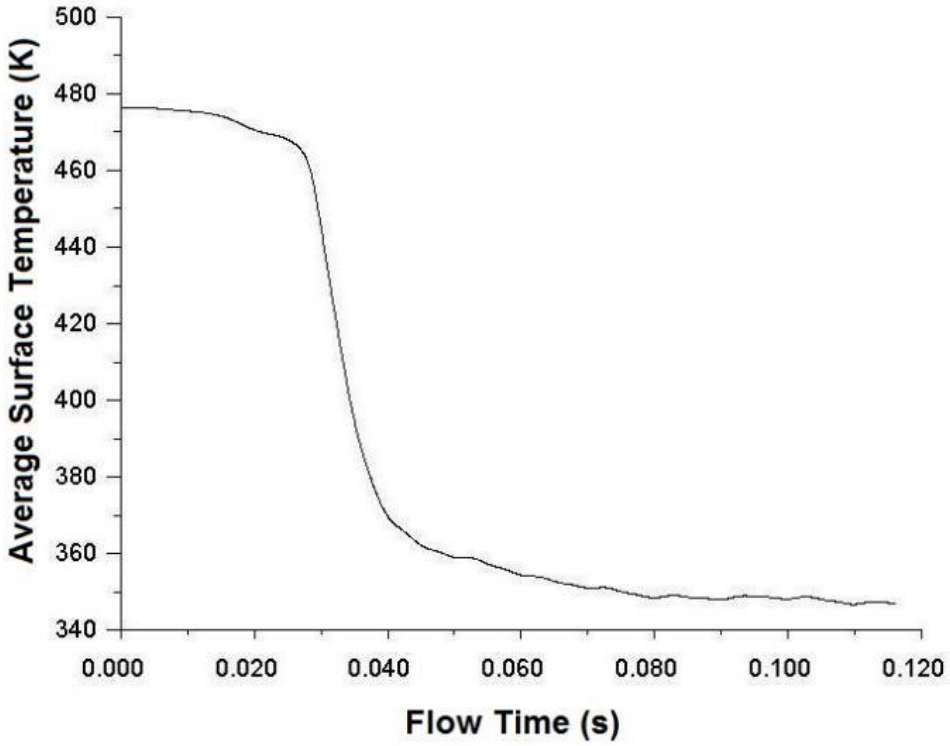

Figure 8.3 Average surface temperature of 2-fin-block

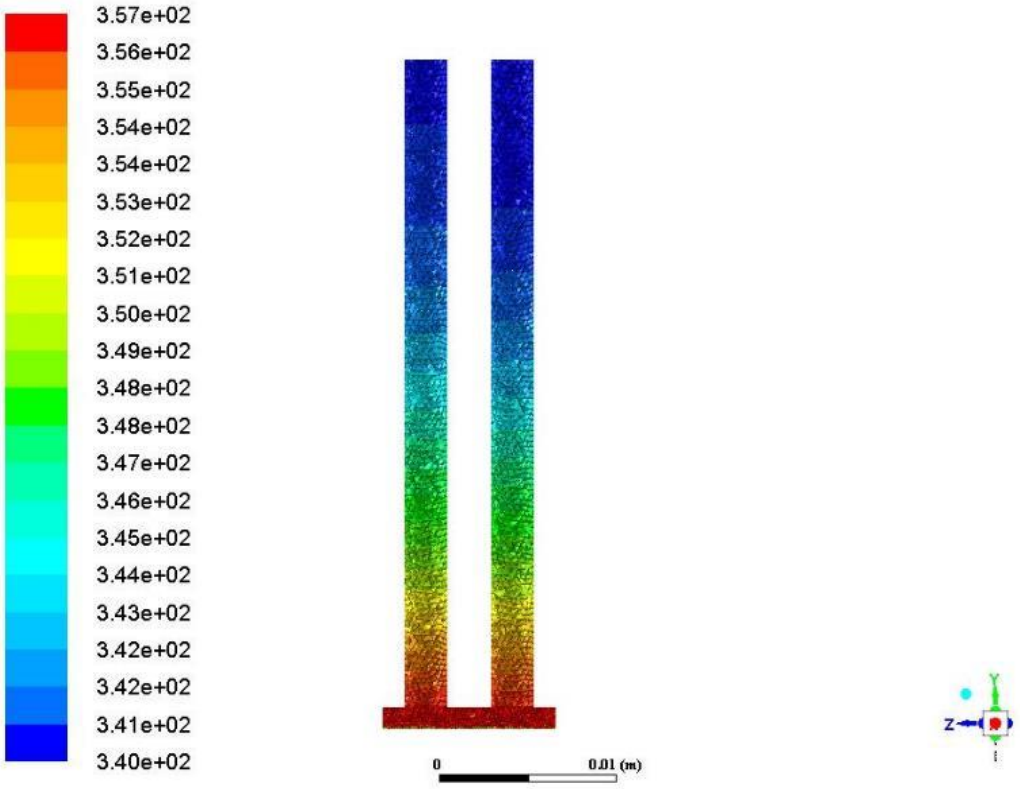

Figure 8.4 Temperature distribution (in K) of 2-fin-block

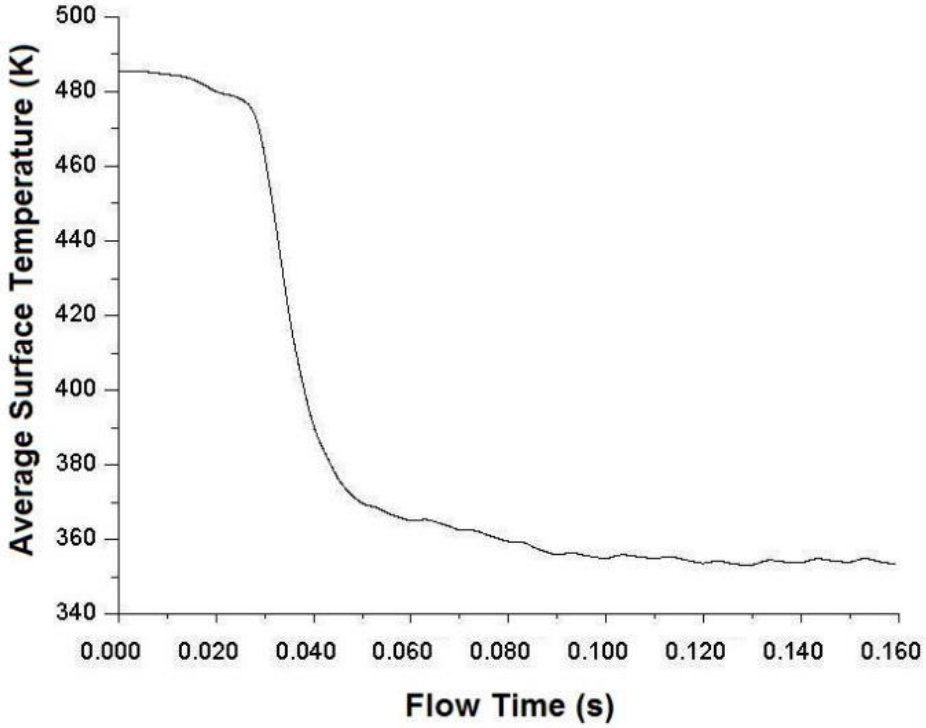

Figure 8.5 Average surface temperature of 3-fin-block

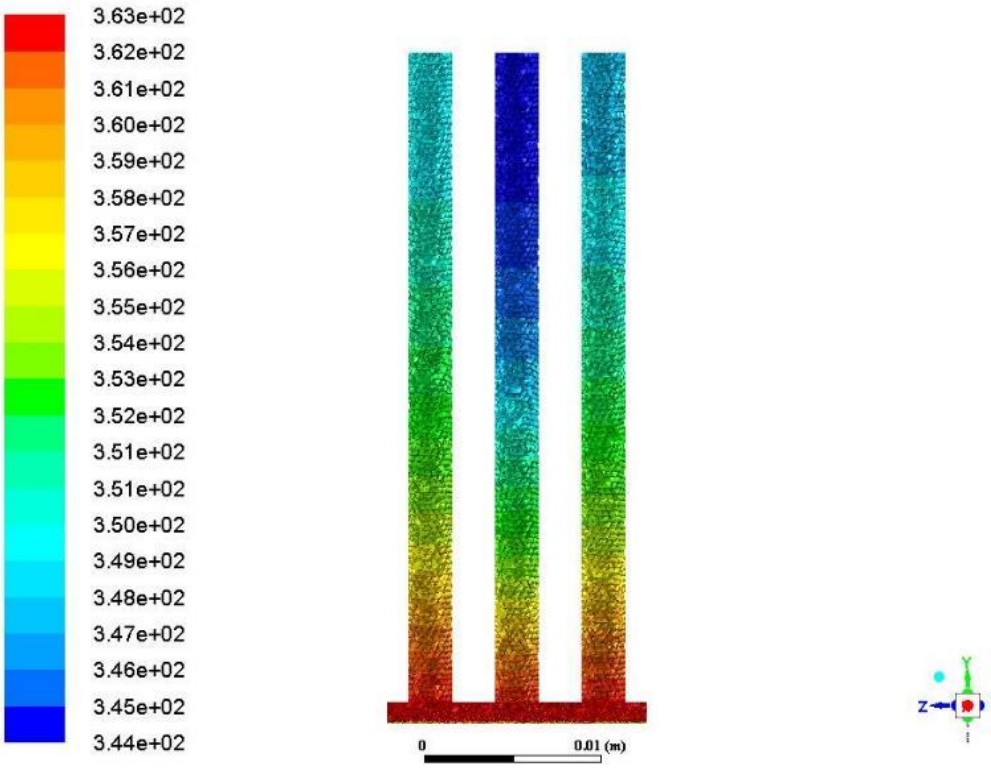

Figure 8.6 Temperature distribution (in K) of 3-fin-block

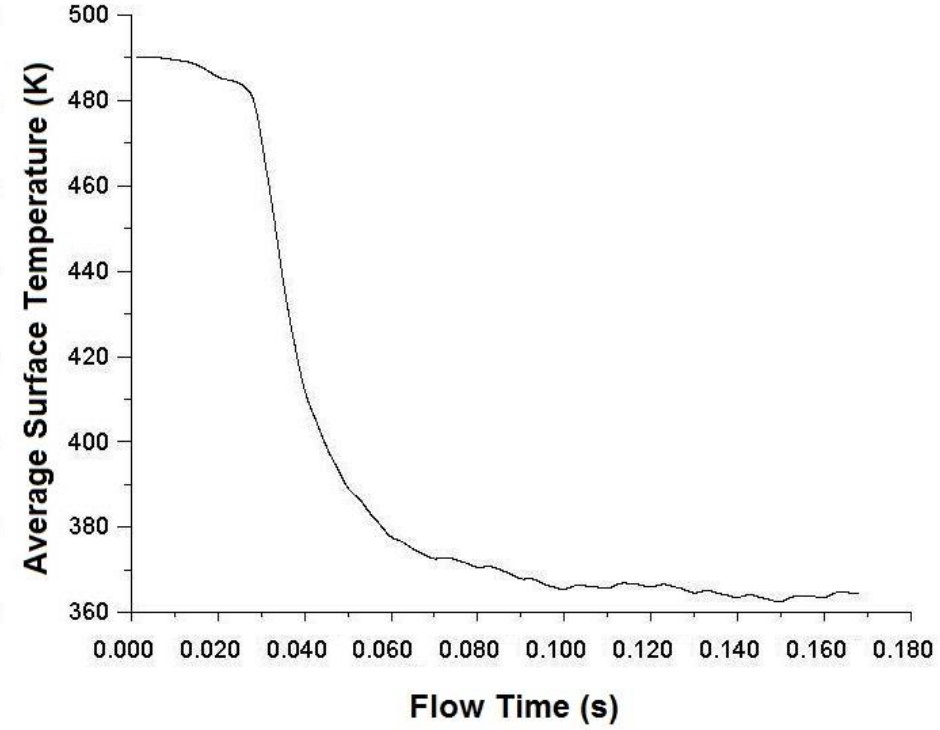

Figure 8.7 Average surface temperature of 4-fin-block

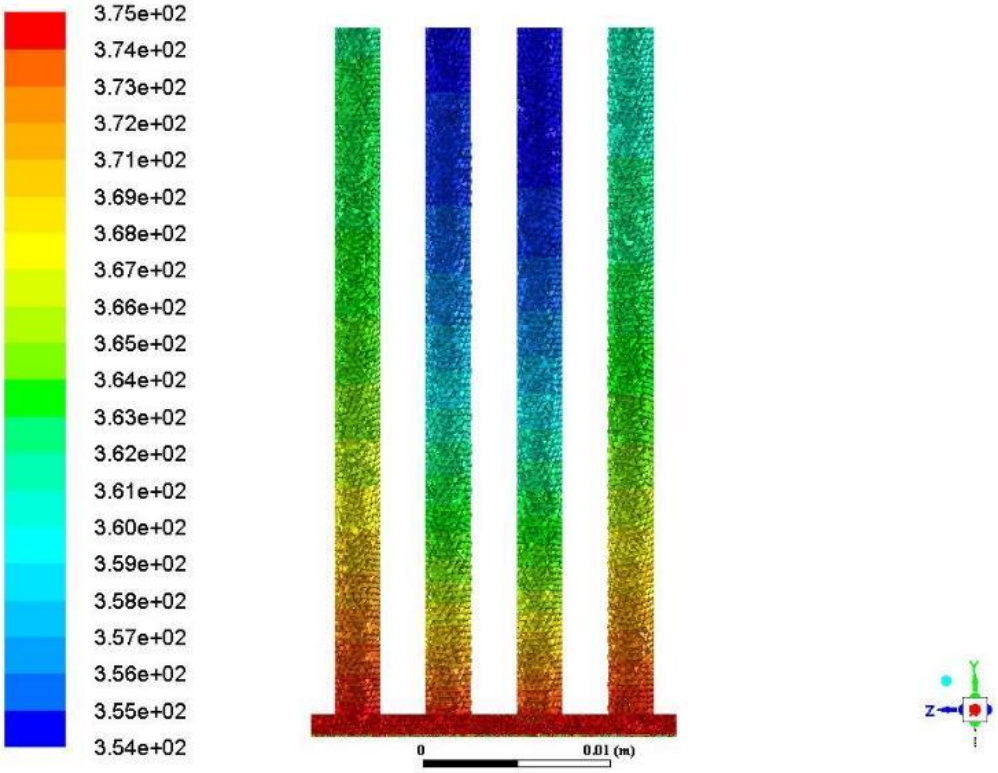

Figure 8.8 Temperature distribution (in K) of 4-fin-block

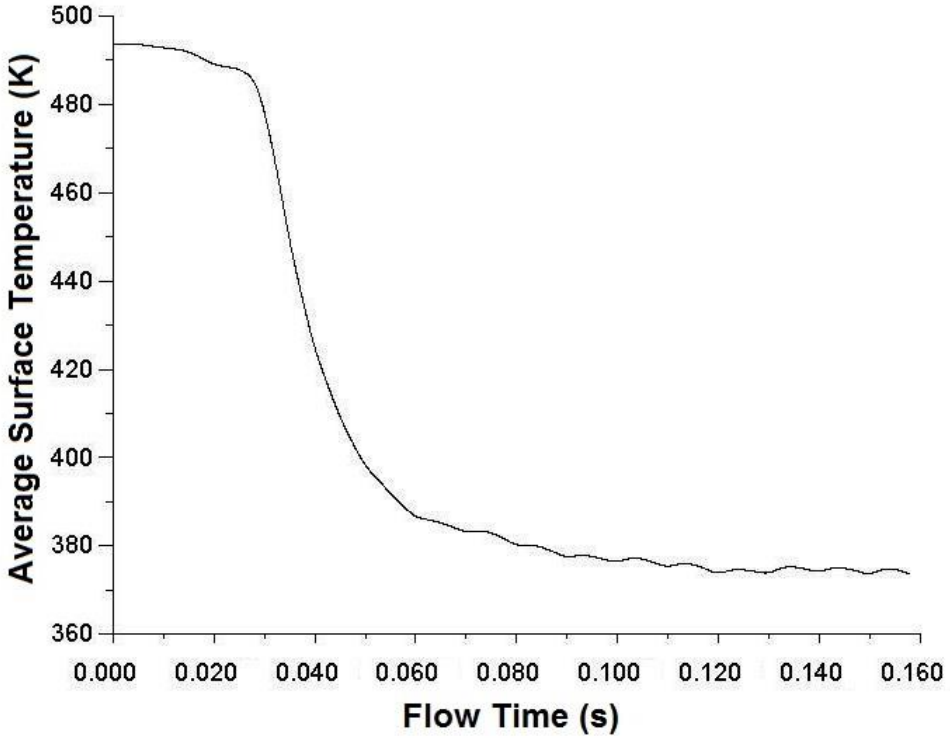

Figure 8.9 Average surface temperature of 5-fin-block

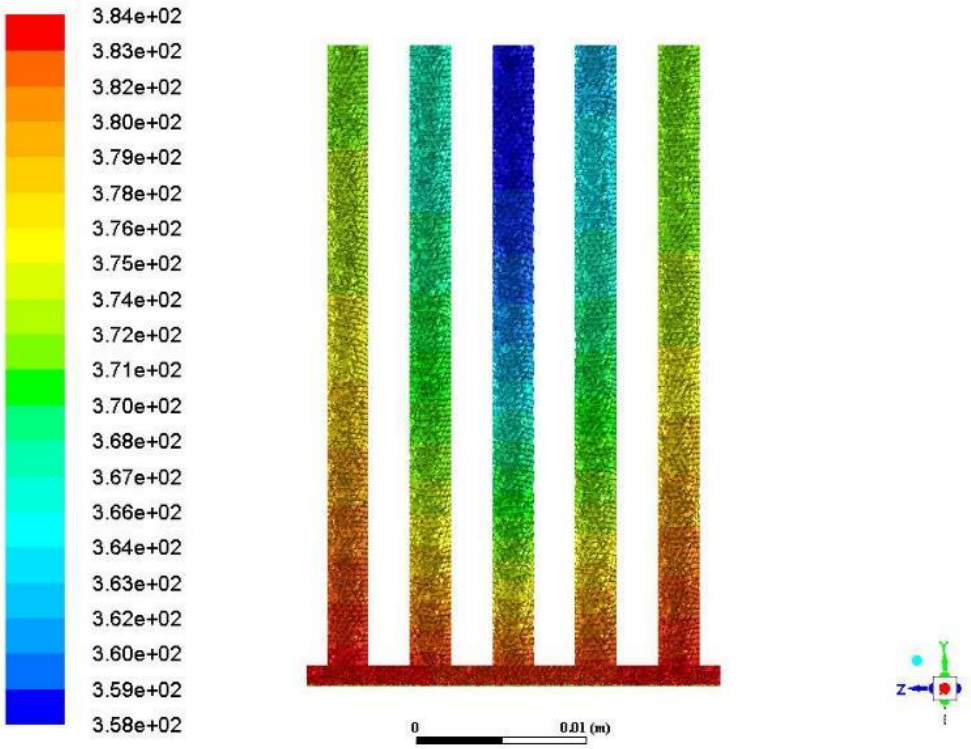

Figure 8.10 Temperature distribution (in K) of 5-fin-block

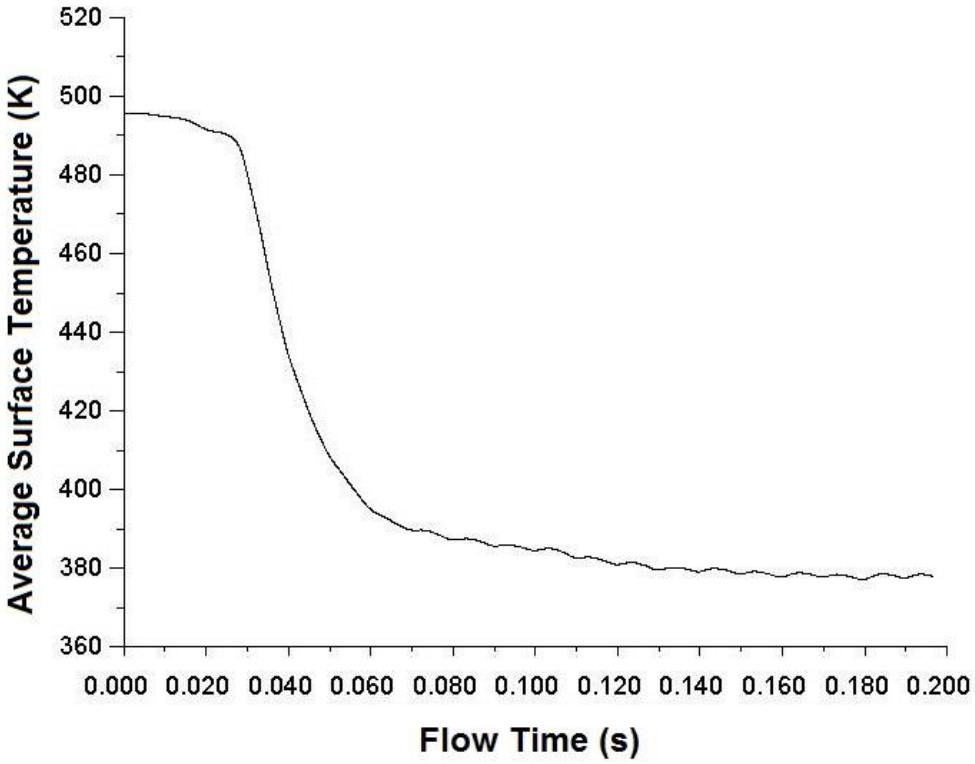

Figure 8.11 Average surface temperature of 6-fin-block

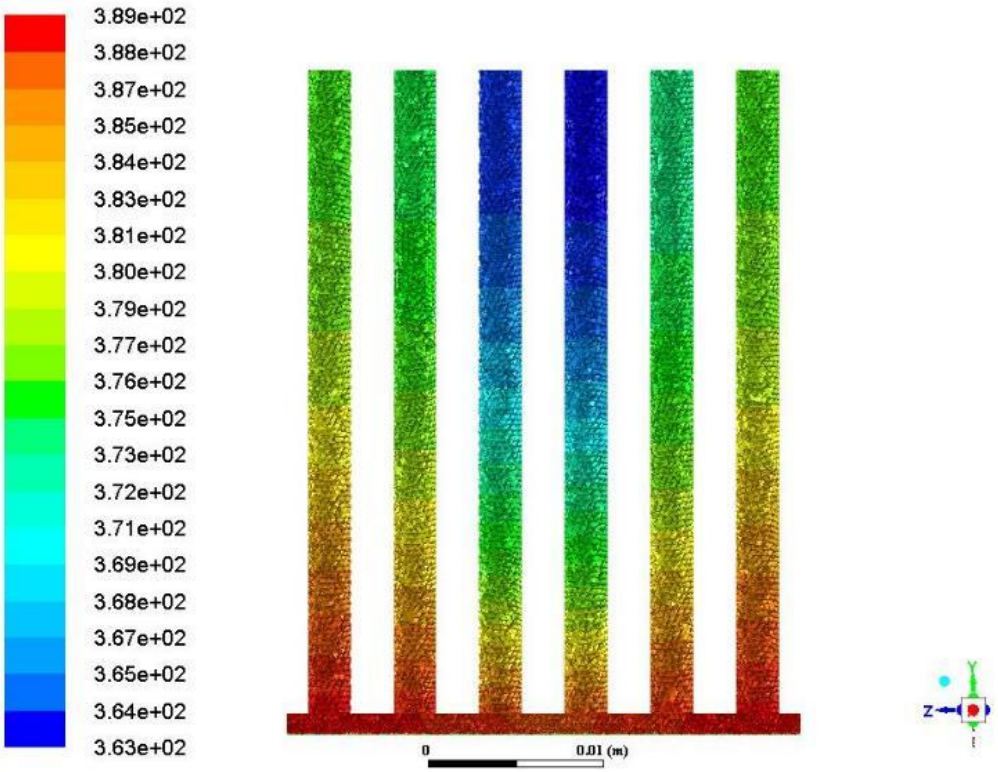

Figure 8.12 Temperature distribution (in K) of 6-fin-block

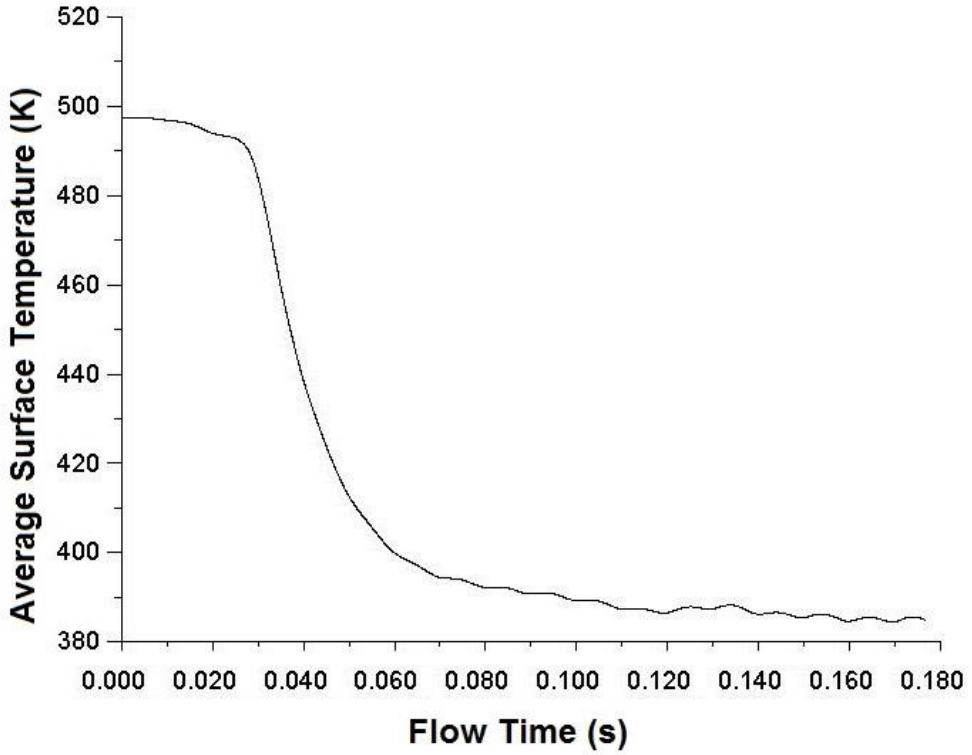

Figure 8.13 Average surface temperature of 7-fin-block

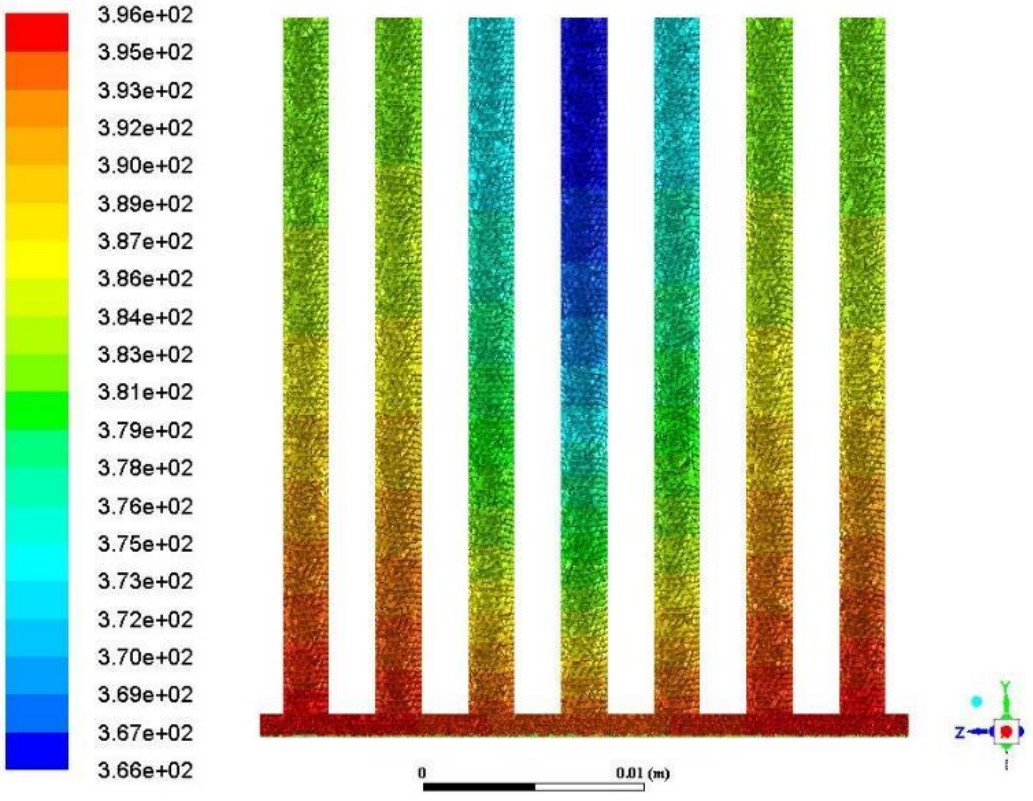

Figure 8.14 Temperature distribution (in K) of 7-fin-block

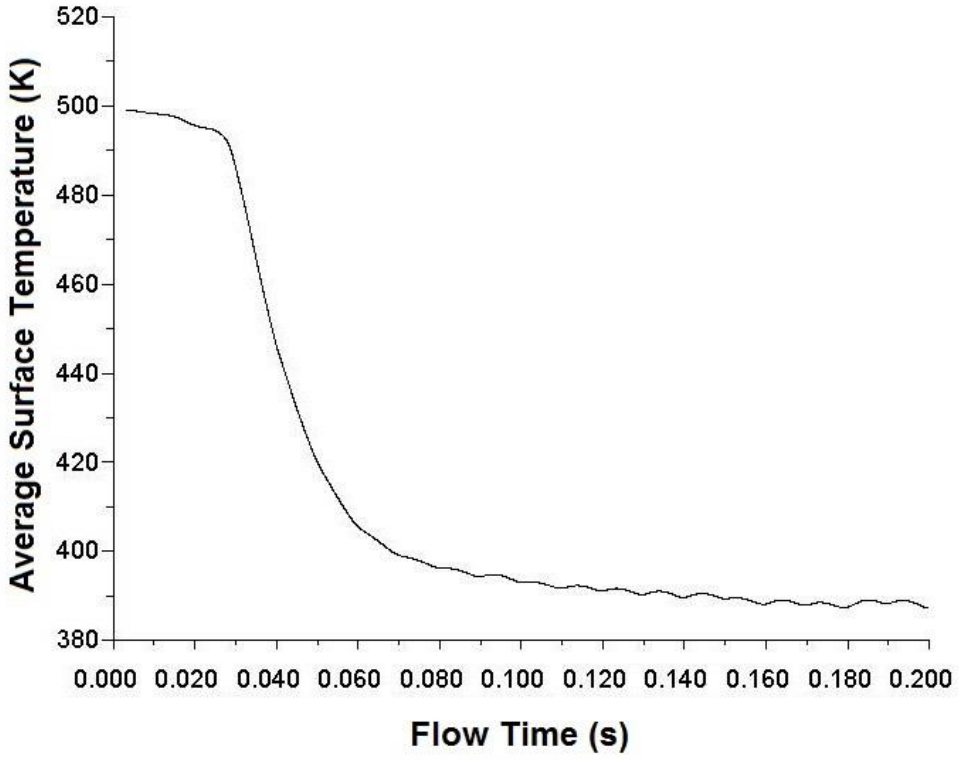

Figure 8.15 Average surface temperature of 8-fin-block

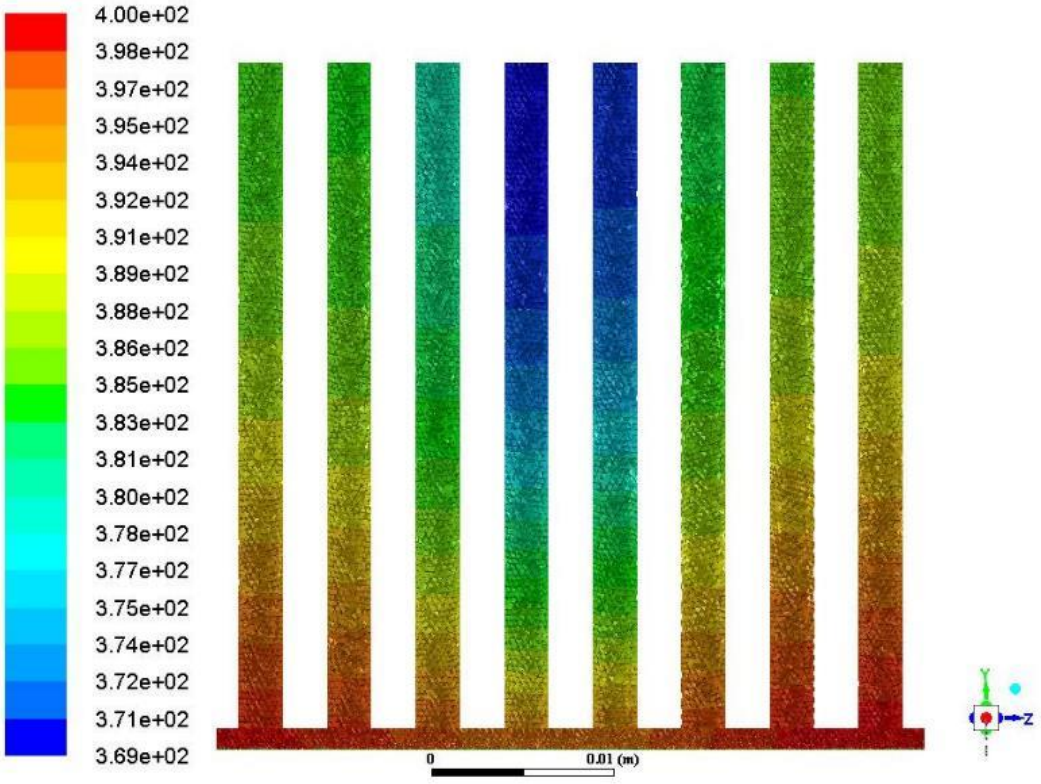

Figure 8.16 Temperature distribution (in K) of 8-fin-block

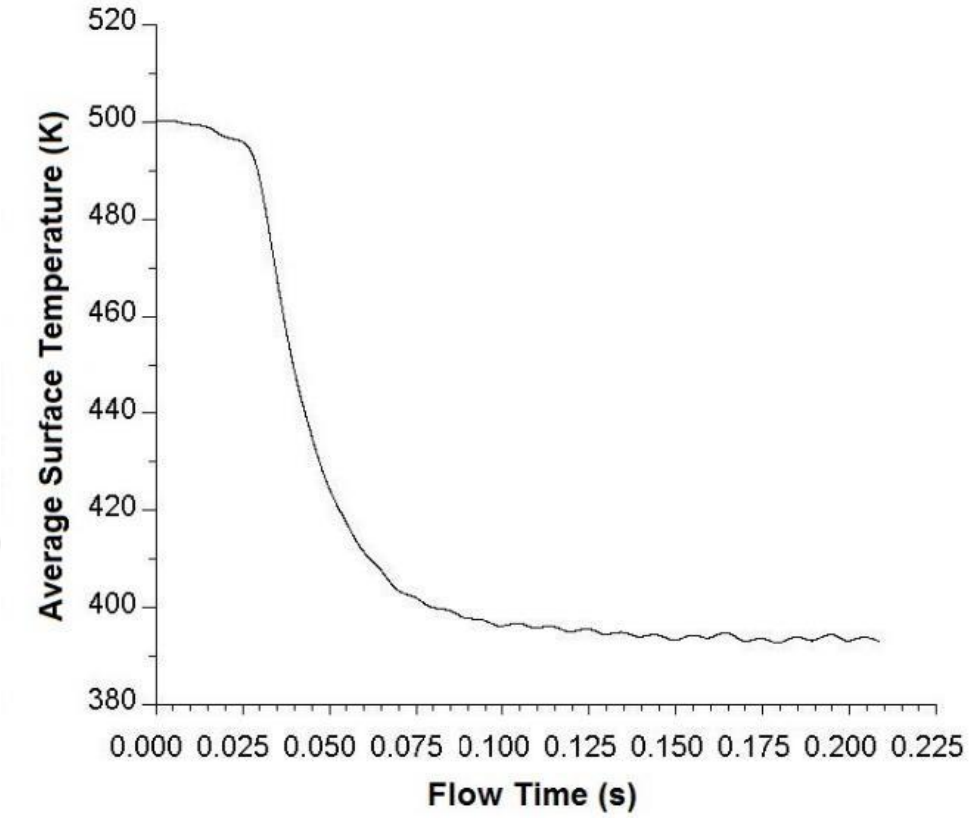

Figure 8.17 Average surface temperature of 9-fin-block

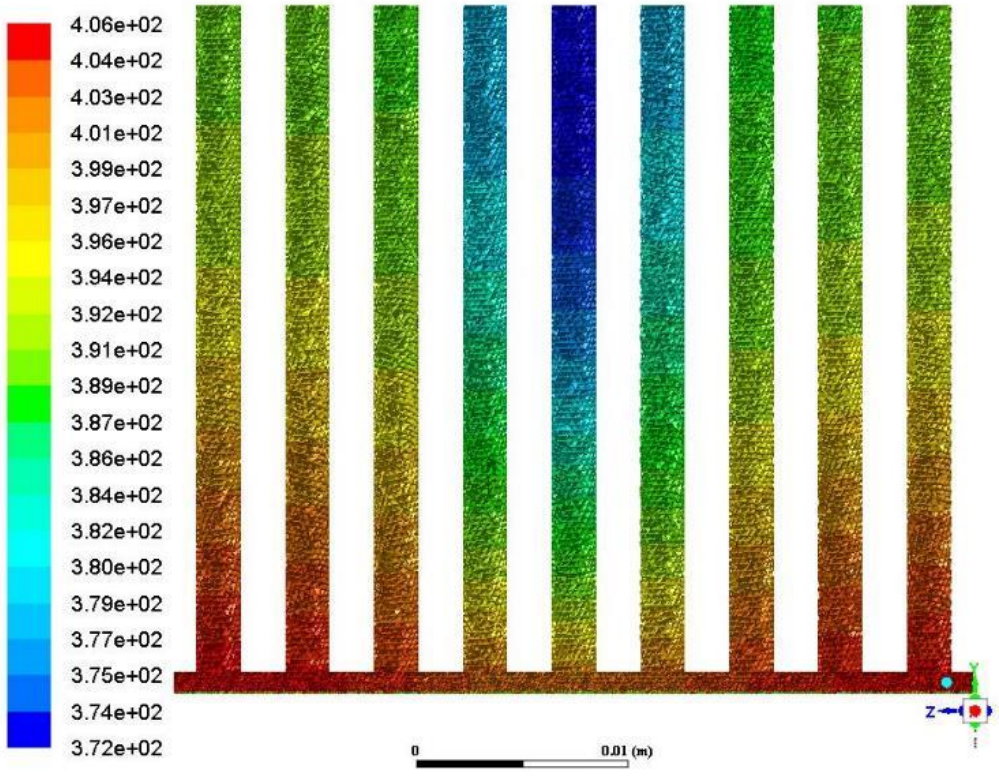

Figure 8.18 Temperature distribution (in K) of 9-fin-block

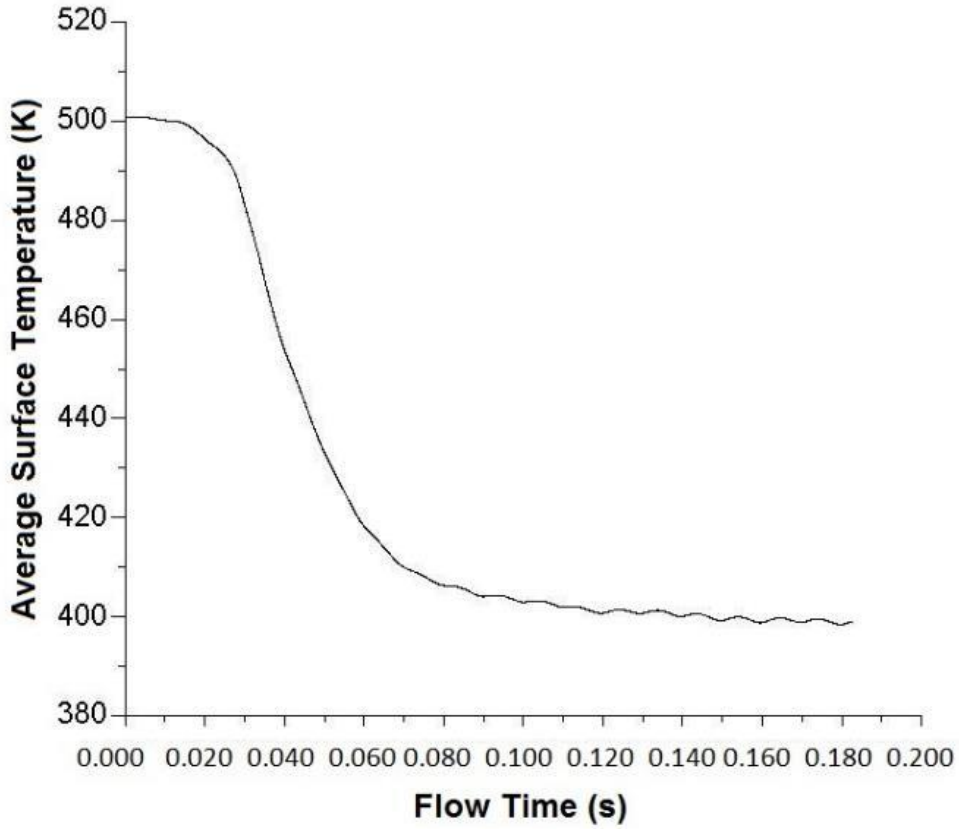

Figure 8.19 Average surface temperature of 10-fin-block

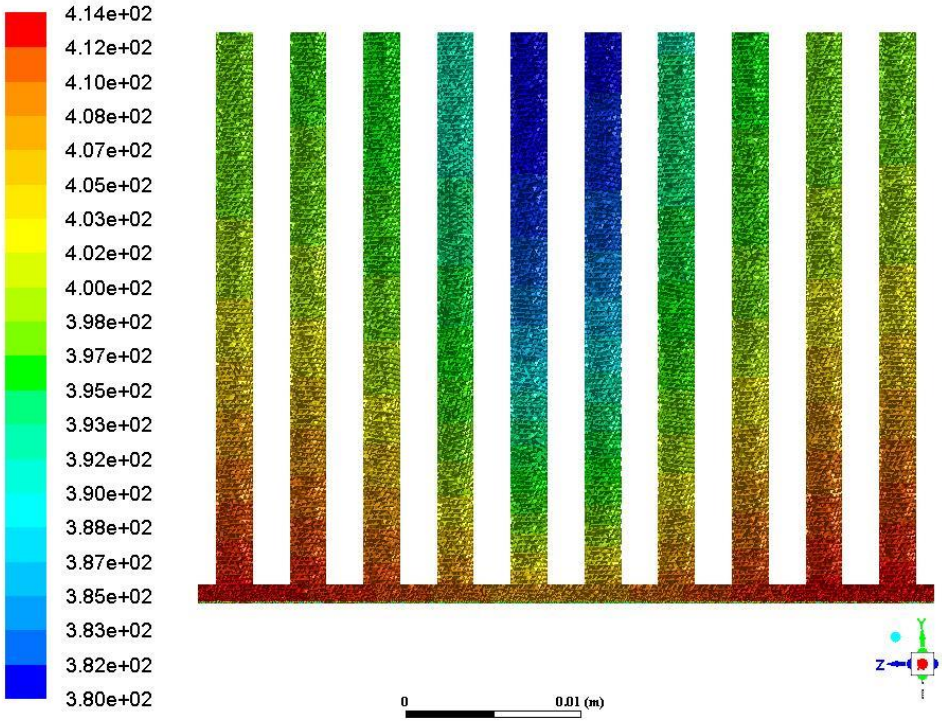

Figure 8.20 Temperature distribution (in K) of 10-fin-block

APPENDIX C

Constant Total Heat - Temperature Distribution in Transient Solution – Vertical Fan Arrangement

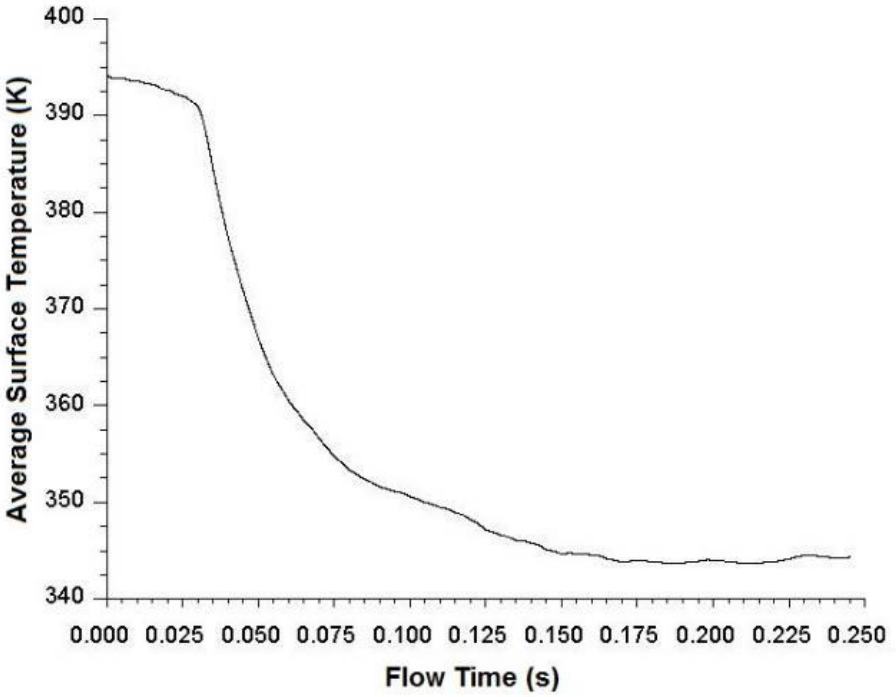

Figure 9.1 Average surface temperature of 2-fin-block

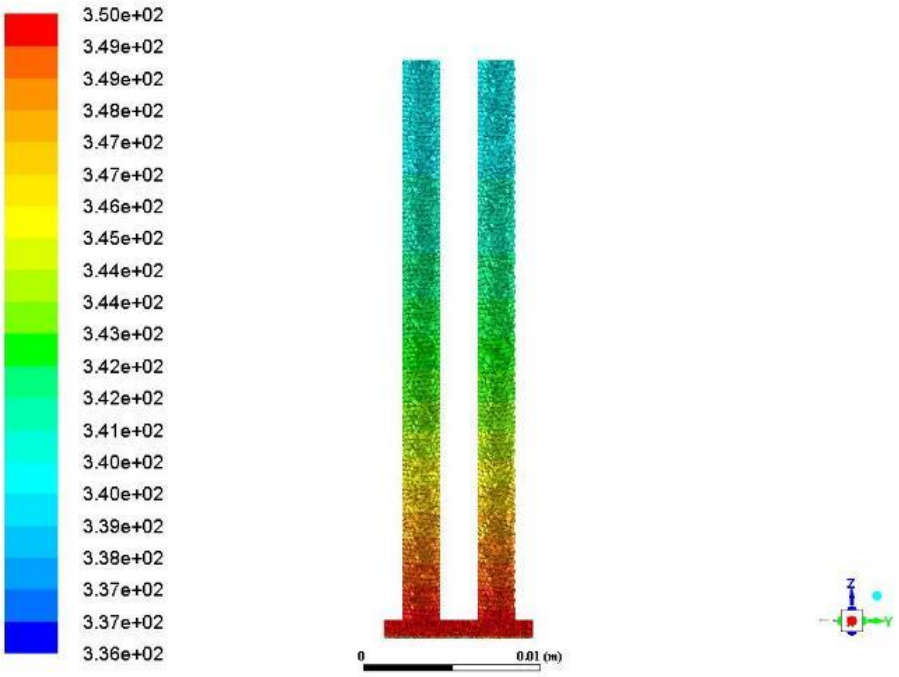

Figure 9.2 Temperature distribution (in K) of 2-fin-block

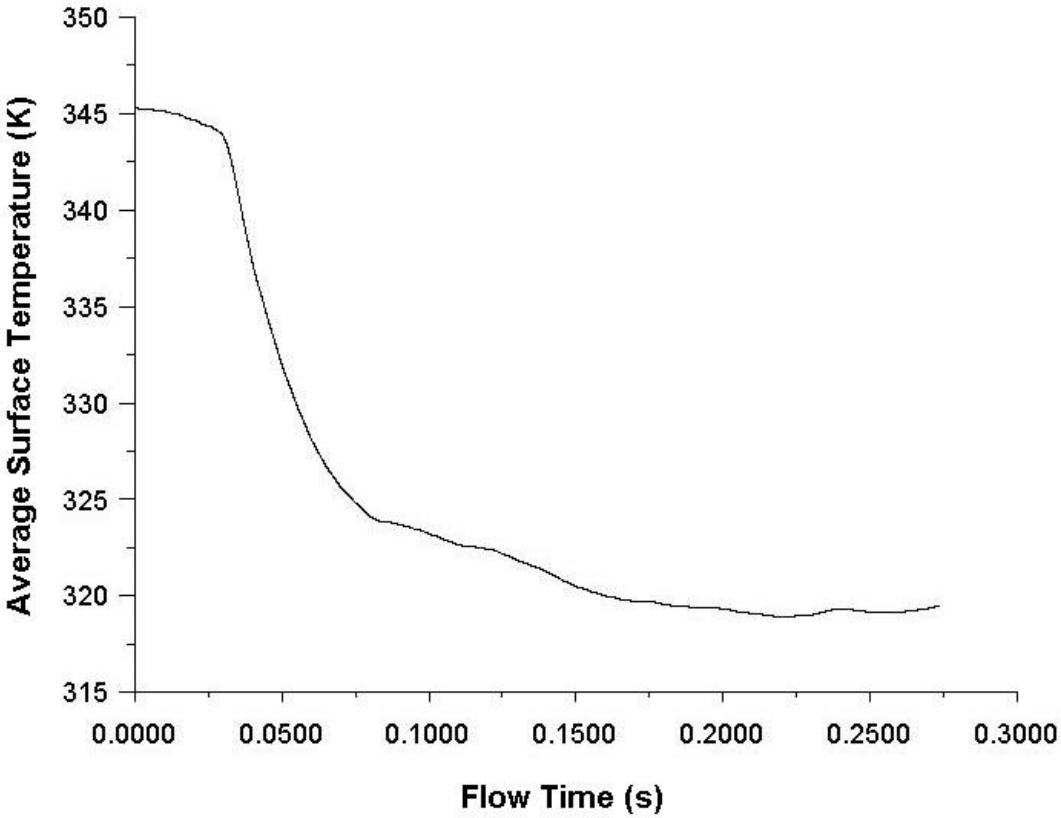

Figure 9.3 Average surface temperature of 5-fin-block

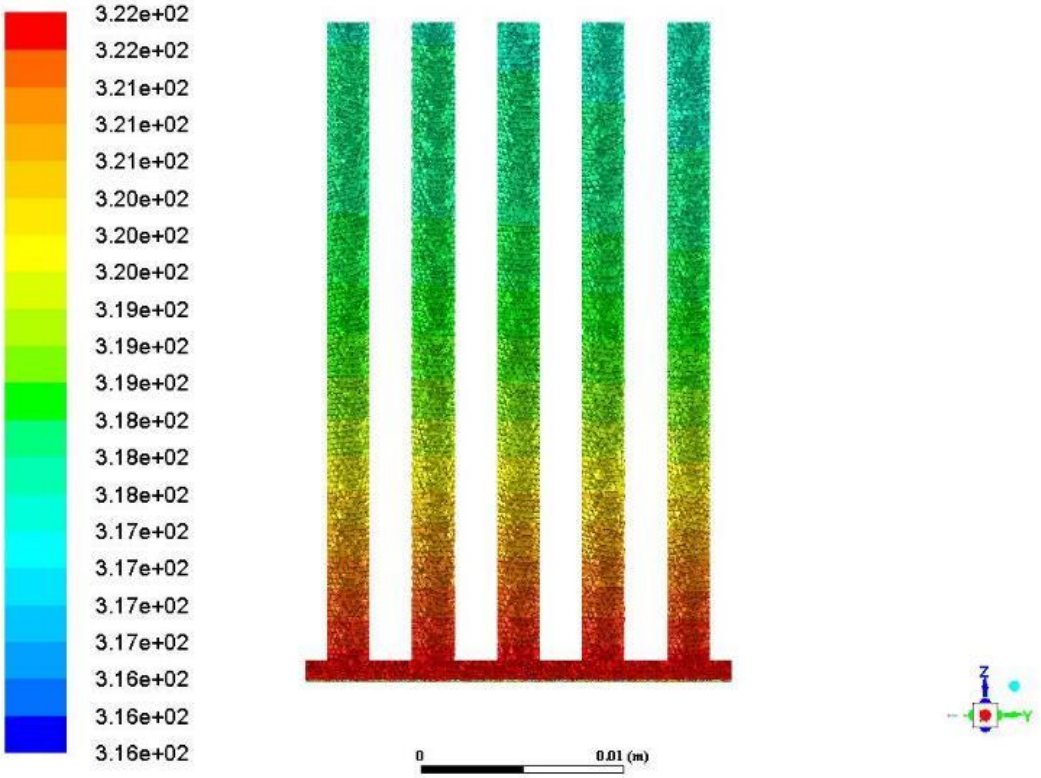

Figure 9.4 Temperature distribution (in K) of 5-fin-block

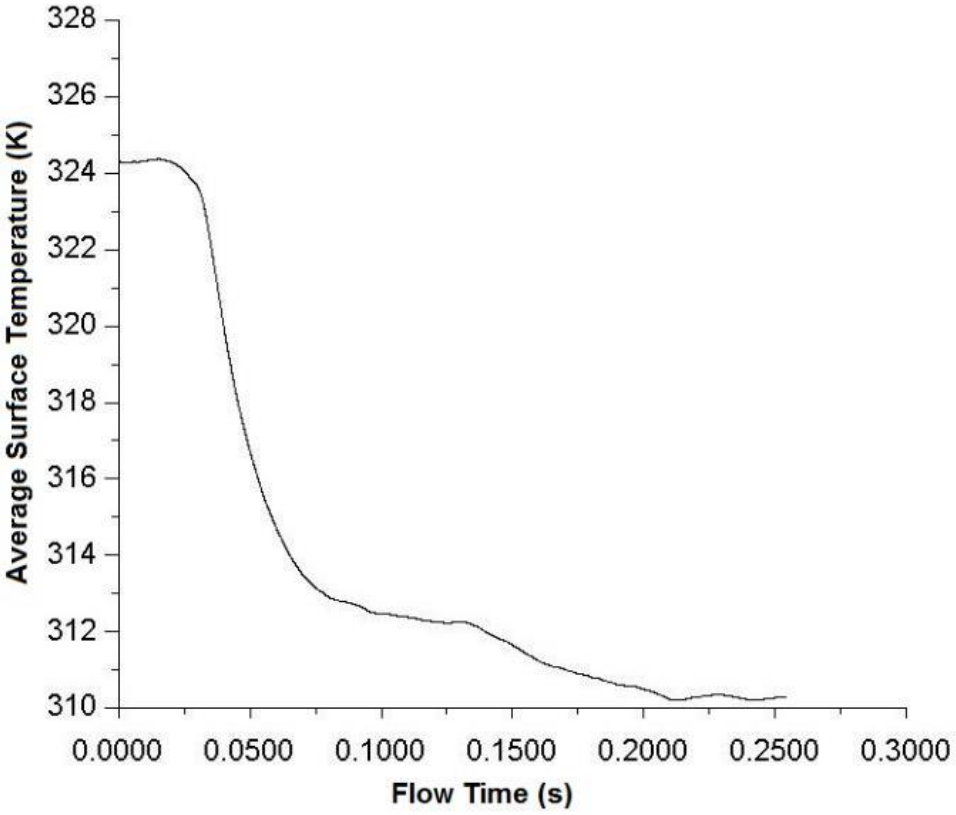

Figure 9.5 Average surface temperature of 10-fin-block

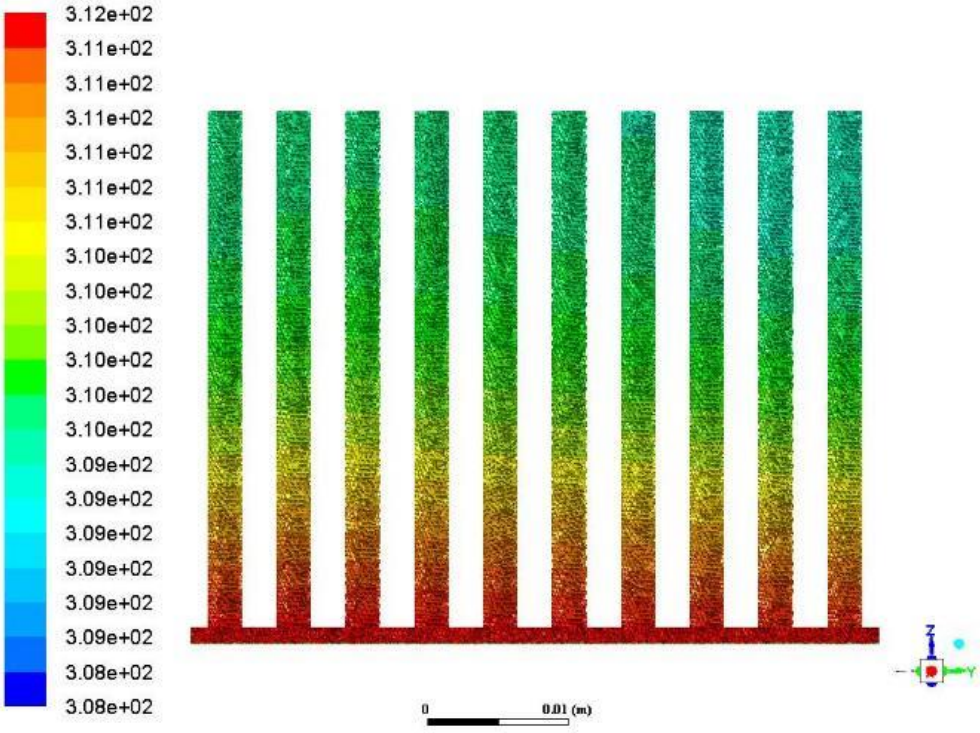

Figure 9.6 Temperature distribution (in K) of 5-fin-block

APPENDIX D

Constant Heat Flux - Temperature Distribution in Transient Solution – Vertical Fan Arrangement

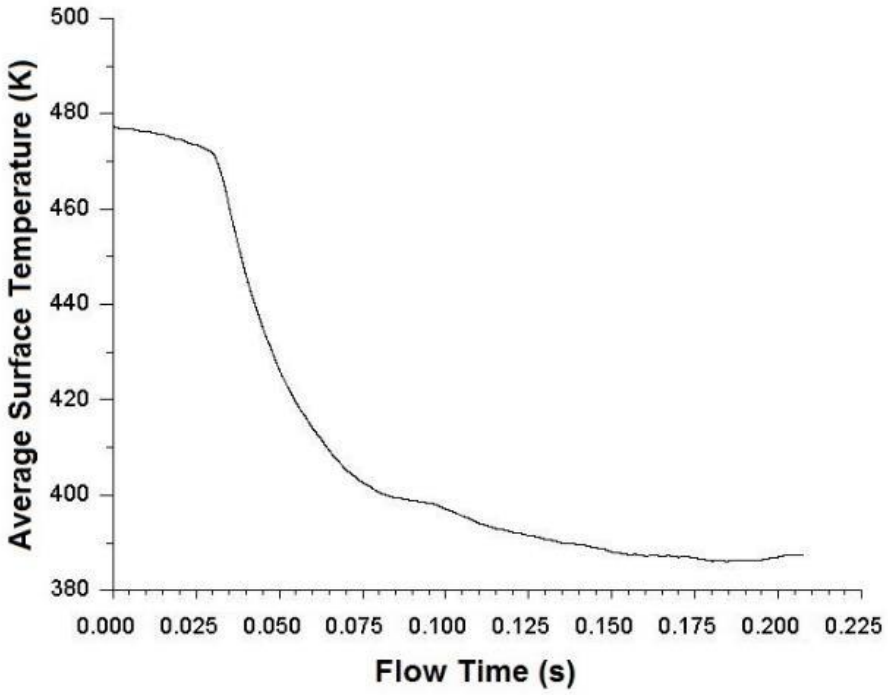

Figure 10.1 Average surface temperature of 2-fin-block

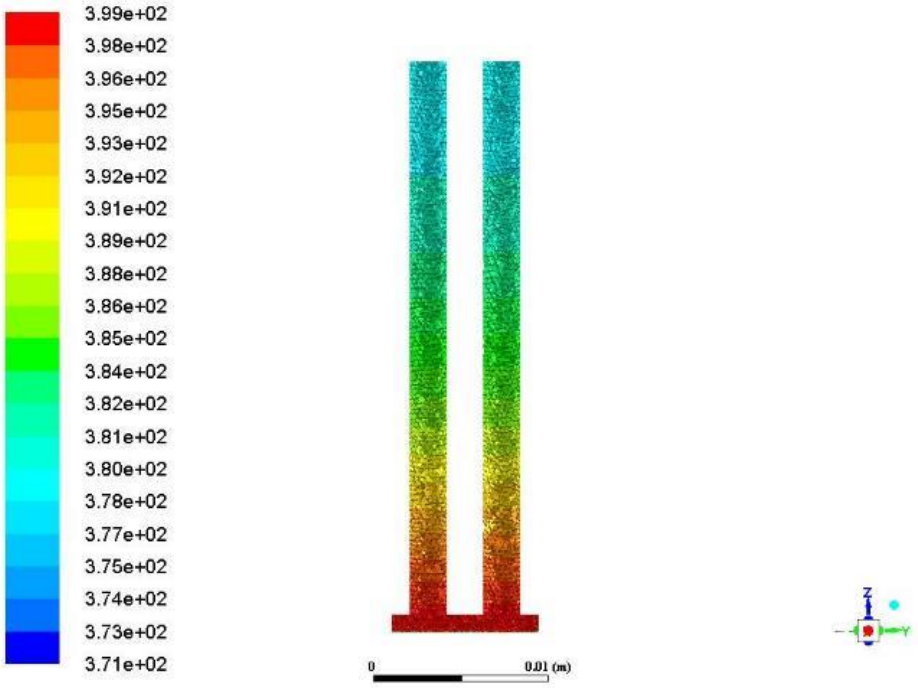

Figure 10.2 Temperature distribution (in K) of 2-fin-block

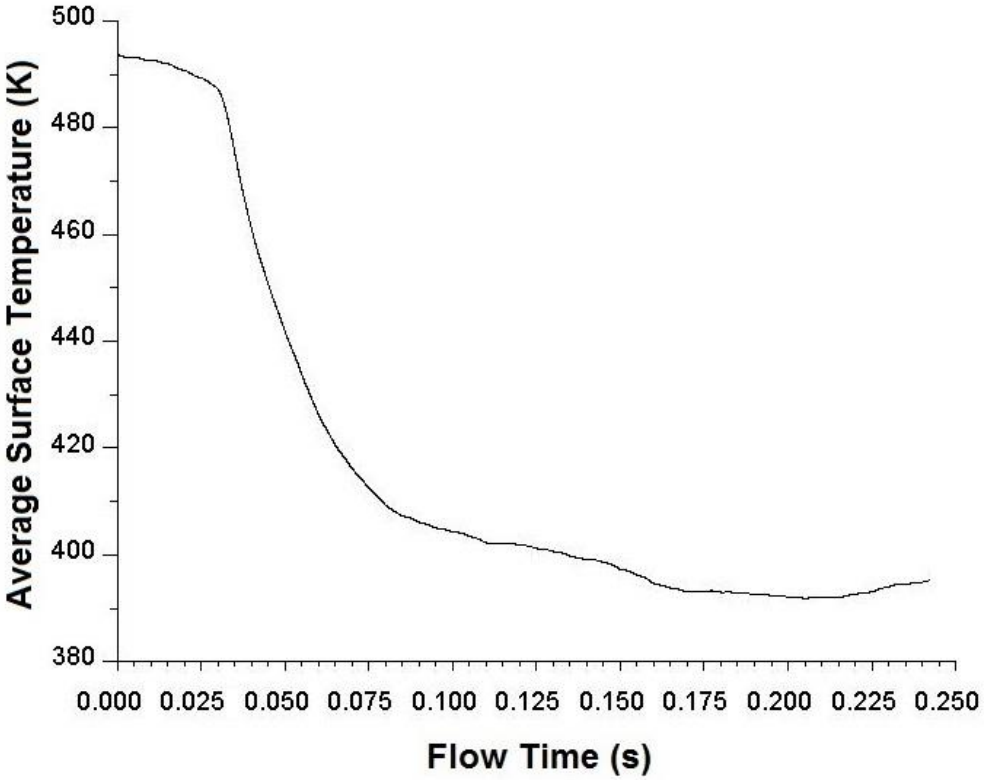

Figure 10.3 Average surface temperature of 5-fin-block

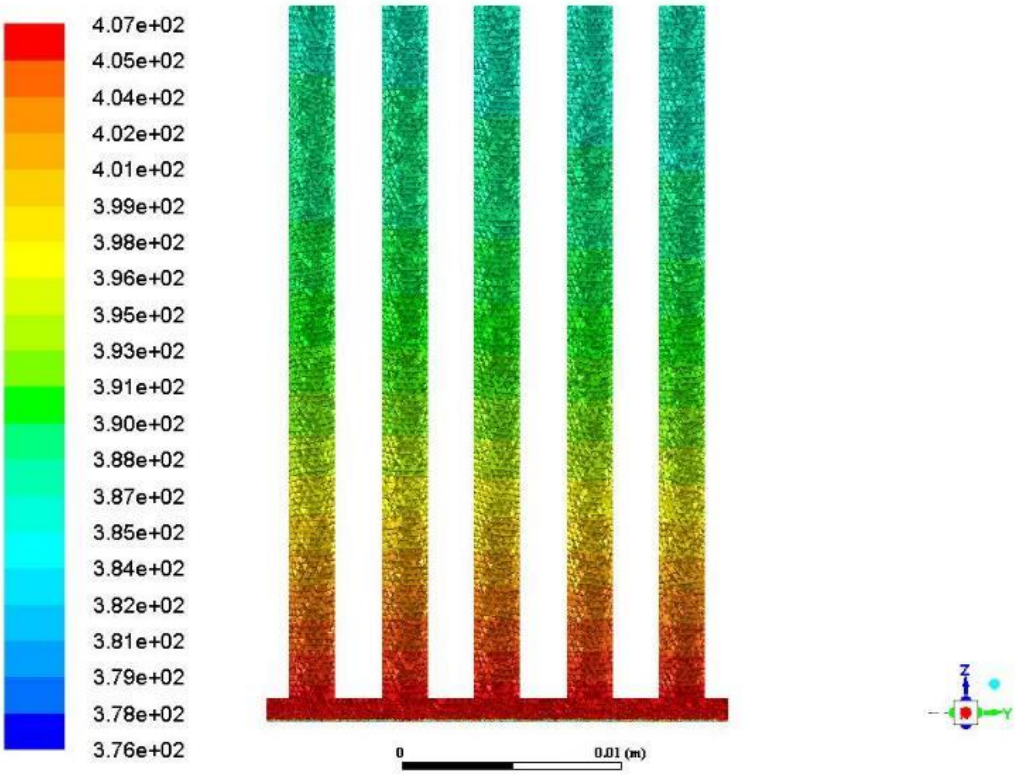

Figure 10.4 Temperature distribution (in K) of 5-fin-block

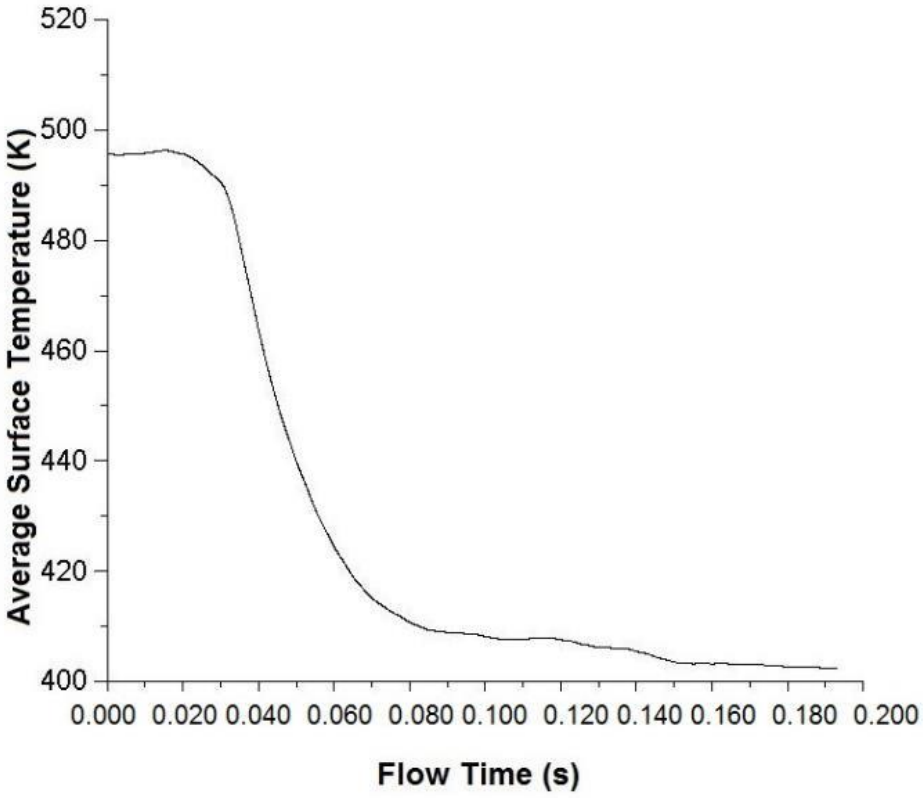

Figure 10.5 Average surface temperature of 10-fin-block

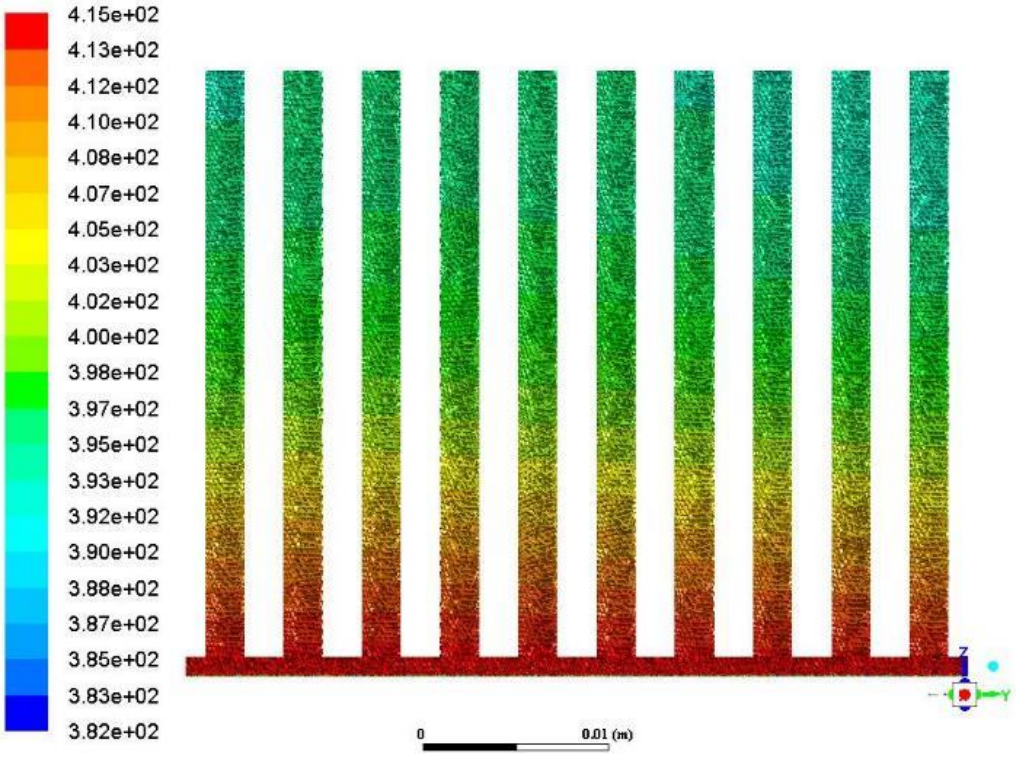

Figure 10.6 Temperature distribution (in K) of 10-fin-block

APPENDIX E

UDF of Thesis Study

```
#include "udf.h"
#define freq 100.0 //hz
#define a0   25.4
#define pi 3.14159

DEFINE_GRID_MOTION(beam,domain,dt,time,dtime)
{
Thread *t=DT_THREAD(dt);
face_t f;
Node *v;
real NV_VEC(omega), NV_VEC(axis), NV_VEC(dx);
real NV_VEC(origin), NV_VEC(rvec);
int n;
SET_DEFORMING_THREAD_FLAG(THREAD_T0(t));
real sign_funq=a0*pi*cos(freq*time*2*pi);

NV_S(omega, =, 0.0);
NV_D(axis, =, 0.0, 0.0, 0.0);
NV_D(origin, =, 0.0, 0.0, 0.0);
begin_f_loop(f,t)
{
f_node_loop(f,t,n)
{
v = F_NODE(f,t,n);
if (NODE_POS_NEED_UPDATE (v))
 {
 NODE_POS_UPDATED(v);
 omega[2] = sign_funq * ((-42.34*pow (NODE_X(v),2.0))+(33587.0*pow
(NODE_X(v),3.0))-(2.732*pow (10,6.0)*pow (NODE_X(v),4.0))+
 (9.053*pow (10,7.0)*pow (NODE_X(v),5.0))-(1.265*pow (10,9.0)*pow
(NODE_X(v),6.0))+(6.34496*pow (10,9.0)*pow (NODE_X(v),7.0)));
```

```
 NV_VV(rvec, =, NODE_COORD(v), -, origin);
 NV_CROSS(dx, omega, rvec);
 NV_S(dx, *=, dtime);
 NV_V(NODE_COORD(v), +=, dx);
 }
}
}
end_f_loop(f,t)
}
```

APPENDIX F

UDF of Validation Study

```
#include "udf.h"

#define freq 35.714 //hz
#define a0   12.7
#define pi 3.14159
#define L1 0.029
#define L2 0.075
#define c0 0.00008772
#define c1 0.00001819
#define c2 0.00007
#define c3 0.0000004763
#define c4 1.159
#define c5 0.09419
#define c6 0.002567
#define c7 0.00002488
#define c8 0.00000009371

DEFINE_GRID_MOTION(beam,domain,dt,time,dtime)
{
Thread *t=DT_THREAD(dt);
face_t f;
Node *v;
real NV_VEC(omega), NV_VEC(axis), NV_VEC(dx);
real NV_VEC(origin), NV_VEC(rvec);
int n;
SET_DEFORMING_THREAD_FLAG(THREAD_T0(t));
real sign_funq=a0*2.0*pi*cos(freq*time*2*pi);

NV_S(omega, =, 0.0);
NV_D(axis, =, 0.0, 0.0, 0.0);
NV_D(origin, =, 0.0, 0.0, 0.0);
```

```
begin_f_loop(f,t)
{
f_node_loop(f,t,n)
{
v = F_NODE(f,t,n);
if (NODE_X(v)<=L1 && NODE_POS_NEED_UPDATE (v))
 {
 NODE_POS_UPDATED(v);
 omega[2] = sign_funq * (-c0+c1*10e3*pow (NODE_X(v),1.0)+c2*10e6*pow
(NODE_X(v),2.0)-c3*10e9*pow (NODE_X(v),3.0));

 NV_VV(rvec, =, NODE_COORD(v), -, origin);
 NV_CROSS(dx, omega, rvec);
 NV_S(dx, *=, dtime);
 NV_V(NODE_COORD(v), +=, dx);
 }
else if (NODE_POS_NEED_UPDATE (v))
 {
 NODE_POS_UPDATED(v);
 omega[2] = sign_funq * (c4-c5*10e3*pow (NODE_X(v),1.0)+c6*10e6*pow
(NODE_X(v),2.0)-c7*10e9*pow (NODE_X(v),3.0)+c8*10e12*pow
(NODE_X(v),4.0));

 NV_VV(rvec, =, NODE_COORD(v), -, origin);
 NV_CROSS(dx, omega, rvec);
 NV_S(dx, *=, dtime);
 NV_V(NODE_COORD(v), +=, dx);
 }
}
}
end_f_loop(f,t)
}
```

CURRICULUM VITAE

Credentials

Name, Surname : Erol, UÇ

Place of Birth : Antalya, Turkey

Marital Status : Married

E-mail : eroluceroluc@gmail.com

Address : Bahçelievler Mh. 315 Sk. No: 3/10 Gölbaşı / ANKARA

Education

B.Sc. : Middle East Technical University, Department of Mechanical Engineering (2012)

M.Sc. : Hacettepe University, Department of Mechanical Engineering (2018)

Foreign Languages

English

Work Experience

System Desing Engineer

Areas of Experience

Thermofluids Sciences, Computational Fluid Dynamics, Piezoelectric Fan

Projects and Budgets

-

Publications

-

Oral and Poster Presentations

-

HACETTEPE UNIVERSITY
GRADUATE SCHOOL OF SCIENCE AND ENGINEERING
THESIS/DISSERTATION ORIGINALITY REPORT

HACETTEPE UNIVERSITY
GRADUATE SCHOOL OF SCIENCE AND ENGINEERING
TO THE DEPARTMENT OF MECHANICAL ENGINEERING

Date: 17/04/2018

Thesis Title / Topic: Fin Optimization in a Flow Field Induced by Piezoelectric Fan

According to the originality report obtained by my thesis advisor by using the *Turnitin* plagiarism detection software and by applying the filtering options stated below on 16/04/2018 for the total of 71 pages including the a) Title Page, b) Introduction, c) Main Chapters, d) Conclusion sections of my thesis entitled as above, the similarity index of my thesis is 7 %.

Filtering options applied:

1. Bibliography/Works Cited excluded
2. Quotes included
3. Match size up to 5 words excluded

I declare that I have carefully read Hacettepe University Graduate School of Sciene and Engineering Guidelines for Obtaining and Using Thesis Originality Reports; that according to the maximum similarity index values specified in the Guidelines, my thesis does not include any form of plagiarism; that in any future detection of possible infringement of the regulations I accept all legal responsibility; and that all the information I have provided is correct to the best of my knowledge.

I respectfully submit this for approval.

17.04.2018

Date and Signature

Name Surname:	Erol UÇ
Student No:	N14321166
Department:	Mechanical Engineering
Program:	Mechanical Engineering
Status:	☒ Masters ☐ Ph.D. ☐ Integrated Ph.D.

ADVISOR APPROVAL

APPROVED.

Assist. Prof. Dr. Özgür EKİCİ

(Title, Name Surname, Signature)